iScience

CellPress
OPEN ACCESS

Review

Solar-driven thermochemical conversion of H_2O and CO_2 into sustainable fuels

Linyang Wei,[1,2,5] Zhefei Pan,[1,5] Xingyi Shi,[1,5] Oladapo Christopher Esan,[1] Guojun Li,[2] Hong Qi,[3] Qixing Wu,[4,*] and Liang An[1,*]

SUMMARY

Solar-driven thermochemical conversion of H_2O and CO_2 into sustainable fuels, based on redox cycle, provides a promising path for alternative energy, as it employs the solar energy as high-temperature heat supply and adopts H_2O and CO_2 as initial feedstock. This review describes the sustainable fuels production system, including a series of physical and chemical processes for converting solar energy into chemical energy in the form of sustainable fuels. Detailed working principles, redox materials, and key devices are reviewed and discussed to provide systematic and in-depth understanding of thermochemical fuels production with the aid of concentrated solar power technology. In addition, limiting factors affecting the solar-to-fuel efficiency are analyzed; meanwhile, the improvement technologies (heat recovery concepts and designs) are summarized. This study therefore sets a pathway for future research works based on the current status and demand for further development of such technologies on a commercial scale.

INTRODUCTION

Energy crisis and carbon neutrality are becoming trending topics across the globe, particularly in the power and energy sector in recent years. Relevant data show that over 80% of the global energy consumption is supplied by fossil fuels while only about 14% are derived from sustainable and renewable energy sources.[1–3] This therefore indicates that the world is experiencing severe challenges in providing clean and sustainable energy for our present society which is confronted by severe energy and environmental issues. It is thus of significant importance to earnestly develop and utilize sustainable and renewable energy sources. The International Renewable Energy Agency (IRENA) recently reported the predicted share of renewable energy to be 28% by 2030 and 66% by 2050 in the global energy outlook.[4] In other words, renewable energy is entering a new stage of development, and its explosive development will occur in the future.

Liquid hydrocarbon fuels (such as methanol, gasoline, diesel, kerosene, etc.) with high energy density have received wide applications in various industries due to their compatibility with existing and relevant infrastructures. In order to achieve the ambitious goal of reducing fossil fuels demand, non-fossil synthetic liquid fuels have become an intensively pursued alternative. At present, the synthetic liquid fuels are usually produced from low energy content carbonaceous sources. Typical representatives are gas-to-liquid[5] and coal-to-liquid[6] technologies which convert natural gas (or other gaseous hydrocarbons) and coal, respectively, into longer-chain liquid hydrocarbons such as gasoline or diesel fuel, on industrial and commercial scales. However, current synthetic liquid fuels technologies are not completely independent of fossil fuels. The upgrading of fuel quality is also accompanied with the consumption of additional energy according to energy conservation. This thus indicates that conventional synthetic liquid fuel technologies cannot meet the global requirement of non-fossil fuels and carbon neutralization.

Solar-driven thermochemical conversion of H_2O and CO_2, using concentrated solar power (CSP), into sustainable liquid fuels can meet this stringent requirement, as it employs only solar energy as high-temperature heat supply and adopts H_2O and CO_2 as initial feedstock.[7] In other words, the conversion of solar energy into chemical energy stored in liquid fuels provides a promising pathway to significantly reduce dependence on fossil fuels. The technological challenge, however, is to produce renewable syngas from H_2O and CO_2 using solar energy. What needs to be explained here is that other existing pathways for H_2O and CO_2 splitting, such as photocatalysis, photo-electrolysis, and water electrolysis, cannot meet the requirements for energy generation. This is because both photocatalysis and photo-electrolysis cannot operate on an industrial scale due to constraints of relevant materials and their poor solar-to-fuel efficiency.[8] Water electrolysis, on the other hand, requires a large amount of electricity source, although it can also adopt inexpensive electricity provided by renewable energy sources (solar or wind power), and multi-step energy conversion which in turn increases costs and reduces conversion efficiency. In contrast, thermochemical

[1]Department of Mechanical Engineering, The Hong Kong Polytechnic University, Hung Hom, Kowloon, Hong Kong SAR, China
[2]School of Metallurgy, Northeastern University, Shenyang 110819, China
[3]School of Energy Science and Engineering, Harbin Institute of Technology, Harbin 150001, China
[4]Shenzhen Key Laboratory of New Lithium-ion Batteries and Mesoporous Materials, College of Chemistry and Environmental Engineering, Shenzhen University, Shenzhen 518060, China
[5]These authors contributed equally
*Correspondence: qxwu@szu.edu.cn (Q.W.), liang.an@polyu.edu.hk (L.A.)
https://doi.org/10.1016/j.isci.2023.108127

splitting of H_2O and CO_2 has a significantly higher energy efficiency potential[9] due to the fact that such technology successfully bypasses intermediate energy conversion, such as the electricity required for electrolysis process, and directly converts solar energy into chemical energy.

Thermochemical fuel production based on redox cycles was initially proposed to produce hydrogen from water-splitting to tackle the first oil crisis in 1970s. Nuclear reactors were therefore employed to provide high-temperature heat source required for thermochemical water splitting. However, the rapid development of such research was not realized until 2000 due to the great potential of concentrated solar energy which can provide high-temperature heat for redox cycle process.[10] Over the past two decades, a large number of research works have been reported and published on redox materials selection, reactors design, thermodynamic analysis, numerical validation and experimental testing.[9,11–17] These studies indicate that solar-driven thermochemical splitting of H_2O and CO_2 based on redox cycles is a significant promising pathway to produce sustainable fuels, even though it is yet to be processed on industrial scale. At present, the major issue limiting the further development of such technology toward commercial production is its very low solar-to-fuel efficiency. However, thermodynamic analyses indicated that the potential solar-to-syngas efficiency can exceed an economically competitive 20% with a suitable heat recovery application.[18,19] How to increase the thermochemical conversion efficiency from solar to fuels therefore becomes a major research focus. Other than the low conversion efficiency, the operating temperature of the entire thermochemical redox cycle is still high, especially in reduction step which usually requires a high temperature >1000°C.[20,21] Such high temperature for the reduction reaction would limit its practicality on large scale, increase energy penalties due to heat losses, as well as place constraints on the redox materials and devices. Therefore, effective and stable redox cycle technology and design under a suitably low temperature for the thermochemical splitting of H_2O and CO_2 are attracting great interest of researchers in this field.[22–29]

Against the backdrop of energy crisis and the pursuit of carbon neutrality, more and more attention is currently given to exploration and utilization of renewable energy, which booms the development of sustainable fuels with concentrated solar energy serving as the high-temperature heat source. To date, several reviews of solar-driven thermochemical redox cycle for splitting of H_2O and CO_2 have been published.[9,14,20,30–35] However, they all focused on one part of thermochemical redox cycles. For instance, Carrillo et al.,[9] Bayon et al.,[14] and Bhosale et al.[33] mainly focused on the redox materials for thermochemical splitting of H_2O and CO_2. Zsembinszki et al.[32] mainly introduced and summarized solar reactors used for thermochemical redox reactions. Pullar et al.[34] only discussed solar thermochemical CO_2 splitting which focused on exploring the advances in the synthesis of ceria materials with specific morphologies or porous macro- and microstructures. To the best of our knowledge, the thorough and comprehensive summary on sustainable fuels production from H_2O and CO_2 with the aid of concentrated solar energy are not covered in the existing published reviews. Hence, a contemporary and comprehensive review of the complete process of solar thermochemical fuel production is of significant importance within the energy and fuel research community for knowledge update. This article therefore presents the development of solar-driven thermochemical conversion of H_2O and CO_2 to sustainable fuels in recent decades. The complete fuel production system including detailed working principles, redox materials, and key devices are extensively discussed, especially for the heat recovery concepts integrating into the reactors. Meanwhile, particular issues for future work on the topic are also identified and discussed. This review therefore provides pathway for future research on solar-driven thermochemical fuel production technologies.

SOLAR-DRIVEN THERMOCHEMICAL CONVERSION

System and key devices

A complete sustainable fuels production system, converting H_2O and CO_2 into sustainable fuels driven by the CSP technology consists of solar energy collection unit, thermochemical reaction unit, and sustainable fuel synthesis unit.[36,37] Since H_2O and CO_2 production belong to another mature technology, it is not repeated here. The solar energy collection unit is employed to track and concentrate the sunlight into dense solar radiation power which serves as high-temperature heat supply to drive thermochemical reaction. Following the heating of the CSP, the thermochemical splitting of H_2O and CO_2 via redox cycle is then used to produce syngas in the thermochemical reaction unit.[38] The syngas produced via the thermochemical reaction can be directly used as a source of pure hydrogen and carbon monoxide,[30,39,40] or further served as basic raw materials to produce synthesis liquid hydrocarbon fuels (such as methanol or kerosene) in a sustainable fuel synthesis unit.[41,42] Through this process, the solar energy therefore can be converted into chemical energy and stored in the form of sustainable liquid fuels as shown in Figure 1.

The key component of the solar energy collection unit is CSP which can provide high solar flux to heat reactor and drive the thermochemical reaction. The CSP can be achieved by a solar collector with a parabolic dish configuration which can provide a three-dimensional (3D) point focusing. Thermochemical splitting cycle of H_2O and CO_2 requires very high temperature (in excess of 1200 K),[31] therefore, only dish solar collector with 3D point focusing can provide sufficient dense solar radiation to obtain such elevated temperature. If large-scale concentration of solar energy is required, a tower solar collector with the aid of a controllable heliostat field can be employed as it has been identified as a favorable path to attain commercial application.[43] The thermochemical reaction unit is the most important part of the complete sustainable fuels production system as it simultaneously connects upstream of solar energy collection and downstream of liquid fuels synthesis. The key device of thermochemical reaction unit is the reactor which provides a place for the thermochemical splitting of H_2O and CO_2. In other words, the syngas (intermediate products for liquid fuels) is produced in the reactor. It should also be noted that the reactor also usually serves as a solar receiver, because the concentrated solar radiation can directly enter the reactor through the aperture. Thus, it is also known as a solar receiver-reactor. A suitable solar receiver-reactor design is required to simultaneously consider redox material, temperature, aperture size, energy loss, stable operation, among others. The detailed description of solar receiver-reactors is presented in

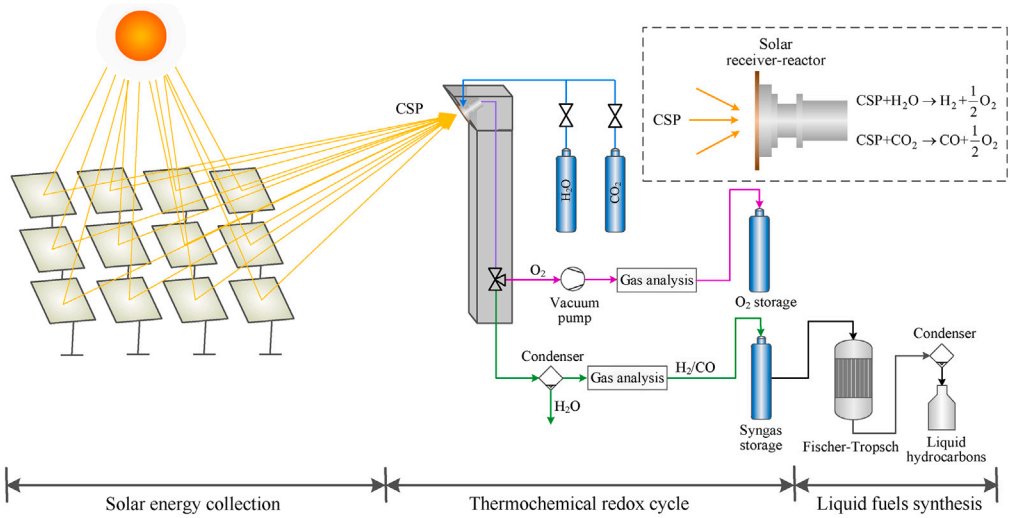

Figure 1. Solar-driven thermochemical fuel production chain from H_2O and CO_2 to sustainable fuels

Converting thermal energy to chemical energy. The liquid fuels are further synthesized in a catalyst packed-bed reactor via the synthesis technology, such as well-known Fischer-Tropsch (FT) synthesis technology.[44] At present, liquid fuels (such as methanol, gasoline, kerosene, etc.) synthesis technologies[41,45–49] are relatively mature and exist in many commercial applications.

In the entire production system from H_2O and CO_2 into sustainable fuels, some auxiliary devices are also necessary. For example, vacuum pumps are employed to control gas pressure in cavity of reactor; condenser is employed to recover liquid water; compressor and storage container are used to store syngas; and other control software and hardware. Therefore, a complete sustainable liquid fuels production chain involves a lot of devices, such that the practical operation is extremely complex, especially when considering the cooperative operation of the above mentioned three units, solar energy discontinuity problem, and heat recovery application. Most studies are still stuck in the conceptual design stage while there are only a few successful cases on an experimental scale. There are still a large number of scientific and technical issues (such as the concentration of solar energy, exploration of redox materials, design of reactor, liquid fuel synthesis, etc.) that need to be resolved for further commercial and industrial production.

Working principle and redox materials

Working principle

The essence of solar-driven thermochemical fuels production is to convert solar energy into chemical energy which is stored in a sustainable liquid fuels carrier. For the entire solar-driven thermochemical fuels production system, the technological challenge is to produce intermediate product syngas from thermochemical splitting of H_2O or/and CO_2, which is our most important concern. Because the solar energy collection (upstream) and final syngas processing to liquid fuels (downstream) can be considered as mature technologies due to the fact that they have realized commercial application, such as solar thermal power plant and FT catalytic synthesis in industrial scale. Therefore, the effective thermochemical splitting of H_2O and CO_2 becomes the first and important problem to be solved.

The thermochemical splitting of H_2O and CO_2 can obtain renewable syngas (H_2 and CO), such as single-step direct thermolysis and two-step thermochemical splitting based on redox cycle. The single-step direct thermolysis of H_2O or/and CO_2 refers to the dissociation of chemical bonds with oxygen atoms at a high temperature. The detailed reaction can be expressed as:

$$H_2O \rightarrow H_2 + \frac{1}{2}O_2 \qquad \text{(Equation 1)}$$

$$CO_2 \rightarrow CO + \frac{1}{2}O_2 \qquad \text{(Equation 2)}$$

Conceptually, direct thermolysis of H_2O or CO_2 seems to be the simplest reaction from Equations 1 and 2, however, it requires an extremely high temperature. Relevant study[20] showed that the direct thermolysis of CO_2 cannot proceed spontaneously below ~3000°C, and even the thermolysis of H_2O needs a higher temperature. Such elevated temperatures seriously hinder the further development toward commercial applications. In additions, the direct thermolysis of H_2O or CO_2 faces some inevitable challenges, for instance, (1) the solar reactors must withstand repeated thermal constraints at high temperatures; (2) H_2 (or CO) and O_2 separation needs to be proceeded at high temperature to avoid recombination of products (reverse reaction); (3) such high temperature required for the reaction is difficult to obtain under direct concentrated solar radiation because of selective absorption of H_2O and CO_2; and (4) even if the high temperature required for reaction is attained, radiation loss would be extremely serious according to the Planck's law, and the solar energy conversion

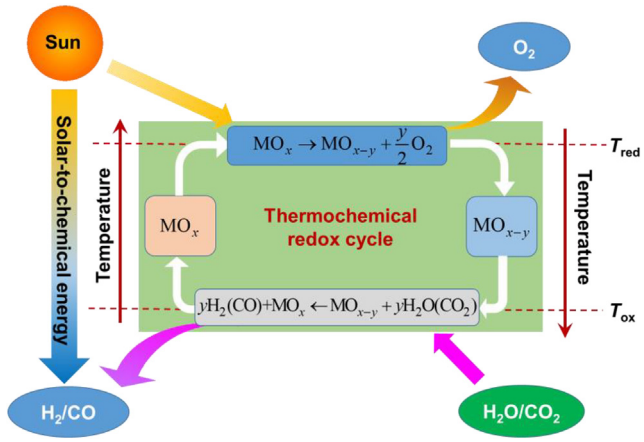

Figure 2. Principle of solar-driven thermochemical redox cycle for production of H_2/CO

efficiency would be very low. At present, no existing technology can address these challenges, which means that alternative suitable routes to split H_2O or/and CO_2 need to be developed.

Thermochemical multistep cycles (≥ 2) is firstly proposed to decompose this direct thermolysis into different steps by Funk and Reinstrom[50] in 1966. The thermochemical cycles are multiple consecutive chemical reactions, and their finial "net" sum is the splitting of $H_2O(CO_2)$ into $H_2(CO)$ and O_2. The initial aim of this study is to produce H_2 from splitting of H_2O using the high-temperature heat (~950°C) supplied by nuclear reactors to face the first oil crisis in 1973. However, the interest in such research decreased drastically in the following two decades. Its real rapid development occurred at the beginning of this current century due to the great progress in alternative concentrated solar energy technologies. A typical thermochemical multistep cycle is two-step thermochemical cycles based on redox materials, which has been successfully applied in the dissociation of H_2O or/and CO_2 with the CSP directly served as the process heat source. Compared with direct thermolysis, the two-step thermochemical splitting cycles significantly reduces the temperature required for reaction, and thereby reduces radiative heat losses. This means a potentially higher solar-to-fuel conversion efficiency and more prospects to realize industrial-scale production. The state-of-the-art and attractive thermochemical cycles for dissociation of H_2O or/and CO_2 are those based on reduction and oxidation reactions of metal oxides.[21,30] The two steps involves – Step 1: endothermic reduction reaction driven by concentrated solar energy, yielding an active oxygen-deficient metal oxides accompanied by pure oxygen release; and Step 2: exothermic oxidation reaction in the presence of H_2O or/and CO_2, regenerating the initial metal oxide and harvesting the products of H_2 or/and CO. The detailed thermochemical cyclic operation is shown in Figure 2, and the reduction and oxidation reactions scheme can be described as:

$$MO_x \rightarrow MO_{x-y} + \frac{y}{2}O_2 \quad \text{(Equation 3)}$$

$$MO_{x-y} + yH_2O(CO_2) \rightarrow MO_x + yH_2(CO) \quad \text{(Equation 4)}$$

where MO_x represents redox materials, such as, metal oxide. It should be noted that the splitting of H_2O and CO_2 obey the same thermochemical principle. The swing of reduction step and oxidation step depends on temperature and oxygen partial pressure. Reduction reaction usually requires a relatively high temperature and low oxygen partial pressure while oxidation reaction need to proceed under a relatively low temperature and in the presence of H_2O or/and CO_2. Thus, O_2 and H_2 (CO or mixture of H_2 and CO) are generated in separate stages (reduction and oxidation steps) in thermochemical cycle process, which eliminates necessary product separation and successfully avoid risk of explosive recombination of O_2 and syngas products in the direct thermolysis.[31] The comparison between direct thermolysis and two-step thermochemical splitting is given in Table 1. An additional advantage of the solar thermochemical two-step redox cycle[51] is that it can co-split H_2O and CO_2 separately or simultaneously, to control the generation of H_2 and CO species suitable for the synthesis of methanol[48] or other liquid fuels (hydrocarbon fuels) by the FT synthesis,[52] which eliminates the energy penalty associated with additional refinement steps for adjusting the syngas mixture (ratio of H_2:CO). Moreover, compared with the electrolytic pathway (called "power-to-X"), the thermochemical approach bypasses the solar electricity generation, the electrolysis, and the reverse water-gas shift reaction steps, directly producing solar syngas.[53]

The solar-to-fuel efficiency is an important indicator that evaluates the performance of reactor.[54] For a closed thermochemical fuel production system, the energy input is assumed to be provided by concentrated solar energy Q_{solar}. The energy loss Q_{loss} includes re-radiation, conduction, and convection losses, and unrecovered sensible and latent heat in the reaction products and materials of construction. The auxiliary work W_{aux} is the additional work that is required for the operation of the reactor, such as pumping work. The chemical energy Q_{chem} is the energy stored in fuels, such as H_2 and CO. It should be noted that the energy loss Q_{loss} and auxiliary work W_{aux} are both assumed to be offset by concentrated solar energy. Thus, a generic energy efficiency is defined as

Table 1. Comparison between direct thermolysis and two-step thermochemical splitting

Styles	Chemical reactions	Required temperature	Gas products separation
Direct thermolysis	Single step	Ultra-high (>2500K)	Required
Thermochemical splitting	Two steps	Depends on redox materials (<2500K)	Not required

$$\eta_{solar-to-fuel} = \frac{Q_{chem}}{Q_{solar}} \times 100\% \quad \text{(Equation 5)}$$

$$Q_{chem} = n_{fuel} \cdot HHV_{fuel} \quad \text{(Equation 6)}$$

where HHV_{fuel} is the higher heating value of fuel.

Due to the temperature-swing of reduction and oxidation steps, the absence of heat recuperation from solids would lead to a significant energy loss to the ambient upon cooling from both. To address this issue, a novel concept of isothermal thermochemical operation has recently emerged as an important special case of two-step solar thermochemical cycle, because isothermal thermochemical cycling successfully doesn't require heat recuperation from solids by eliminating the temperature difference.[55–58] However, in fact, "isothermal" is just an idealized condition, because the absolute isothermal thermochemical cycling is hard to achieve. Thus, the near-isothermal thermochemical cycles with a relatively small temperature variation, such as $\Delta T < 150°C$, is considered, which can take advantage of both high efficiency of two-temperature cycling and simple reactor design of isothermal cycling. At present, the pros and cons of isothermal versus two-temperature thermochemical cycling are still under debate. This is because the thermodynamic properties of redox materials play a significant role in the reactor design and energy conversion performance, which means selection of isothermal or two-temperature thermochemical cycling depends on redox materials. It is well known that materials with a lower reduction enthalpy and a higher reduction entropy are easier to be reduced while more difficult to be re-oxidized. For example, ceria-based materials with high reduction enthalpy and high reduction entropy, requires high temperature and low oxygen partial pressure to be reduced, but has favorable oxidation thermodynamics. Conversely, some perovskite oxides are easy to be reduced but require a large amount of H_2O/CO_2 gas or a lower oxidation temperature to be re-oxidized due to contradictory thermodynamic forces. Taking ceria as example, if the redox temperature is too high, the oxidation kinetics would be decreased, which is not conducive to oxidation step; if the redox temperature is too low, a lower oxygen partial pressure is required to drive reduction reaction, which means a higher energy consumption associated with vacuum pump or inert gas sweep. Whether final isothermal operation can improve the solar conversion efficiency needs further verification.

Redox materials

The oxygen exchange capacity in one cycle (i.e., reduction extent of redox materials from highest-metal-valence oxide to lower-metal-valence/zero-metal-valence oxide) is not only related to the temperature and/or oxygen partial pressure conditions, but also depends on the redox material itself. Redox materials developed for thermochemical conversion process can be divided into three categories: (1) volatile redox materials, (2) non-volatile stoichiometric redox materials, and (3) non-stoichiometric redox materials. The volatile redox materials include: ZnO/Zn redox pair,[59–63] CdO/Cd redox pair,[64–66] SnO2/SnO redox pair,[67–70] and GeO_2/GeO redox pair.[71] This category of materials are accompanied by a phase change during redox cycles, since the temperature required for reduction step exceeds the boiling temperatures of the reduced species. Although the phase change is thermodynamically beneficial for redox cycles, oxygen products mixed with gaseous metal or lower valence oxide would face significant challenges of recombination issues back to the initial reactants in the product gas stream, particularly if they are not separated in time. The non-volatile stoichiometric redox materials include: Fe_3O_4/FeO redox pair,[72–74] CeO_2/Ce_2O_3 redox pair,[75] and hercynite redox material.[76–78] They would not change into gaseous state during the entire redox cycles process, thereby successfully bypass the recombination issues. In addition, the stoichiometric reactions involve a change in crystal structure during redox cycle and have a great oxygen exchange capacity. However, a complete reduction reaction usually requires a very high temperature (such as 2100k for Fe_3O_4 reduction[20]) under which the redox materials would change into liquid, meanwhile the oxidation reaction process requires a relatively low temperature (such as the minimum temperature 450K for FeO oxidation[79]). Solid-to-liquid phase change during reduction step and large temperature difference between reduction and oxidation steps would not only cause poor stability and slower reaction kinetics, but also seriously decrease the solar-to-fuel efficiency. Compared with these two categories, the non-stoichiometric redox materials are more advanced in term of operation, efficiency, and stability. The materials comparatively presented in recent publications are ferrites,[80–83] ceria,[33,75,84–86] and perovskites.[14,87–91] The maximum difference from non-volatile stoichiometric redox materials is that the non-stoichiometric redox materials only involve partial reduction during cycle, while maintaining the crystallographic structure. Although oxygen generated in reduction step and syngas generated in subsequent oxidation step are both decreased, this can avoid phase transformations which can induce structure disruption, and make redox cycle operate more stably and efficiently. A detailed introduction of prominent non-stoichiometric redox materials is presented in subsequent sections.

Ferrite materials

The initial research works on non-stoichiometric redox materials referred to ferrite system, which were experimentally tested for hydrogen production from the splitting of H_2O.[80] Nowadays, it has become one of the most advanced systems and been tested to the stage of a 100 kW

(using a solar tower) pilot-scale demonstrator.[92] The initial ferrite redox materials usually require a high temperature for thermal reduction (TR) in thermochemical cycle, however, such high temperature would cause significant sintering of the oxides. For example, the Fe_3O_4/FeO redox pair requires a temperature of 2100K during reduction step, while the melting temperatures of Fe_3O_4 and FeO are 1811K and 1650K, respectively. Thus, the Fe_3O_4/FeO redox pair need a milling to obtain a fine powder to warrant a sufficient specific surface area to process repeated redox cycle, which would make redox cycle seriously complicated to be implemented. In addition, a quenching below 570°C is required to avoid the formation of Fe_3O_4 and metallic Fe from the produced FeO species by disproportionation reaction. Ferrite materials usually do not have a sufficient cycling stability because of unavoidable sintering and induced losses of redox activity and fuel production capacity.

To decrease the redox cycle temperature of ferrites, the metallic dopant idea (i.e., replacing some iron atoms in the lattice with other metals) has been proposed and investigated. Some other more readily reducible metals (like Mg, Mn, Co, Ni, Zn, etc.) are inserted into Fe_3O_4 to form $(Fe_{1-x}M_x)_3O_4$ formula. Although the reactivity of the doped metals to the oxidant (H_2O or CO_2) becomes relatively low, the reduction step is further facilitated because such a doping creates a structural deformation of the spinel, thereby favoring oxygen mobility. Thus, the doped ferrites can participate in non-stoichiometric redox cycle under a lower temperature than pure Fe_3O_4. A series of ferrites has been developed including only one bivalent metal cations in the A site such as $MnFe_2O_4$,[80] $ZnFe_2O_4$,[93] $NiFe_2O_4$,[94] $CoFe_2O_4$,[95] and two bivalent metal cations in the A site such as $Ni_{0.5}Mn_{0.5}Fe_2O_4$,[96] and $Mn_{0.5}Zn_{0.5}Fe_2O_4$.[97] Numerous experimental testing and thermodynamic studies of ferrites for splitting of H_2O or/and CO_2 via two-step redox cycle indicated that the nickel-based ferrites that are operated under a reduction step temperature below ~1400°C–1500°C have an optimal performance in terms of fuel production yield and thermochemical stability.[81,98,99] However, the improved reduction temperature is still high for the operating process which would be accompanied by sintering, and induced losses of redox activity and fuel production capacity. To further enhance cycling stability of ferrites, an idea supporting the redox reagent on high-temperature-stable ceramic support was widely considered.[82,83] It was reported that the yttrium-stabilized zirconia (YSZ)[100] and monoclinic zirconia (*m*-ZrO_2)[22] have been adopted to serve as substrates of ferrites. In addition, Coker et al.[101,102] found that Fe ions dissolved within the YSZ lattice are more "redox-active", which would lead to higher oxygen yields accompanied with more H_2 or CO produced per cycle.

Reaction kinetic of ferrites for thermochemical redox cycle (such as establishment of kinetic models, extraction of the kinetic parameters of ferrites during redox reactions, etc.) have been studied by many experts. For example, Go et al.[103] adopted thermogravimetric analyzer to determine reaction kinetics of Mn and Zn doped ferrites during redox cycle for splitting of H_2O. They found that the reduction conversion of the ferrites increased with temperature (above 1073K) and the oxidation reaction was controlled by the product-layer diffusion mechanism. Neises et al.[104] built a laboratory scale test rig to examine and monitor the hydrogen production in oxidation step by analyzing the product gas. They also investigated the effects of temperature and water concentration on the hydrogen production, and thereafter calculated the activation energy from the experimental data. Kostoglou et al.[99] proposed an improved kinetic model of nickel-based ferrite for thermochemical splitting of H_2O via redox cycles. They considered two oxygen storage regions existing in ferrite material and thought that the oxygen storage regions communicate to each other by a solid-state diffusion mechanism, which can well explain why thermochemical cycles converge to a periodic steady state. In addition, an interesting phenomenon that the oxidation reaction of ferrites is much faster than corresponding reduction reaction during splitting of H_2O or/and CO_2 cycle, which means a shorter time for one cycle (i.e., more H_2 or/and CO yield at the same time), was also discovered from these investigations.

Ceria materials

Ceria is an excellent catalytic material used for oxidizing exhaust gases to reduce gaseous pollutants due to its facilitated solid-state diffusion and exchange of oxygen ion in crystalline lattice. It is just suitable for thermochemical redox cycle for splitting of H_2O or/and CO_2, which attracts a great deal of research interests of experts from all over the world. Furthermore, ceria can maintain its cubic fluorite structure without sintering due to its high melting temperature. Compared with ferrites, ceria has better stability, cyclability during the long-term operation. Thus, since ceria was firstly proposed to serve as redox materials for splitting of H_2O via two-step thermochemical cycle in 2006,[75] its attractive research interest has continued until now. It is regarded as the current state-of-the-art redox material due to several desirable thermodynamic and physicochemical properties (i.e., favorable oxidation thermodynamics, rapid reaction kinetics, and morphological stability). For the pure ceria, only a partial Ce^{4+} in CeO_2 is reduced during reduction step (non-stoichiometric reduction). Thus, the redox of ceria can be described as

$$CeO_2 \rightarrow CeO_{2-\delta} + \frac{\delta}{2}O_2 \qquad \text{(Equation 7)}$$

$$CeO_{2-\delta} + \delta H_2O / CO_2 \rightarrow CeO_2 + \delta H_2 / CO \qquad \text{(Equation 8)}$$

where δ is the non-stoichiometry which represents reaction extent of CeO_2 in one redox cycle. The reaction extent of CeO_2 depends on the reduction temperature and oxygen partial pressure which are usually adopted as swing between reduction and oxidation reactions. Usually the non-stoichiometry parameter is very small in the thermochemical redox cycle. It is reported that a maximum non-stoichiometry without changing the fluorite structure of CeO_2 for redox recycling of ceria was 0.286 at 1000°C. The oxygen evolution kinetics of CeO_2 during reduction step are also limited by the heating rate,[7] while reaction rate during oxidation step is primarily dictated by the chemical kinetics which mainly depends on chemical composition, as well as microstructure and available surface area of the material. For the $CeO_2/CeO_{2-\delta}$ redox pair, if the reduction temperature is decreased, the reaction extent would be low, which limits the H_2 or/and CO yields per cycle. However, it should also be noted that oxidation reaction rate is high due to rapid oxidation kinetics of $CeO_{2-\delta}$, which means a great deal of cycles can be completed in limited sunny time.

To further improve the reaction extent of CeO_2 for H_2 or/and CO production, the cationic-dopant scheme is proposed and applied, namely, by substituting transition metal and rare earth metal oxides (such as Li^{2+}, Sr^{2+}, Ca^{2+}, Mg^{2+}, Sc^{3+}, Dy^{3+}, La^{3+}, Sm^{3+}, Gd^{3+}, Y^{3+}, Pr^{3+}, Hf^{4+}, and Zr^{4+}) into the crystal structure, the thermodynamic properties and redox performance of CeO_2 may be tuned. For instance, if the tetravalent cationic Zr^{4+} was employed to dope the CeO_2, the reduction extent would be improved, but the oxidation kinetics of doped CeO_2 would decrease compared with pure CeO_2.[25,105,106] The trivalent cations La^{3+}, Gd^{3+}, and Y^{3+} are further doped into the Zr^{4+} doped CeO_2, which can continue to improve reduction extents and fuel yields. Meanwhile, it was also found that trivalent cation La^{3+} dopant can improve the thermal stability and resistance to material deactivation during cyclic operation.[107] Meng et al.[26,108] investigated a series of doping schemes including Mg^{2+}, Sc^{3+}, Hf^{4+} and Pr^{3+}, and they found these dopants all improve the reduction extent compared with pure CeO_2. Among them, Mg^{2+}, Sc^{3+}, and Hf^{4+} dopants schemes can yield a smaller effective cation radius to obtain greater reducibility, and Pr^{3+} dopant of 5 mol % and 10 mol % can improve O_2 and H_2 yields due to a reduced enthalpic energy penalty, though Pr did not participate in oxidation reaction. In contrast, Hf^{4+} dopant exhibited the largest improvement in O_2 evolution at the expense of a lower H_2 production rate than undoped CeO_2. Scheffe et al.[18] performed a thermodynamic analysis of Gd^{3+}, Y^{3+}, Sm^{3+}, Ca^{2+}, and Sr^{2+} doped CeO_2 during redox cycle for solar thermochemical fuel production, and observed an interesting phenomenon that the dopants are not always of better performance. For example, at high reduction temperature larger than 1700K, the reduction extents of pure CeO_2 are larger than those of the dopants, while at lower reduction temperature, just the opposite is achieved. If the dopant concentrations were too large, the entropy change during oxidation with H_2O or CO_2 would be decreased, which means that the oxidation of pure CeO_2 is more favorable than that of doped CeO_2 at temperatures below 1200K. At present, the development of new formulations for doped CeO_2 become a research trend, various novel research results (including their chemical synthesis, performance testing, and reaction kinetics) are reported continuously.[109–116]

In addition to the ceria material's own performance, heat transfer behavior related to structure and morphology of the material is also a limiting factor. When the concentrated solar radiation enters reactors through the aperture, ceria exposed directly to the high-flux radiant energy will first raise the temperature to the reduction temperature, while other ceria remains in low temperature due to its low thermal conductivity. Inhomogeneous temperature distribution limits the majority of reduction reaction to the near-surface layer closed to the aperture.[117] To address this limitation, the structure and morphology of the ceria need to be designed to improve the heat transfer performance. Porous structure concepts (like reticulated porous ceramic foam) become an attractive choice because of their excellent volumetric absorption of incident radiation.[118,119] A macro-porous structure can make radiation pass through internal medium (i.e., enhancing heat transfer capability) and make the entire porous structure ceria be heated more homogeneously (i.e., a lower temperature gradient throughout the ceria material). Furler et al.[120] observed that the average efficiency increased by over a factor of 10 by adopting reticulated porous ceria redox system. Another study[121] found that the oxidation kinetics of the porous ceria would be limited by its relatively low specific surface area. Consequently, they proposed the concept of CeO_2-based porous structures with dual-scale porosities, in which the millimeter-sized pores can enhance heat transfer behavior and the micrometer-sized pores can improve specific surface area. The dual-scale porosities structure perfectly solve the low reduction kinetics issue.[122,123] Marxer et al.[41,124] investigated thermochemical splitting of H_2O and CO_2 based on CeO_2-based porous structures with dual-scale porosities, and they obtained a solar-to-fuel energy conversion efficiency of 5.25%. Recently, Oliveira et al.[125–127] proposed a novel concept of three-dimensionally ordered macroporous structures (such as cork-templated or wood-templated ceria) based on biomimetic approaches to improve the redox cycle performance of ceria for splitting of H_2O and CO_2.

At present, the ceria-based redox materials are experiencing explosive development, and various recent advances in the field are continuously reported.[128–132] However, there are still several aspects that need to be further developed before commercial application. To plainly take profit of the advantages of ceria-based redox cycles, Abanades[20] reviewed the development of ceria-based redox materials and gave some suggestions: (1) the dopant schemes of ceria need to be further optimized including development of new dopants and utilization of composite materials; (2) synthesis method is also an important aspect, especially when the powdered ceria-based material is adopted, synthesis material must be warranted high-temperature resistance; and (3) for porous structure ceria-based material, thermally resistant supports and efficient coating methods are needed, and elaboration of architecture porous structures (such as biomimetics, 3D printing, etc.) are good choices.

Perovskites materials

Perovskites are regarded as a type of crystal structure with a general formula ABO_3 where A and B are both cations with the oxygen in the edge centers. Research indicate that the A cation is 12-fold coordinated with oxygen while the B atom is 6-fold coordinated. Thus, perovskites are commonly cubic, but sometimes may exhibit orthorhombic and rhombohedral crystal structures. Such structures allow some A and B sites to be substituted with other cations, which means that the structural stability may be altered by creating defects. Perovskite materials have been discovered for a long time and become well known for their applications in fuel cells based on reversibility in delivering and picking up oxygen at high temperatures.[133] However, perovskites as non-stoichiometric redox materials for thermochemical splitting of H_2O and CO_2 first appeared in the publication in 2013.[134] In other words, the development of perovskites for thermochemical redox cycle is less than a decade.

Reasonable selection of cations in A and B sites and dopant schemes can make perovskites become excellent redox materials with high non-stoichiometric oxygen exchange capacities and diffusion rates. The two-step thermochemical redox non-stoichiometric reactions based on perovskites can be described as:

$$ABO_3 \rightarrow ABO_{3-\delta} + \frac{\delta}{2}O_2 \qquad \text{(Equation 9)}$$

$$ABO_{3-\delta} + \delta H_2O / CO_2 \rightarrow ABO_3 + H_2 / CO \quad \text{(Equation 10)}$$

where δ is the non-stoichiometry which represents reaction extent of ABO_3 in one redox cycle. Similar to the ceria-based materials, the non-stoichiometry is also small and determined by temperature and oxygen partial pressure. It is reported that a general range of non-stoichiometry between 0.03 and 0.23. At present, perovskites used for thermochemical fuel production have attracts great interests of experts. In design aspect, Ezbiri et al.[135] gave the design principles of perovskites with balanced redox energetics, in which the electronic structure computations were adopted to predict the activity of lattice oxygen vacancies and stability against crystal phase changes and detrimental carbonate formation, and they also experimentally validated the predicted perovskite materials. Antoine et al.[136] presented a high-throughput computational screening strategy to select the potential candidates of perovskite ABO_3 for splitting of H_2O in term of thermodynamic stability and oxygen vacancy formation energy, and they finally identified 139 perovskites favorable for application. In kinetics study aspect, to better characterize a material for thermochemical splitting of H_2O and CO_2, various kinetics methods have been proposed and implemented, such as, mechanistic model-fitting method and non-mechanistic isoconversional method.[137] Reduction kinetics focus on oxygen evolution of perovskites, while oxidation kinetics focus on splitting reaction. Kinetics study aims to determine the maximum fuel amount which can be produced in a reasonable duration. Existing research works indicate that the oxidation kinetics of perovskites are lower than that of pure ceria while their oxygen exchange capacity (namely, fuel productivity per mass of material) is higher. In thermodynamic study aspect, a series of thermodynamic analysis on ceria for redox cycle have been reported.[138–141] In contrast, corresponding related works on perovskites are very few. Muhich et al.[142] pioneered a thermodynamic analysis of perovskites for thermochemical splitting of H_2O and CO_2, and comparison indicated that the solar-to-fuel efficiency of perovskites is lower than that of ceria due to their relative reducibility and re-oxidizability. However, opposite results are observed in the work of Vieten et al.,[87] in which they found that many perovskite materials have higher H_2/CO production. This therefore suggests that the performance and types of perovskite materials need to be further developed.

Doping scheme of perovskites is another research content, and a series of doped perovskites as redox materials have been reported.[143–151] Typical perovskites materials include lanthanum-manganite perovskites, lanthanum-cobalt perovskites, and yttrium-manganese perovskites. For lanthanum-manganite perovskites, the most studied is $La_{1-x}Sr_xMnO_3$. The presence of Sr in the A-site significantly increases reduction extent,[134,152] thereby can obtain a higher fuel production. In addition, the use of Sr as dopant can also affect grain morphology[153] and increase the characteristic time during the oxidation step.[154] For lanthanum-cobalt perovskites, Ca, Sr, and Fe dopants are proposed to substitute in the A or/and B-site. Studies concluded that Ca dopant in the A-site can promote oxygen production, but if Ca content is too high (such as >40%), hydrogen production would decrease. The $La_{0.6}Ca_{0.4}CoO_3$ is regarded as the most promising material in Ca dopant scheme in term of O_2 and CO production.[155] Sr dopant instead of partial La in material can improve reduction extent, and even $La_{0.6}Sr_{0.4}CoO_3$ can achieve a higher H_2 yield (514 μmol/g) than that of $La_{0.6}Sr_{0.4}MnO_3$ (234 μmol/g).[156] However, Orfila et al.[157] found that the fuel production of the Sr doped perovskites would decrease after 4 consecutive cycles, which means its stability need to be further improved. Fe as dopant in $LaCoO_3$ neither improve the stability of material nor re-oxidation yield.[158] Even the presence of Fe would decrease the O_2 production. For yttrium-manganese perovskites, Sr as dopant ($Y_{0.5}Sr_{0.5}MnO_3$) exhibited a higher reduction extent than $La_{0.5}Sr_{0.5}MnO_3$ in similar conditions,[159] which can be attributed to a smaller ionic radius of Y^{3+}. This smaller ionic radius increases the MnO_6 octahedron inclination and the lattice distortion, thereby promoting oxygen departure. At the same time, a lack of CO (a lower re-oxidation) was observed in both Chan[160] and Nair et al.,[159] which means the re-oxidation ability of such perovskites needs to be improved. Ca dopant was also investigated in yttrium-manganese perovskites. Both yttrium and calcium can increase the reduction extent compared with lanthanum and strontium.[161]

Perovskites as a relatively "new" redox material have exhibited a great potential for solar fuel production via thermochemical redox cycle. For example, Barcellos et al.[162] discussed the $BaCe_{0.25}Mn_{0.75}O_3$ (BCM) within the context of thermochemical water splitting materials, and this novel material exhibited a polymorph phase transition during thermal reduction and yielded nearly three times H_2 more than ceria when adopting a reduction temperature of 1350°C. Moreover, BCM exhibited faster oxidation kinetics and higher water-splitting favorability than popular Mn-based perovskite $Sr_xLa_{1-x}Mn_yAl_{1-y}O_3$ (x, y = 0.4, 0.6). Although perovskite materials may exhibit superior redox performance but have not yet proven to be as stable as ceria.[36] Bayon et al.[14] therefore suggested that perovskites should be further developed toward adequate thermochemical properties, large redox extents, fast redox kinetics, high mechanical stability and sintering resistance, adequate vapor pressure at working temperatures, high thermal conductivity, and ultimately, abundance, low toxicity and low cost.

CONCENTRATING SOLAR ENERGY TO THERMAL ENERGY

Research on thermochemical redox cycle for splitting H_2O or/and CO_2 instigated an explosive development in the current century, which also benefit from the aid of CSP technologies. For such evaluated temperature required for thermochemical redox reaction, the high-flux solar energy with high concentration ratio (generally >2000 suns) is required. The open market currently provides four types of CSP technologies, including parabolic troughs, fresnel mirrors, power towers, and solar dish concentrators.[163] However, only solar dish and tower concentrators can provide such high-temperature heat source for thermochemical cycle process,[164] because they both provide 3D point-focus concentration. The applications of these two types of solar concentrators for the thermochemical splitting cycles of H_2O or/and CO_2 are described and discussed in subsequent sections.

Parabolic dish concentrator

Parabolic dish solar concentrator can be used to reflect, concentrate, and deliver sunlight onto a receiver at the focal point.[165] Its high concentration ratio and optical efficiency position it as one of the most perfect solar concentrators for high-temperature heat source. A typical

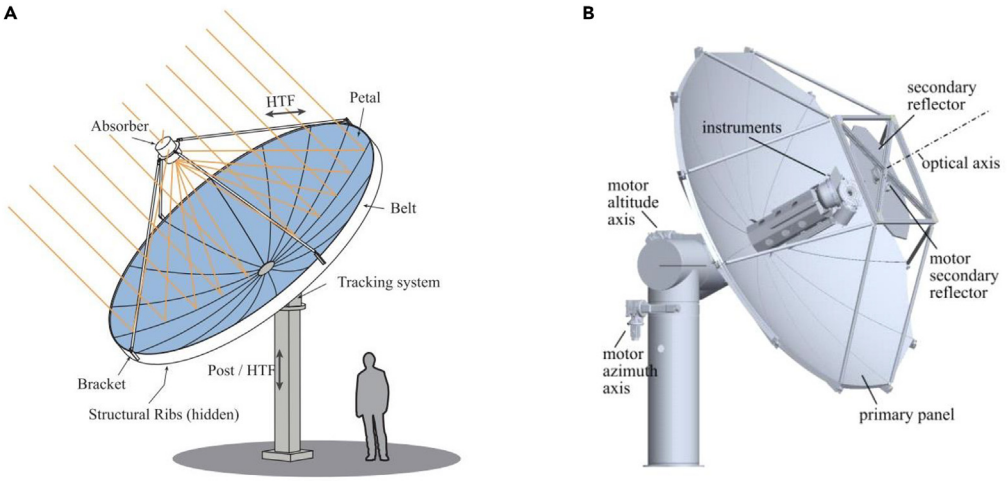

Figure 3. Configuration of parabolic dish concentrators

(A) Parabolic dish concentrator with only primary reflector; Reproduced with permission.[168] Copyright 2020, Elsevier.

(B) Parabolic dish concentrator with another secondary reflector. Reproduced with permission.[169] Copyright 2018, Elsevier.

parabolic dish concentrator consists of a parabolic dish reflector which is usually made up of a set of mirrors, solar receiver which collects concentrated solar energy and solar tracing devices.[166–168] If needed, a secondary reflector can also be integrated into the solar concentrating dish system to change sunlight pathway, to make the whole system more compact at the expense of increasing optical loss. In addition, a secondary reflector (flat or hyperboloid) can flexibly change focal point while keeping the whole system stationary, which is very suitable for the simultaneous operation of two or more adjacent solar receiver-reactors.[169] The generic configuration of parabolic dish concentrator is shown in Figure 3.

At present, most studies on solar-driven thermochemical redox cycle were conducted for performance testing and validation of numerical models.[4,31,170,171] Thus, parabolic dish concentrator was employed to supply high-temperature heat by establishing ray tracing model in theoretical or modeling research works on solar-driven thermochemical redox cycle. For example, Monte Carlo ray tracing method was employed to design the parabolic dish system.[172] The model-generated concentrated radiant fluxes served as CSP to provide high-temperature energy for two-step solar thermochemical splitting of CO_2 in the established CFD model whose numerical results were employed to analyze the influences of geometric factors on the performance. The ceria-based thermodynamic cycle combined with parabolic dish for solar hydrogen production is developed and achieved as high as a solar-to-fuel efficiency of 21.2% after optimizing the concentration ratio, reactor pressures and temperatures.[173] If the parabolic dish concentrator (optimal diameter is 5.168m) is optimized, the amount of hydrogen produced can reach 34 mol m^{-3} in a 10 kWth solar reactor.[174] In addition, some researchers even used the simulated concentrated solar light to power the reaction and directly equated the concentrated solar energy to a specific value or assumed the temperatures provided by concentrated solar energy to be known to simplify the model in their numerical studies.[175–177] This is majorly because their focus is on thermochemical redox cycle process and its performance, rather than concentrated solar technology.

Most experimental studies on thermochemical redox cycle adopted indoor solar simulators to provide high-temperature heat sources in laboratory scale.[70,120,123,125,178] In order to be closer to the real conditions, some researchers designed parabolic dish concentrators to investigate solar-driven thermochemical redox cycle for splitting H_2O or/and CO_2 outdoors. For example, Dähler et al.[169] designed several parabolic dish concentrators for successive thermochemical splitting of H_2O and CO_2 based on redox cycles. They obtained a peak solar concentration ratio of 5,010 suns and an average of 2,710 suns over the 30 mm-radius apertures of the solar reactor. Schäppi et al.[179] applied a parabolic dish concentrator to provide concentrated solar energy for the thermochemical splitting of CO_2, and a secondary rotating reflector was designed to alternate the concentrated solar input between two reactors, which ensure simultaneous operation of both reactors. The team[36] later presented a complete solar fuels production chain based on the above study, which can directly produce methanol from sunlight and air with the aid of parabolic dish concentrator. Abanades et al.[131] adopted parabolic dish concentrator to directly and indirectly provide high-temperature heat for H_2O and CO_2 dissociation in solar reactors, and they observed highest fuel production rate of ~9.5 mL g^{-1} min^{-1} and peak solar-to-fuel energy efficiency of ~9.4% from directly irradiation style.

It can be known from the above research examples (including simulations and experiments) that the parabolic dish concentrator with high concentration ratio and optical efficiency has been successfully applied in solar-driven thermochemical splitting of H_2O or/and CO_2 based on redox cycle. A series of experimental data indicated that the combination of concentrated solar energy and thermochemical conversion is a perfect pathway to produce syngas with only H_2O and CO_2 as feedstock. It should be noted that intercept losses are unavoidable due to inaccurate tracking in practice. To achieve enough high concentration ratio, sunlight needs to be reflected multiple times and finally concentrated to the designated focus position, which causes some solar energy loss but can reduce re-radiation from aperture of reactor. At present, the parabolic dish concentrator is just suitable for experimental research in laboratory scale, due to the limitation of size. Scale-up of solar-driven

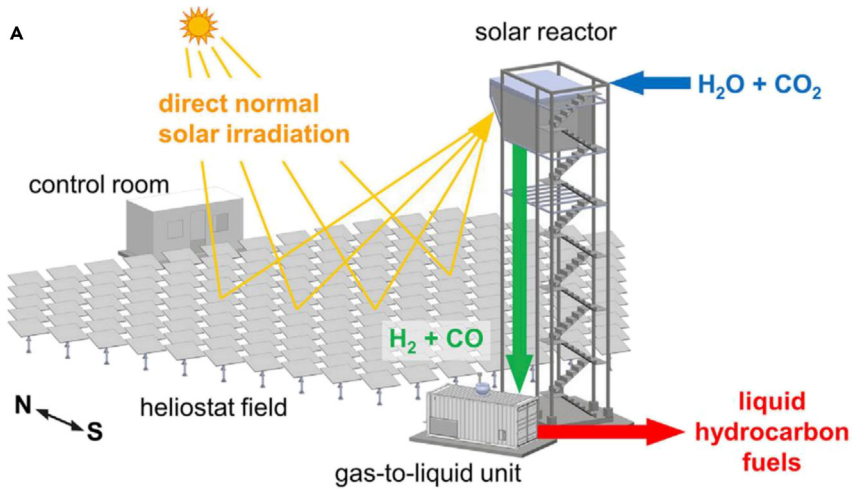

Figure 4. Configuration of solar tower with a heliostat field
Reproduced with permission.[53] Copyright 2022, Elsevier.

thermochemical splitting of H_2O or/and CO_2 based on redox cycle can consider solar tower system with a heliostat field concentrator, which is introduced in the following section.

Heliostat field concentrator

Large scale application of concentrated solar energy focuses on solar tower technology with a heliostat field concentrator,[180–185] because the parabolic dish concentrator configuration is limited in size considering mechanical constraints caused by wind and weight loads.[53] There is no commercial parabolic dish whose diameter is over 10 m in the current market. Although employing a group of solar parabolic dishes can increase the scale of solar energy collection, its investment and cost will be lost to those of solar tower configuration with significant economy-of-scale advantages.[186] At present, solar towers are considered as the most suitable CSP technology to carry out solar-driven thermochemical cycle processes on industrial scale due to it can provide high-power CSP with relatively low cost.[43] A typical concentrated solar tower system usually consists of (1) solar receiver mounted on top of the tower, (2) heliostat field concentrating and delivering solar irradiation onto the aperture of receiver; (3) control room adapting the angle of heliostat to optimize solar collection. These three parts collaboratively operate to finish the tracking, concentrating, and delivering of sunlight. A complete solar tower configuration is depicted in Figure 4.

The heliostat field concentrator is made up of a family of heliostats. A single heliostat is composed of a set of reflect mirrors, a tracking system, a frame, a structure foundation, and control system[187] as shown in Figure 5. The optical efficiency of heliostat field mainly depends on cosine effect, shadowing effect, blocking effect, mirror reflectivity, atmospheric attenuation, and receiver spillage. For the entire solar tower system with a heliostat field concentrator, the almost 50% of investment and 40% of energy loss are attributed to the heliostat field. Thus, optimal design of heliostat and optimal layout of heliostat field are significantly important to improve solar efficiency and reduce the capital cost. In heliostat field layout design aspects, Wei et al.[184,188–191] have done a lot of works involving mechanism, method, and optimization of heliostat field layout design toward the performance improvement of solar tower system. Till date, the heliostat field concentrator technology is one of the most effective methods providing high concentrated solar energy whose scale is far larger than other solar concentrators.

Laboratory-scale research usually adopted indoor solar simulators or outdoor solar parabolic dish concentrator configuration. In contrast, published literatures on the use of concentrated solar tower to drive thermochemical redox cycle for dissociation of H_2O or/and CO_2 are relatively few. This is due to the fact that a relatively large-scale study of thermochemical redox cycle based on concentrated solar tower configuration needs a lot of manpower and financial support. The concept of combination of a high-temperature (~1000°C) power tower and a sulfuric acid/hybrid thermochemical cycle is proposed by Kolb et al.[192] using a combination of thermal input and an electrolyzer to produce hydrogen, and they predicted the solar thermochemical plant will have a much lower cost of hydrogen product than a solar-electrolyzer plant of similar size. After that, solar thermochemical processes based on solar tower is thoroughly studied, including design,[193] control strategy, and validation.[194] And even a successful test operation of a 100 kW pilot plant for thermochemical water splitting is implemented on a solar tower platform under real conditions.[92] More recently, Zoller et al.[53] experimentally demonstrated a fully integrated thermochemical production chain from H_2O and CO_2 to kerosene for the first time, and adopted solar tower with a controllable heliostat field to provide high solar flux (2500 suns) to achieve a solar-to-syngas energy conversion efficiency of 4.1% in the absence of any heat recovery system.

Above studies successfully push solar tower technology toward application in large-scale solar-driven thermochemical fuel production. However, up to now, no solar tower plants for thermochemical fuel production are employed on a commercial scale, because there are still many scientific and technical issues, including efficiency, cost, intermittent solar energy, weather, seasons, operation maintenance that all need to be resolved in the future. Nevertheless, existing publications have proven that the solar tower with heliostat field concentrator is

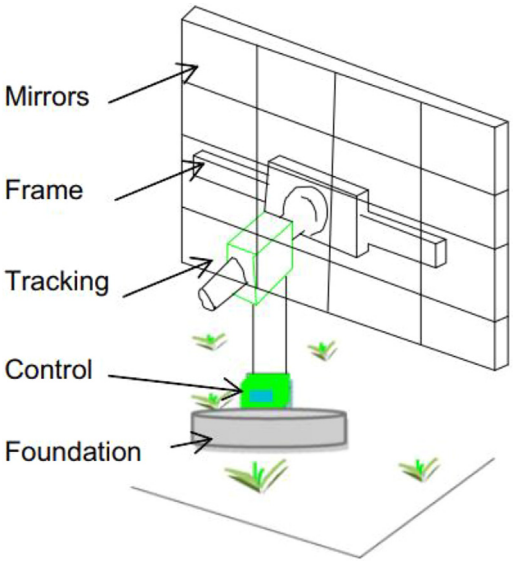

Figure 5. Configuration of single heliostat
Reproduced with permission.[187] Copyright 2013, Elsevier.

the most promising pathway to provide high-temperature heat supply for realizing large scale commercial application of thermochemical conversion process of H_2O and CO_2 to sustainable liquid fuels.

CONVERTING THERMAL ENERGY TO CHEMICAL ENERGY

Once the solar energy has been concentrated to the intensive thermal energy, the next step is transferring the thermal energy to the thermochemical reactor to trigger the thermochemical conversion of H_2O or/and CO_2 to H_2 or/and CO. The energy transfer can be generally divided into two categories according to the mechanism of transfer: one is the indirect irradiation, during which absorbing surfaces are exposed to the concentrated solar radiation with heat conducted across their walls to the thermal fluid, and the other is direct irradiation, during which fluid streams or solid particles/structures are directly exposed to the concentrated solar radiation.[195] A typical example of the indirect irradiation is conventional tubular reactors consisting of absorbing surfaces exposed to concentrated solar irradiation while the heat transfer fluid is moving in a direction vertical to that of the incident solar radiation.[196] The later type is also known as "volumetric" reactor that enables the concentrated solar radiation to penetrate and be absorbed by the absorber without the transfer through the wall.[38] The majority of reactors are in the category of direct irradiation that use solid particles or structures directly exposed to concentrated solar radiation. Hence, the reactors must be equipped with a transparent window, which allows concentrated light to enter the receiver while isolating the working gas from ambient air.[197]

Continuous utilization of thermal energy

There are two types of solar reactors based on the redox chemistry of volatile and non-volatile redox cycles. A gaseous mixture of the reduced phase and oxygen occurs during the TR phase, and special treatment is required to prevent its recombination back to its original oxidized form, which is a common feature of all proposed volatile cycles. As a result, each of these systems has two distinct reactors: one that plays out the TR step from which a dense decreased stage is gotten along with vaporous oxygen and a second one where this consolidated stage is oxidized and plays out the necessary splitting of H_2O or CO_2 step.[198] The cyclic operation can thus be separated into two stages: one during the day for thermal reduction and one at night for the production of syngas. Therefore, the thermal energy is difficult to be continuously used by one reactor in this manner. As a result, we include and discuss the reactors that intend to carry out the TR step and innovative reactors that could continuously use thermal energy in this section. Partial reactor designs are presented in Figure 6 while their main characteristics are summarized in Table 2.

Reactors performing only the reduction step

The reduced materials and evolved O_2 are inherently separated in this reactor concept, which operates isothermally throughout the day and decouples the reduction and oxidation processes in space and time for potential 24-h syngas generation. Haueter et al.[204] described the solar thermochemical reactor's design, fabrication and initial testing, which uses a windowed rotating cavity-receiver lined with ZnO particles held by centrifugal force to conduct the thermal dissociation of ZnO into zinc and oxygen at temperatures above 2000 K. ZnO functions as a radiant absorber, a thermal insulator, and a chemical reactant in this arrangement while also being directly exposed to high-flux solar radiation. The limitations imposed by the chemistry of the decomposition reaction and the transitory nature of solar energy are considered when designing the reactor. The high-temperature thermal dissociation of ZnO in a solar-powered thermochemical pilot plant was also planned, built, and tested by Villasmil et al.[205] They tested the solar reactor by exposing it to concentrated radiation fluxes of up to 4477 suns and a peak solar radiation power input of

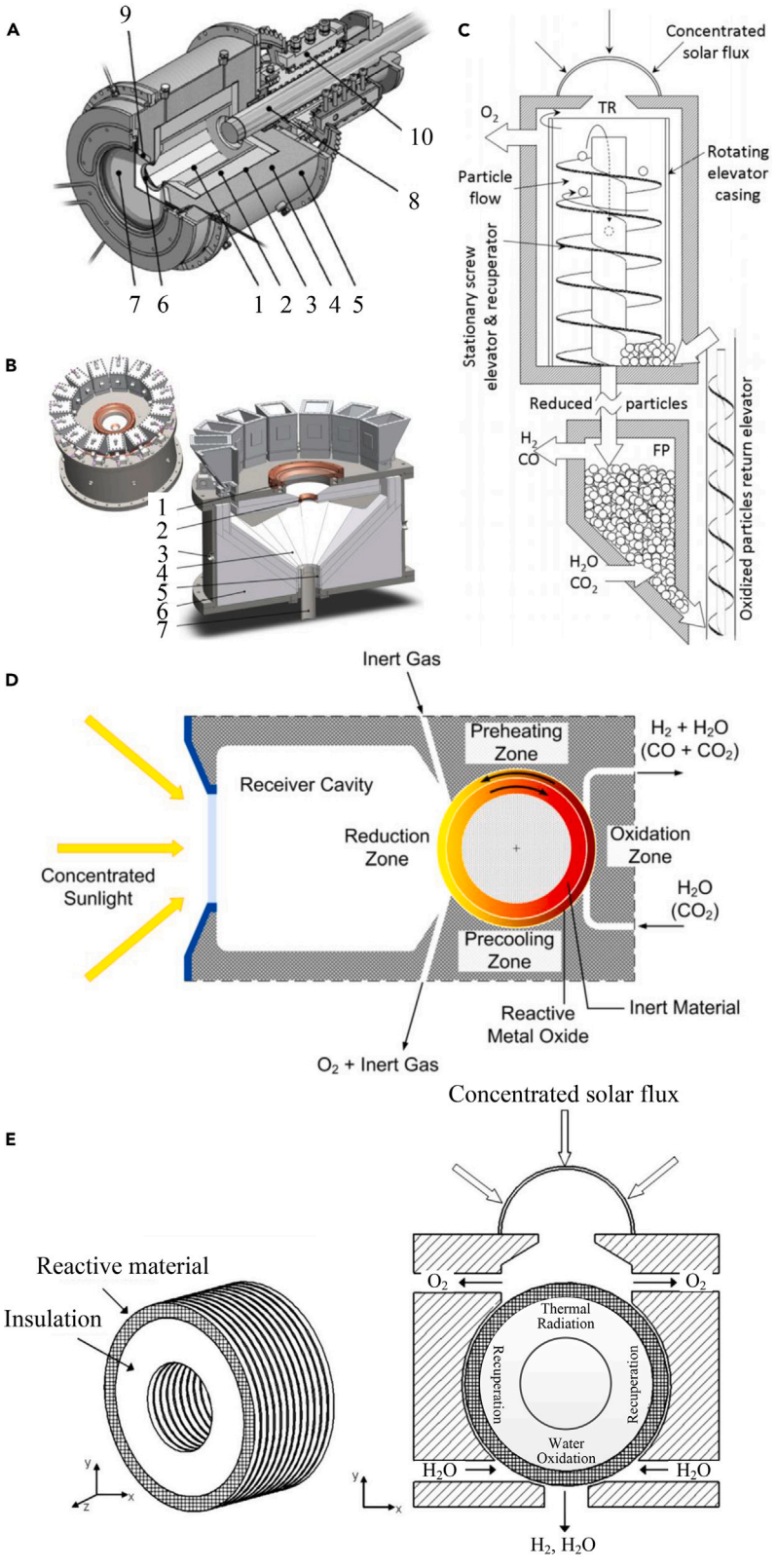
A
9
10
8
7 6
1 2 3 4 5
B
1
2
3
4
5
6
7
C
Concentrated solar flux
TR
O_2
Particle flow
Rotating elevator casing
Stationary screw elevator & recuperator
Reduced particles
H_2
CO
FP
H_2O
CO_2
Oxidized particles return elevator
D
Inert Gas
Preheating Zone
$H_2 + H_2O$
$(CO + CO_2)$
Receiver Cavity
Reduction Zone
Oxidation Zone
Concentrated Sunlight
H_2O
(CO_2)
Precooling Zone
Reactive Metal Oxide
Inert Material
O_2 + Inert Gas
E
Concentrated solar flux
Reactive material
Insulation
O_2
O_2
Thermal Radiation
Recuperation
Recuperation
Water Oxidation
H_2O
H_2O
H_2, H_2O

Figure 6. Schematic of thermochemical reactors

(A) Solar thermochemical reactor with a rotating cavity-receiver: 1-rotating cavity, 2-insulation, 3-ceramic matrix composite, 4-alumina fibers, 5-Al reactor shell, 6-aperture, 7-quartz window, 8-dynamic feeder, 9-conical frustum, and 10-rotary joint; Reproduced with permission.[199] Copyright 2009, Elsevier.

(B) Beam-down solar thermochemical reactor: 1-water-cooled window mount and vortex-flow generation, 2-water-cooled cavity aperture, 3-BOP and data-acquisition cavity access ports, 4-alumina-tile reaction surface, 5-annular solid ZnO exit, 6-bulk insulation and cavity-shape support, 7-central product-vapor and gas exit; Reproduced with permission.[200] Copyright 2012, Elsevier.

(C) Moving packed particle bed reactor; Reproduced with permission.[201] Copyright 2013, The American Society Mechanical Engineers.

(D) Solar thermochemical reactor realizing a nonstoichiometric partial redox cycle with solid-solid heat recuperation; Reproduced with permission.[202] Copyright 2013, The American Society Mechanical Engineers.

(E) Counter-rotating-ring receiver/reactor/recuperation (CR5). Reproduced with permission.[203] Copyright 2008, The American Society Mechanical Engineers.

140 kW_{th} at the PROMES-CNRS large-scale solar concentrating facility. The solar reactor operated at temperatures as high as 1936 K, producing a Zn molar fraction of 12–49% of the condensed products. This Zn molar fraction was largely determined by the flow rate of Ar that was injected into the reactor to cool the gaseous products that were forming. Chambon et al.[206] designed, constructed and operated a prototype high-temperature lab-scale solar reactor based on a rotating cavity-type solar radiation absorber made of standard refractory materials that allow continuous ZnO thermal dissociation in a controlled atmosphere at lower pressure. By increasing the rate of dissociation and operating at lower temperatures, lower pressures increase the overall dissociation yield by thermodynamic displacement toward the gaseous products. The reactant oxide powder is infused persistently inside the hole and the created Zn particles are recuperated in a downstream fired channel. With a neutral gas flow rate of 5 NL/min and a typical dilution ratio of 300, the filter produced a maximum yield of 21% for particle recovery and a dissociation yield of up to 87% (Zn weight content in the final powder). The gravity-fed, entrained-bed reactor proposed by Koepf et al.,[200] which is abbreviated as GRAFSTRR (Gravity-Fed Solar-Thermochemical Receiver/Reactor), is closed off from the outside and has a reaction surface in the shape of an inverted conical. Along this surface, reactant powder continuously descends as a moving bed, undergoing a thermochemical reaction at high temperatures when exposed to highly concentrated sunlight within the reaction cavity. Chambon et al.[207] investigated the high-temperature thermal dissociation reaction of ZnO and SnO_2 simultaneously. To ensure continuous reactant feeding, the reactor's design permits the movement of the reaction front. Thermal dissociation of ZnO and SnO_2 was carried out successfully at around 1900 K, resulting in the recovery of up to 50% of the products as nano powders with high specific surface areas (between 20 and 60 m^2/g) and mass fractions of reduced species of up to 48 wt. % for Zn and 72 wt. % for SnO. Perkins et al.[208] conducted an experimental investigation into how ZnO particles break apart at room temperature in aerosol flow, and used a cooling lance and quench tube to reduce product recombination and sharpen residence time determination. Chemical analysis revealed that the

Table 2. Comparison among different types of reactors for continuous utilization of thermal energy

Reactors	Solar irradiation types	Thermochemical process	Redox material and its shape	Power	Maximum temperature	Solar conversion efficiency	Reference
Stacked bed-rotary reactor	Directly	Dissociation of ZnO	ZnO particles	~10 kW	~2136 K	~3.1%	Schunk et al.[199]
Stacked bed-mobile bed	Directly	Dissociation of H_2O	ZnO powders	~10 kW	~1900 K	/	Koepf et al.[200]
Moving packed bed	Directly	Dissociation of H_2O or CO_2	CeO_2 particles	/	~1500°C	~30%	Ermanoski et al.[201]
Directly-irradiated reactor	Directly	Dissociation of H_2O or CO_2	Ceria porous medium	/	~2203 K	/	Lapp et al.[202]
CR5 reactor	Directly	Dissociation of H_2O	Ferrite fins	~36 kW	~2300 K	~29.9%	Diver et al.[203]
Solar chemical reactor	Directly	Dissociation of ZnO	ZnO particles	~10 kW	>2000 K	/	Haueter et al.[204]
Solar reactor	Directly	Dissociation of ZnO	ZnO particles	~100 kW	~1936 K	/	Villasmil et al.[205]
Rotary cavity-type reactor	Directly	Dissociation of H_2O	ZnO powders	~1.4 kW	~1600°C	/	Chambon et al.[206]
Moving-front reactor	Directly	Dissociation of H_2O	ZnO and SnO_2 powders	~1 kW	~1993 K	~2.9%	Chambon et al.[207]
Rapid reaction aerosol flow reactor	Indirectly	Dissociation of H_2O	ZnO particles	/	~2123 K	/	Perkins et al.[208]
Circulating fluidized bed	Directly	Dissociation of H_2O	$NiFe_2O_4$/m-ZrO_2 particles	2.6 kW	~1200°C	<1%	Gokon et al.[209]
Rotary-type reactor	Directly	Dissociation of H_2O	CeO_2 or Ni, Mn-ferrite ceramics	/	~1623 K	/	Kaneko et al.[210]

material in the gravity vessel lack significant reaction. Particles collected in the quench tube and filter were found to have undergone some recombination and conversion to Zn through physical and chemical analysis. After recombination, the net conversions had a maximum value of 18% and a mean value of 8%. The surface area of the product particles, which ranged from 5 to 70 nm, was anticipated to accelerate the Zn hydrolysis step of the cycle.

Moving packed bed reactors

Gokon et al.[209] demonstrated a single reactor of an internally circulating fluidized bed, with which thermochemical hydrogen production by a two-step reaction on a laboratory scale can be achieved. In the TR step, the internally circulating fluidized bed was subjected to simulated solar light from Xe lamps with input powers of 2.4-2.6 kW_{th} and 1.6-1.7 kW_{th}, respectively. The fed gas was changed from an inert gas (N_2) to a mixture of N_2 and steam in the splitting of H_2O step. As a fluidized bed of reacting particles, $NiFe_2O_4$/m-ZrO_2 and unsupported $NiFe_2O_4$ particles were evaluated, and the reactivity of reacting particles as well as the rate and productivity of hydrogen production were examined. The ferrite conversion was 35% and the hydrogen productivity was 951 Ncm^3 for the $NiFe_2O_4$/m-ZrO_2 particles. The hydrogen productivity of the unsupported $NiFe_2O_4$ particles was 1072 Ncm^3 while the ferrite conversion rate was 5%. Ermanski et al.[211] evaluated the effectiveness of a reactor that makes use of a moving packed bed of reactive particles and concluded that the packed bed reactor must possess the following characteristics to achieve high efficiency: the reactor's pressure and temperature, reaction products being separated spatially, sensible heat recovery throughout the process of reaction, continuous use of the irradiation, and the working material being directly illuminated. In addition, it was demonstrated that vacuum pumping outperformed inert gas sweeping in terms of efficiency owing to the pressure separation technique and the conversion efficiency of solar energy into H_2 and CO that could exceed 30% in a fully developed system employing CeO_2 as a reactive material. Effective heat recuperation is the central idea, with the packed bed of reduced particles supposed to move downward through a connecting tube in a counter-flow arrangement with the oxidized particles moving upward, essentially pre-heating them.

Rotary-type reactors

To decouple the reduction and oxidation processes in space and time for potential 24-h syngas generation, Kaneko et al.[212] used a special reactive ceramic to develop and fabricate the rotary-type reactor for the production of solar hydrogen through a two-step WS reaction. The dual-cell rotary-type reactor has two distinct types of reaction rooms: one for oxygen discharge and the other for splitting of H_2O. Its efficiency and detailed specifications were examined. In oxygen discharging and H_2O-splitting reaction cells, oxygen and hydrogen underwent successive evolutions, respectively. With Ni and Mn-ferrite, the optimal reaction temperatures for the reactions were 1173 K and 1473 K, respectively. The same research group further[210] used the rotary solar reactor with CeO_2 and found that the optimal reaction temperatures of the O_2-releasing and H_2O-splitting were 1623 K and 1273 K, respectively. It was demonstrated that the approximately 10-fold scaled-up rotary-type reactor was able to achieve a higher O_2-releasing reaction temperature of over 1800 K. Lapp et al.[202] predicted heat transfer for a rotary-type reactor that uses direct radiation to create a metal oxide-based nonstoichiometric redox cycle for making synthesis gas from CO_2 and H_2O. In this reactor, the reactive porous medium forms the outer cylinder, which alternates between the high-temperature reduction zone and the low-temperature oxidation zone. Chemically inert and heat-recovering solid makes up the inner cylinder. This system therefore can transfer heat from a porous reactive material's rotating hollow cylinder to an inert solid cylinder in form of radiation. A parametric study of the geometric and material parameters resulted in a heat recovery efficiency of more than 50%.

The CR5 reactor

The CR5 reactor has the most distinctive feature of a stack of counter-rotating rings or disks that are surrounded by fins made of a redox metal oxide. The reactive material moves back and forth between a relatively low-temperature hydrolysis reactor where the reactant material undergoes a H_2O-splitting reaction and a solar-irradiated high-temperature TR as the rings rotate. After rotating, each ring rotates in the opposite direction of its neighbor. The oxidized redox material in the fins meets hotter fins leaving the TR reactor on both sides as it enters the recuperator from the H_2O-splitting reactor. As the adjacent fins moving in the opposite direction cool, it heats up in the recuperator. Diver et al.[213] first invented the CR5 two-step solar-driven thermochemical heat engines based on working materials made of iron oxide and iron oxide mixed with other metal oxides (ferrites). A major obstacle to achieving highly efficient thermal recuperation between solids in effective counter-current arrangements was overcome by employing two sets of moving beds that are adjacent to one another but moving in opposite directions. They also naturally separated the product of hydrogen and oxygen. The core of the CR5 system is a set of annular rings made of reactive solid ferrite. These rings are cycled chemically and thermally to produce O_2 and H_2 from H_2O in separate steps. From a material standpoint, this design is extremely demanding. After months of thermal cycling and exposure to temperatures greater than 1100°C, the ferrite rings must maintain their high reactivity and structural integrity. In addition, the rings must have a large geometric surface area to adsorb incident solar radiation and make contact with the solids.

As successful application of ceria-based materials in thermochemical redox cycle, Diver et al.[178] further designed and built a CR5 thermochemical heat engine prototype made of ceria, and tested its redox cycle performance in the 16 kWt National Solar Thermal Test Facility (NSTTF) solar furnace in Albuquerque, NM. The initial tests indicated the CR5 was promising thermochemical heat engine concept for fuel production and would achieve ultimate goal of 20% efficiency in the future. Miller et al.[214–216] carried out a series of initial screenings, selected $Co_{0.67}Fe_{2.33}O_4$ as the starting point for demonstration of the CR5 and further characterized and developed this material. Robocasting was used to produce monolithic structures with intricate three-dimensional geometries for chemical, physical, and mechanical evaluation concurrently with the powder studies. Ferrite/zirconia mixtures can be made into small, 3D and monolithic lattice structures that gave

Table 3. Comparison among different types of reactors for intermittent utilization of thermal energy

Reactors	Solar irradiation types	Thermochemical process	Redox material and its shape	Power	Maximum temperature	Solar conversion efficiency	Reference
Packed bed reactor	Directly	Dissociation of H_2O	$Ni_{0.5}Mn_{0.5}Fe_2O_4$ powder	~15 kW	~1373 K	/	Tamaura et al.[218]
Internally circulating fluidized bed	Directly	Dissociation of H_2O	$NiFe_2O_4$/m-ZrO_2 particles	~1.2 kW	/	<1%	Gokon et al.[219]
Internally circulating fluidized bed	Directly	Dissociation of H_2O	$NiFe_2O_4$/m-ZrO_2 particles	~1 kW	~1500°C	/	Gokon et al.[220]
Windowed solar chemical reactor	Directly	/	Coal coke particles	~0.94 kW	~850°C	12%	Kodama et al.[221]
Stacked bed-Fixed bed	Directly	Dissociation of H_2O	Ferrite-coated monoliths	~100 kW	~1473 K	/	Roeb et al.[222]
Solar receiver-reactors	Directly	Dissociation of H_2O	Iron-oxides coated on ceramic substrate	~100 kW	1200°C	/	Neises et al.[223]
Monolithic reactor	Directly	Dissociation of H_2O	Ferrites ceramic honeycombs	/	1300°C	/	Agrafiotis et al.[224]
Monolithic reactor	Directly	Dissociation of H_2O	Monolith coated with $Zn_xFe_{1-x}O$	/	/	/	Roeb et al.[225]
Honeycomb reactor	Directly	Dissociation of CO_2	Zirconia and iron oxide ceramic honeycombs	/	1200°C	/	Walker et al.[226]
Solar cavity reactor	Directly	Dissociation of H_2O	/	~1 MW	1020°C	/	Houaijia et al.[227]
Foam reactor	Directly	Dissociation of H_2O	Fe_3O_4 or $NiFe_2O_4$ reticulated ceramic foam	~0.7 kW	1773 K	/	Gokon et al.[228]
Quartz reactor	Directly	Dissociation of H_2O	Fe3O4/c-YSZ particles	7 kW	1450°C	/	Gokon et al.[100]
Foam reactor	Directly	Dissociation of H_2O	$NiFe_2O_4$/m-ZrO_2 or Fe_3O_4/m-ZrO_2 powders	7 kW	1450°C	/	Gokon et al.[22]

consistent hydrogen yields over multiple cycles. Kim et al.[217] presented a comparison of the environmental effects of gasoline derived from petroleum and sunshine to petrol (S2P) using a life cycle assessment (LCA) method. According to the findings, S2P gasoline scored lower than conventional gasoline in all of the impact categories. The environmental benefits, such as the reduction of greenhouse gases and the reduction of external costs, were then examined in light of the findings of the LCA. Based on the current fleet of vehicles, it was determined that 3.6 Mt CO_2-eq of greenhouse gas emissions (77% of the total regional emissions) would be mitigated if S2P gasoline could be successfully introduced to satisfy the gasoline demand. In addition, the reduced impact results in annual cost savings of 4.2 million dollars due to avoided environmental damage.

Intermittent utilization of thermal energy

In contrast to the continuous utilization of thermal energy, another strategy where the thermal energy is being used intermittently has also been studied worldwide. The intermittent utilization of thermal energy enables the reduction and oxidation steps to happen separately or within the same system. The major types of such reactor structures include packed bed reactors, spouted bed reactors, honeycomb reactors and foam reactors. Their partial representatives are summarized in Table 3. The details are discussed in the following sections.

Packed bed reactors

In 1995, Steinfeld et al. reported their work on utilizing a packed bed solar reactor for the two-step water splitting cycle.[218] The design of the reactor is as shown in Figure 7, which is composed of a 2 cm-diameter quartz tube containing a packed-bed of powder reactants. The reactants were made of $Ni_{0.5}Mn_{0.5}Fe_2O_4$ powder mixed with Al_2O_3 grains for avoiding sintering. During its operation, the reactor was first heated to about 1373 K by directly exposing it to the solar flux for releasing the oxygen from the ferrite lattice with the carrying gas of a flow of 0.3 L min^{-1} Ar passing through the sample. Thereafter, the reactor would be cooled down to 573 K while 0.04 L min^{-1} steam carried by 0.8 L min^{-1} Ar passing through the sample for 5 min. By further raising the reactor temperature to 773 K, 823 K, and 873 K, the oxidation process would take place and H_2 would be produced. Such a novel design thus eliminated the need for high-temperature gas separation while proving the capability of this designed system for reduction and oxidation reactions in the same structure.

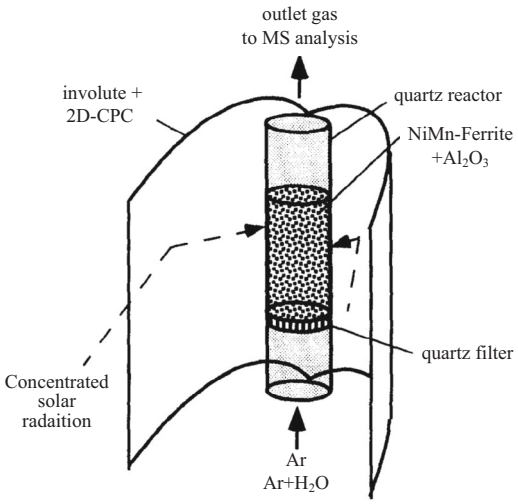

Figure 7. Design of packed bed reactor
Reproduced with permission.[218] Copyright 1995, Elsevier.

Spouted bed reactors

Apart from the packed-bed reactors, a series of works have been conducted by Goken et al. from the Niigata University for examining the spouted bed solar reactor design.[209,219–221,229] Through combining the windowed fluidized bed reactor with beam-down type solar concentrator, as shown in Figure 8, the two-step WS cycle has been successfully demonstrated.[219] In this system, the fluidized bed reactor is composed of a stainless-steel cylindrical reactor body, a transparent quartz window and a draft tube at the center region. During its operation, the solar-heated particles will be transported upward in the draft tube and move downward in the annulus region, through which the solar energy can be transferred from top to bottom and thus create a more uniform temperature distribution. It is reported that, with this design, during the reduction step, an operating temperature of 1500–1600°C can be reached in the draft region, while a temperature of 1100–1250°C can be attained in the annulus region. Using this reactor, the *m*-ZrO_2-supported $NiFe_2O_4$ and unsupported $NiFe_2O_4$ particles were tested, both of which did not sinter nor coagulate during the whole test verifying the feasibility of this reactor design for successive reduction and oxidation reactions. Furthermore, it is also found that, with the $NiFe_2O_4$/m-ZrO_2 particles, this reactor design is able to achieve a hydrogen

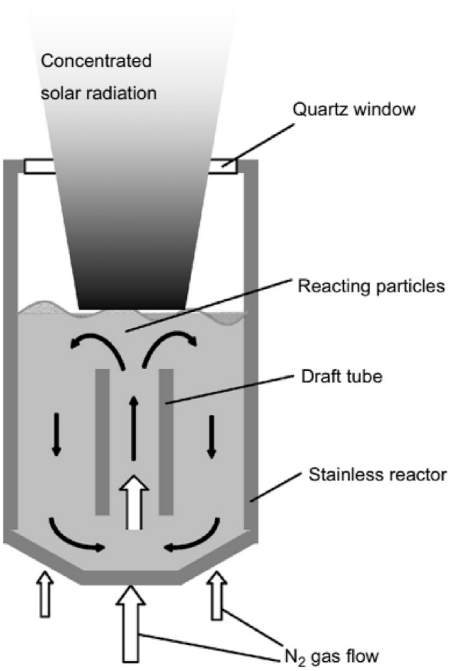

Figure 8. Design of fluidized bed reactor
Reproduced with permission.[219] Copyright 2008, Elsevier.

Figure 9. Design of honeycomb solar reactor

(A) Prototype of honeycomb solar reactor.

(B) Extruded re-crystallized silicon carbide honeycombs (carriers) and cast parts (housing vessel).

Reproduced with permission.[224] Copyright 2005, Elsevier.

productivity of 951 N cm^3 with the ferrite conversion of 3% demonstrating the superiority of this reactor design for efficient solar hydrogen production.

Honeycomb reactors

In addition to the aforementioned solar reactor structures, another type of reactor design adopting the ceramic honeycombs has recently attracted much attentions and been studied worldwide.[95,203,222,223,230–235] In comparison to the packed bed and spouted bed reactors, the honeycomb reactors have the following three major advantages.[234] First, attributed to the thin walls of the honeycomb structure, a low resistance to the reactants/flushing gas flow can be achieved, which thus can offer low pressure drop and fast mass transport. Second, the honeycomb structure can provide large geometric surface area, and hence allow good gas-solid contact to attain high efficiency. Third, such a structure can secure good mechanical stability at a light weight, thereby bearing the high operating temperature required during reduction and oxidation steps.

One good example of utilizing the honeycomb structure for solar reactor is demonstrated by Agrafiotis et al. in 2005.[224] Adopting the multi-channeled honeycomb ceramic supports coated with active redox reagent powders, a solar reactor for splitting of H_2O and H_2 production is fabricated as shown in Figure 9A. The multi-channeled honeycomb ceramic made of re-crystallized silicon carbide is fabricated to serve as the catalyst carrier (Figure 9B), while the iron-oxide-based redox material was synthesized for the reduction-oxidation cycle. During operation, the operating temperature of the solar reactor will swing between 800°C and 1300°C for H_2 production and O_2 regeneration, respectively. Optimizing the operating condition of this system showed that the entire honeycomb embedded inside the solar reactor could achieve a uniform temperature up to 1300°C proving its capability for the reduction and oxidation reactions within the same structure. The system operation is then studied as shown in Figure 10. It is found that a weight loss of 0.68% can be achieved during the heating process under argon flush, while the same weight was recovered when O_2 mixture was fed, proving the capability of this system for stable H_2 production, though intermittent due to the need of changing operating temperature during its operation. In an attempt to achieve the continuous production of hydrogen, the same group[225] thereafter designed and fabricated a reactor with dual chambers (Figure 11A). Such a design allows the concentrated solar radiation to heat these two reactor chambers independently (Figure 11B),[222] so that when one reactor chamber is being heated to split water, the other one can be cooled down to regenerate the O_2 and wait for the next cycle. Through such process as shown in Figure 11B, a quasi-continuous utilization of solar energy can therefore be attained. Due to the modularity of this developed system and in order to verify the ability of this system for scale up, a model has also been constructed for simulating the transient thermal and chemical behaviors inside the reactor while the design of a 100 kW system has been completed and the pilot plant has been installed and tested for demonstration.[92]

Other than coating the redox reagents onto a honeycomb structure supports, another effective method is to synthesis the reactive material into the honeycomb structure directly. With this thought, Luke et al. manufactured the ceramic honeycombs based on the composites of zirconia and iron oxide for splitting of CO_2.[226] During the system operation, it is found that the melting of FeO within the system allows the full reduction of the substrate system in a very short time (<60 min), which thus present this material as a promising candidate for splitting of CO_2. Furthermore, the honeycomb structure is also demonstrated to sustain 6-10 cycles with good structure stability.

In addition to the fabrication of the honeycomb structure shape reactors, the design of the absorber is also of vital importance to the system performance and has been studied and modified by Houaijia et al.[227] As the key to decrease exergy destruction lies on the realization of smaller radiation losses, the screening process was first conducted on analyzing the possible absorber shapes so that a better thermal performance can be achieved. It is found that in comparison to the flat shape and conical shape absorbers, the spherical shape absorber is able to provide a better performance, while the best performance is attained for the absorber of hemispherical shape, making it a promising candidate for real applications. Based on these findings, a solar reactor has been designed as shown in Figure 12, which is demonstrated to provide a more homogeneous distribution of solar flux and thereby a more even distribution of temperature than the flat

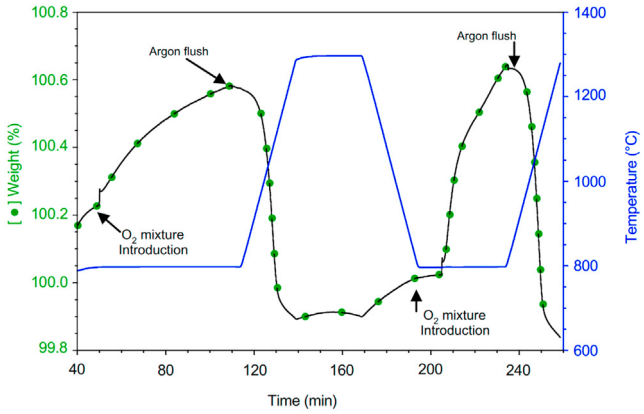

Figure 10. Weight loss and temperature curves obtained during TGA study of a sintered SSS MnZn ferrite
Reproduced with permission.[224] Copyright 2005, Elsevier.

shape absorber. Furthermore, the adoption of such design is analyzed and found to be capable of achieving an increase of thermal reactor efficiency above 25%.

Foam reactors

The adoption of the foam structured reactors for splitting of H_2O and CO_2 was not started until most recently. The first work utilizing the foam-based structure for WS is reported by Gokon et al.[22] The reactive materials made of monoclinic ZrO_2 supported $NiFe_2O_4$ and Fe_3O_4 were first examined for the H_2 production, where a higher O_2 and H_2 production rates was achieved by the $NiFe_2O_4$. Therefore, utilizing the $NiFe_2O_4$/m-ZrO_2/MPSZ foam device (Figure 13A), the experimental set-up for the reduction and oxidation reactions is then developed as shown in Figures 13C and 13D, respectively. Utilizing this system, the H_2O splitting reaction can successfully last for 10 cycles while the foam device is found to be slightly damaged (Figure 13B) in the fringe. Thereafter, another work utilizing the zirconia supported $NiFe_2O_4$ as reactive material was synthesized through the spin-coating method.[228] In contrast to the previous work, this spin coated $NiFe_2O_4$/m-ZrO_2/MPSZ foam device is demonstrated to achieve an improved performance with a H_2 production rate of 1.1–4.6 cm^3 per gram of device through 20 cycles with a maximum ferrite conversion of 60%. It is also reported that, utilizing this material, a solar reactor incorporated with a 5 kWt dish

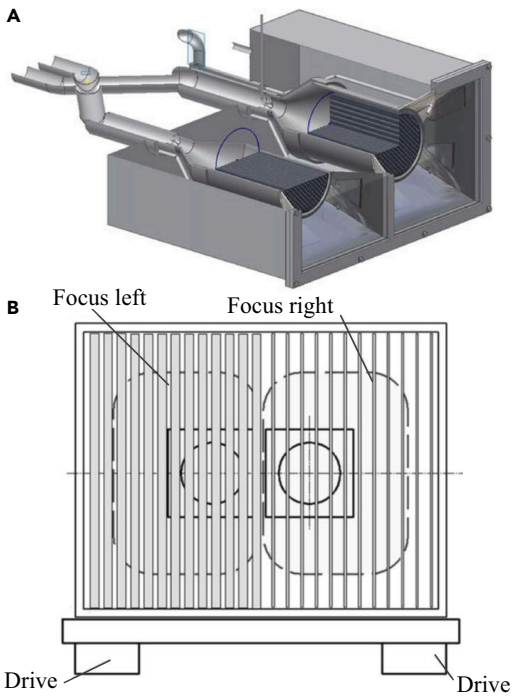

Figure 11. Design of two-chamber solar reactor
(A) Vertical-horizontal cut of two-chamber reactor.
(B) Schematic view of the lamellae shutter.
Reproduced with permission.[222] Copyright 2009, Elsevier.

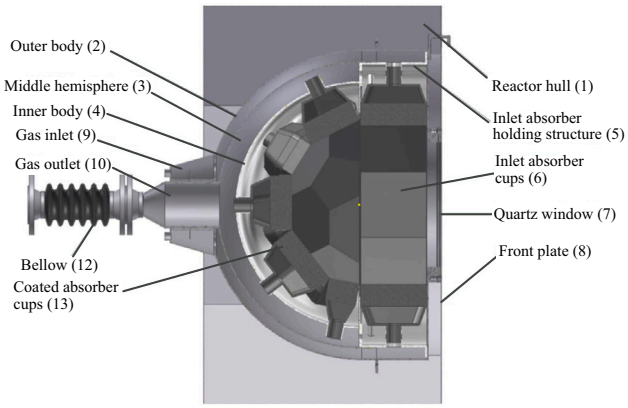

Figure 12. Design of the honeycomb solar reactor with a spherical shape absorber
Reproduced with permission.[227] Copyright 2013, Elsevier.

concentrator is now also under development for demonstration. While the previous work found the Fe_3O_4 to be relatively poorer in comparison to the $NiFe_2O_4$ when supported by the zirconia, another trial of using the Fe_3O_4 supported on cubic yttria-stabilized zirconia (Fe_3O_4/c-YSZ) stated otherwise.[100] The Fe_3O_4/YSZ powder was first examined for the H_2 and O_2 production and then coated on a ceramic foam device similar as the previous work. When applied in the foam device, it is found that, the Fe_3O_4/YSZ/MPSZ is able to achieve an operation of 32 cycles before any crack and broken are identified. Such a superior performance thus indicates the good stability of this material, though the structure integrity of the reactive material become more and more important as the cycle number increases.

Other than the aforementioned materials, using cerium oxide, Chueh et al.[7] reported a solar reactor achieving a stable and rapid fuel generation for 500 cycles. The structure of the solar reactor is shown in Figure 14A, inside which a porous ceria tube is embedded for H_2 and CO production. During its operation for the uninterrupted 500 cycles (Figure 14B), an initial stabilization period of 100 cycles is presented, where the oxygen and hydrogen evolution rates was found to decrease. However, in the following 400 cycles, a stable production rates of hydrogen and oxygen is achieved, indicating the superior stability of this system. Later, employing the ceria felt, another work has been conducted for the syngas production from H_2O and CO_2.[236] The study reported that over 8 h of operation and ten consecutive H_2O/CO_2 gas splitting cycles

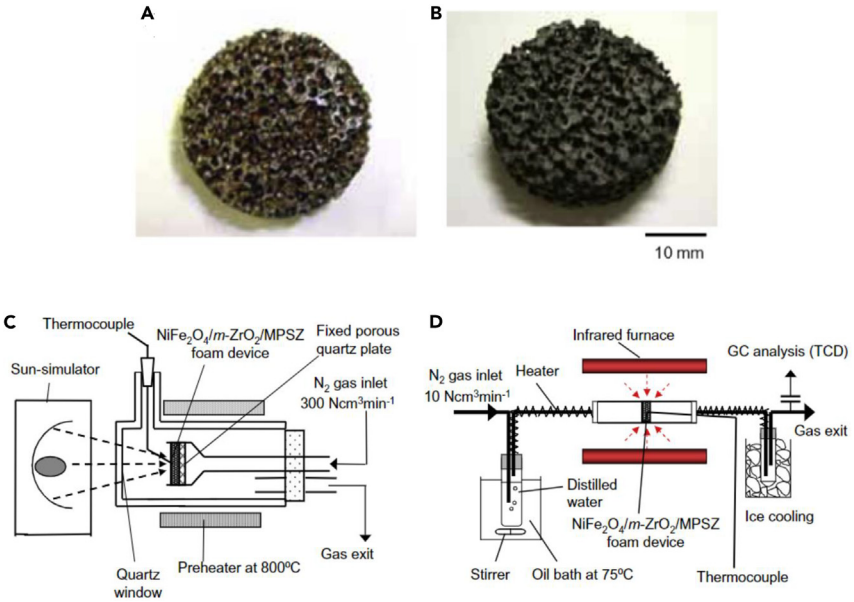

Figure 13. $NiFe_2O_4$/m-ZrO_2/MPSZ foam device and experimental setups
(A) $NiFe_2O_4$/m-ZrO_2/MPSZ foam before testing.
(B) $NiFe_2O_4$/m-ZrO_2/MPSZ foam after 10 cycles of repetition test.
(C) Experimental setup for thermal-reduction step.
(D) Experimental setup for water-decomposition step.
Reproduced with permission.[22] Copyright 2009, Elsevier.

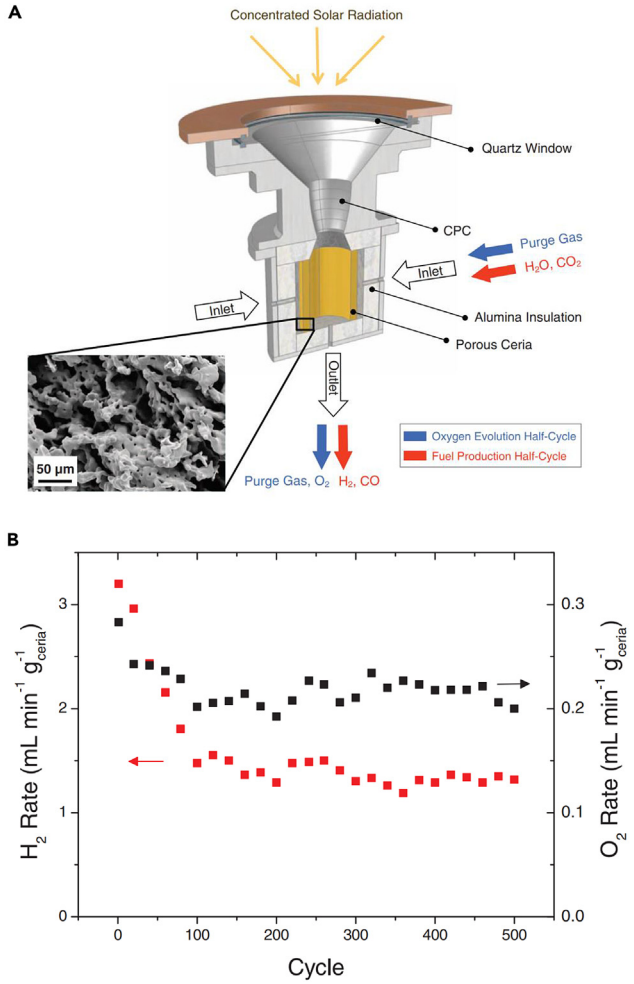

Figure 14. Design of foam-based solar reactor for thermochemical fuels production

(A) Structure and composition of reactor.

(B) Performance of reactor: H_2 and O_2 evolution rates for 500 water-splitting cycles.

Reproduced with permission.[7] Copyright 2010, The American Association for the Advancement of Science.

have been performed while a stable syngas production has been demonstrated. These works therefore proved the ceria-based materials as a promising candidate for application in solar reactors with superior performance.

Other new reactor concepts for converting solar energy to chemical energy

For the conventional solar thermochemical reactors, the reduction step usually requires a very high temperature and a very low oxygen partial pressure to increase the reduction extent which is significant for syngas yield. However, high temperature and low oxygen partial pressure environment means a serious heat loss, which can be considered as a limiting factor for the practical implementation. To reduce the demanding heat requirement, reducing the reduction temperature is necessary. Meanwhile, to ensure the reduction extent, what can be done is to obtain a low oxygen partial pressure with less or no additional energy requirement. Following this, some new reactor design concepts have been developed in recent years.

Reactor integrated with thermochemical oxygen pump

To obtain a low oxygen partial pressure, some methods, such as vacuum pumping and inert gas sweeping, have been proposed. However, both methods require additional electric energy, which would limit solar-to-fuel efficiency. Brendelberger et al.[237] therefore proposed a novel design idea that adopt thermochemical oxygen pump instead of conventional mechanical pump to maintain low partial pressure of oxygen with a lower energy input. As shown in Figure 15, there are two horizontal tube furnaces (i.e., splitting furnace and pumping furnace) in the test rig, and redox materials (ceria and $SrFeO_3$) are placed in the tubes in ceramic crucibles. When the reduction reaction takes place in the splitting furnace, the oxidation reaction starts in the pumping furnace. The O_2 released from ceria during reduction step would be absorbed by the

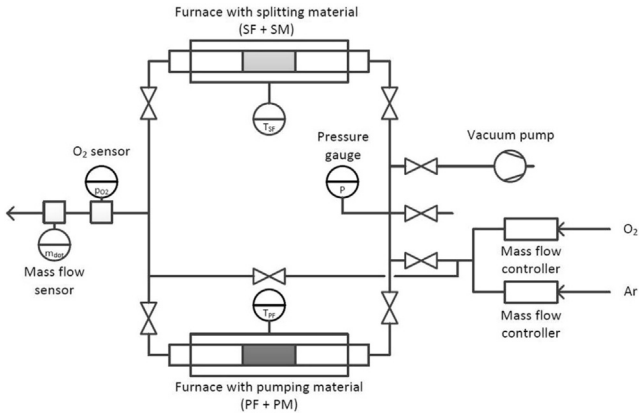

Figure 15. The test rig of reactor integrated with thermochemical oxygen pump
Reproduced with permission.[237] Copyright 2018, Elsevier.

$SrFeO_3$ that is undergoing oxidation reaction. The O_2 released can then be moved out of the splitting furnace in time, which can maintain a lower oxygen partial pressure and enhance reduction extent. Comparison experiments demonstrated that application of thermochemical oxygen pump can make the reduction extent of ceria increase from 0.005 to 0.0108; if the doubled amount of $SrFeO_3$ was used, the reduction extent can further increase to 0.0145; if the oxidation temperature of $SrFeO_3$ is reduced, the reduction extent can finally increase to 0.0181. In other words, the largest increase of reduction extent measured can reach 265% which successfully prove the advantage of such reactor design. Meanwhile, such technology has the potential advantage of low energy consumption, which is limited to some extent by the kinetics of the oxidation reaction. The authors also pointed out that their subsequent study will focus on the application of such thermochemical oxygen pump in solar thermochemical reactor in a real case scenario.

Reactor integrated with electrochemical oxygen pump

Similar with the last reactor design, Bai et al.[238] designed a novel solar thermochemical reactor integrated with electrochemical oxygen pump (EOP) which is employed for *in situ* oxygen removal with a low heating load. The design idea is shown in Figure 16. The majority of solar energy (98%) is used to heat the reticulated porous ceramic ceria (redox material), and the other (2%) is employed to generate electricity which provides energy required for EOP. The cathode of EOP is placed adjacent to the ceria and the anode is facing the inner channel exposed to the ambient. When the ceria is heated to reduction temperature by the concentrated solar energy, the thermochemical reduction of ceria occurs and O_2 is released from ceria. The O_2 moves to the cathode of EOP and electrochemical reduction converts O_2 into O^{2-}. The generated O^{2-} thereafter moves to the anode by diffusing through the electrolyte and re-converts into O_2 by electrochemical oxidation. Finally, the O_2 is moved out from

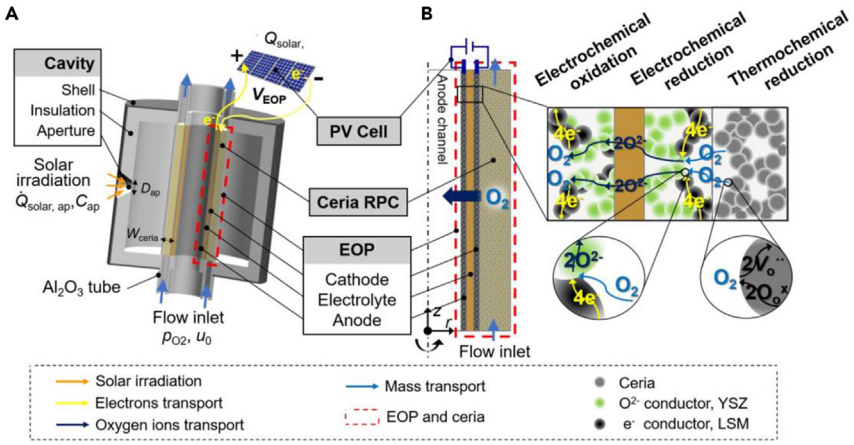

Figure 16. Schematic of solar thermochemical reactor integrated with EOP
(A) Structure and composition of reactor.
(B) Multiphysical model of EOP.
Reproduced with permission.[238] Copyright 2022, American Chemical Society.

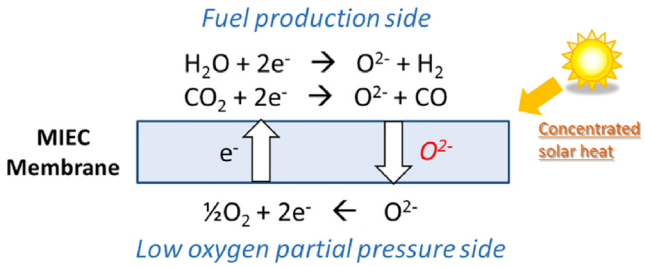

Figure 17. Membrane reactor concept: oxygen ions and electrons transport across the MIEC membrane
Reproduced with permission.[129] Copyright 2021, Elsevier.

thermochemical reduction zone and escapes into the ambient. Consequently, the application of EOP can maintain a low oxygen partial pressure and enhance the reduction extent of ceria. The authors numerically resolved the coupled physical process including the multimode heat transfer and the mass transfer, as well as electrochemical and thermochemical reactions to quantify the reactor performance. The calculation results indicated that the reduction extent increased by 56.8% compared to the nitrogen sweeping scheme. In addition, the EOP scheme can obtain more uniform temperature and species concentration distributions, which is beneficial for thermo-mechanical stability.

Reactor integrated with reactant membrane

Alternatively, a novel solar reactor integrated with reactant membrane is developed to implement thermochemical splitting of H_2O and CO_2 driven by concentrated solar energy.[129,239–241] Operation principle of the reactant membrane reactor is shown in Figure 17, the reduction zone and oxidation zone is separated by a dense mixed-ion-electron-conducting (MIEC) membrane. The oxidation reaction occurs at the fuel production side accompanied with production of H_2(CO) and O^{2-}, while reduction reaction occurs at the low oxygen partial pressure side to generate O_2. The key is that MIEC membrane can transport the charge carriers (oxygen, vacancies, and electrons) through the bulk via a thermally activated process. Thus, such membrane reactor has two advantages: (1) the reduction and oxidation reactions (production of O_2 and H_2/CO) can be carried out simultaneously at the same temperature in two distinct compartments and (2) an external electrical supply for electronic transfer can be avoided to reduce energy required for redox cycle.

Based on the above idea, Abanades et al.[129] presented a novel solar ceria membrane reactor as shown in Figure 18. The high temperature isothermal continuous splitting of CO_2 is carried out in such membrane reactor with two separate compartments. In other words, the high

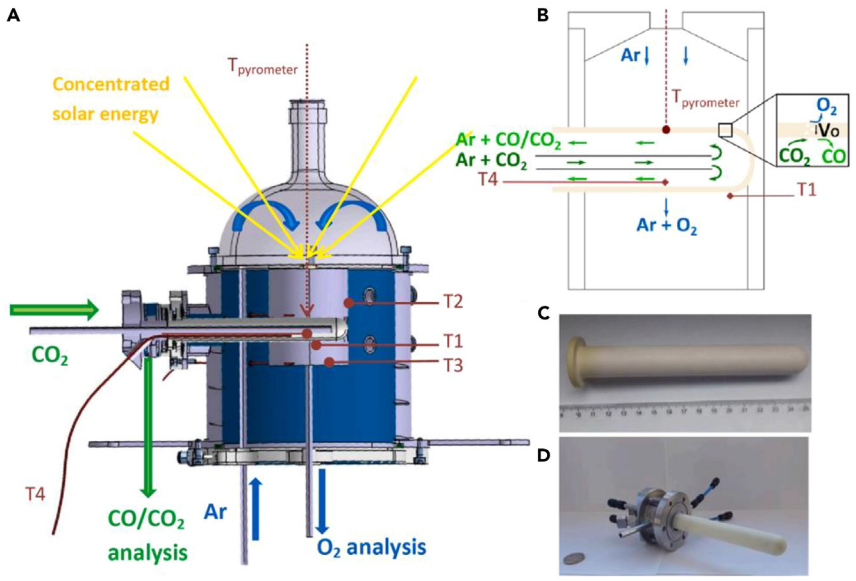

Figure 18. Design of solar membrane reactor for thermochemical splitting of CO_2
(A) Structure of the solar membrane reactor.
(B) Principle of *in-situ* separation of CO and O_2 across ceria redox tubular membrane.
(C) A tubular ceria membrane.
(D) A membrane fixed on the water-cooled support.
Reproduced with permission.[129] Copyright 2021, Elsevier.

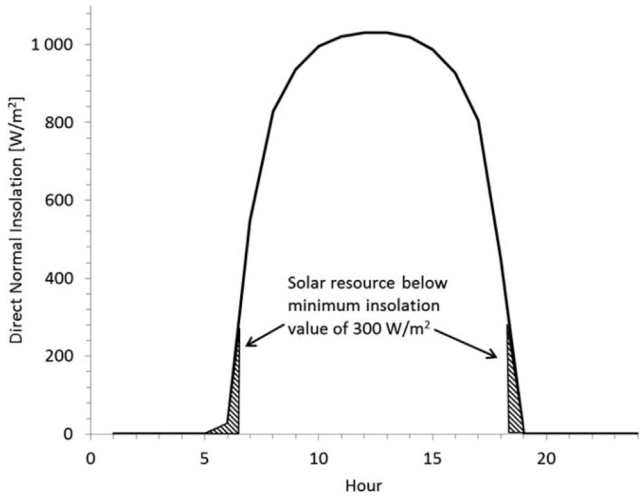

Figure 19. The DNI in Daggett, CA, on March 20th based on hourly TMY2 data
Reproduced with permission.[242] Copyright 2013, American Chemical Society.

temperature reduction and CO_2-splitting reactions can be simultaneously operated at both sides of the membrane. With the aid of concentrated solar energy, the required temperature can be achieved and the thermally favored reduction reaction of the MIEC oxide material occurs at the outer side of the membrane. The inert gas is supplied to sweep reduction side to control the oxygen partial pressure in the cavity. Meanwhile, CO_2 enters the inner side of the membrane and backflows in the annular space to achieve a suitable solid/gas contact with the membrane surface. In such process, CO and O_2 are generated at the inner and outer sides of the membrane, respectively. A stable and unprecedented CO production rate up to 0.071 μmol/cm^2/s at 1550°C and CO/O_2 ratio of 2 is observed in the experimental measurement, which proved remarkable thermochemical CO_2 splitting performance of such membrane reactor design. The authors pointed out that the analogous direct H_2O splitting can be carried out in the same reactor to produce H_2/O_2. In addition, the author also thought that other MIEC materials, such as perovskites, may further lower temperature required for reaction to decrease thermal press imposed to the membrane. Meanwhile, it can be also noted that excessive reactant gas is required in this reactor to increase fuel yield, which means a very low conversion rate of H_2O/CO_2 into H_2/CO and a more high-energy consumption. Therefore, enhancing conversion rate of reactant gas needs to be further studied in the future.

LIMITING FACTORS AND HEAT RECOVERY CONCEPTS FOR SOLAR CONVERSION EFFICIENCY

Limiting factors

The entire production chain from H_2O and CO_2 into sustainable fuels based on thermochemical redox cycle driven by concentrated solar energy demonstrates the completed physical and chemical process of converting solar energy to chemical energy stored in liquid hydrocarbon fuels. Solar energy is tracked, concentrated, and delivered into the receiver-reactor through aperture, in which solar energy is converted into thermal energy. Thermal energy is thereafter converted into chemical energy via thermochemical redox cycle and fuel synthesis processes. Thus, energy losses occur during the delivery and conversion process of solar energy, which limits the solar-to-fuel conversion efficiency. According to the production chain described in System and key devices, the energy losses includes: (1) solar energy loss which is associated with available solar radiation collection process from incident onto reflectors (parabolic dish or heliostats) to entering receiver-reactor; (2) thermal energy loss which exists in the heat transfer and thermochemical reaction process in the solar receiver-reactor; and (3) energy loss determined by the existing level of sustainable fuels synthesis technologies from syngas to liquid hydrocarbon fuels (such as FT technology). The three parts mainly determine the solar-to-fuel conversion efficiency which can be employed to evaluate whether such technology has compelling advantages over existing or competing liquid hydrocarbon fuels synthesis technologies.

Solar energy loss is also called optical loss occurring along its delivery path. It is noted that not all solar energy is effective. Siegel et al.[242] proposed available solar radiation concept and suggested that available solar radiation must exceed a minimum value of direct normal insolation (DNI) to provide heat for thermochemical reaction. This is because a partial additional energy is needed to offset thermal losses and parasitic loads within the system. In their research, a conservative value of 300 W/m^2 was adopted and the variation of DNI at Daggett on the Spring Equinox (March 20th) is presented in Figure 19 from which it can be seen that the DNI during most daytime can meet the minimum insolation value except for in the early morning, late afternoon, and during periods of extensive cloud cover. Except for unavailable solar radiation loss, another optical loss can be summarized as equipment loss and operating loss. Equipment loss is defined as optical loss due to structure and characteristics of equipment itself. Real solar concentrators are not ideal models, and their own structure will also cause optical losses, such as blocking of components, incomplete reflect of primary reflector and secondary reflector (if needed), long term dirt accumulation on reflect mirrors, and reflection of aperture mounted on the solar receiver. Operating loss are the optical loss during the operating

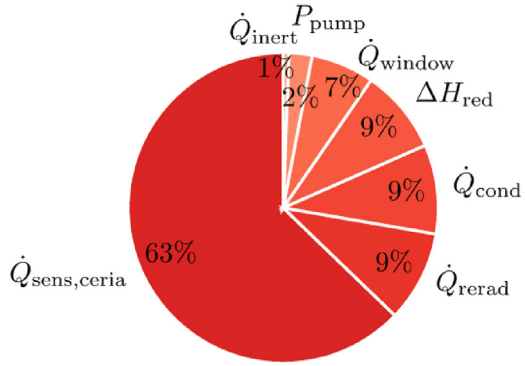

Figure 20. A typical distribution of thermal energy in one thermochemical system
Reproduced with permission.[243] Copyright 2019, The American Society Mechanical Engineers.

process. Solar concentrators collecting and delivering the available solar radiation into receiver-reactor cannot work all the time, because they need regular outages for maintenance. For example, for parabolic dish concentrator, it is only on operation for 97% of the time, based on the experience of Sandia National Laboratories.[242] In addition, inaccurate tracking of sunlight can also result in spillage of useful energy, which is inevitable in operation of solar concentrators. These optical losses in the delivery of solar energy can account for nearly 20% of total solar energy incident onto solar concentrators.[242]

Thermal energy loss mainly occurs at thermochemical reactor where two-step thermochemical redox reaction cycles for splitting of H_2O or/and CO_2 take place after absorbing concentrated solar energy. Taking a 4 kW ceria-based solar reactor as example, under a solar flux irradiation with a 3000 concentration ratio, the energy distribution in the thermochemical system[243] is presented in Figure 20. It can be seen that the sensible heat of redox material accounts for over 60% of the total energy in the reactor. This is because endothermic reduction reaction requires a very high temperature to drive redox material to release O_2, while exothermic oxidation reaction is carried out at a lower temperature without external energy input. Large temperature difference (usually over several hundred degrees) would cause great sensible heat loss which includes solid phase sensible heat of redox materials and gas phase sensible heat of products syngas and oxygen (or mixed with inert gas). Sensible heat is unavoidable due to the characteristic of two-step thermochemical redox reaction. Re-radiation loss refers to the high temperature within the reactor. It is well known that radiation is proportional to the fourth power of temperature according to the Stephen-Boltzmann law. An amount part of energy, in form of radiation, therefore escapes from the reactor through aperture which is designed to receive concentrated solar energy. In addition, an amount of energy, in form of conduction and convection, leaves the reactor to the surroundings through insulation layer and steel layer, or quartz window on the aperture. If the insulation of the reactor is not good or the aperture is not designed reasonably, energy loss caused by heat transfer (radiation, conduction, and convection) would be larger. It can be also noted that only a small percentage of solar energy (9% as shown in Figure 20) is converted into chemical energy, which thus explains why the solar-to-syngas conversion efficiency is so low in reported experimental testing data. To make the two-step thermochemical redox reaction operate more efficiently, some additional work needs to be included (such as pump) to enhance thermochemical reaction kinetics. This additional energy input should be also considered in the solar-to-syngas conversion efficiency.

Except for heat loss caused by temperature-swing, re-radiation and imperfect insulation, the deoxygenation energy consumption in the reduction step is also not ignored. The oxygen partial pressure in the reduction step has a significant effect on the reduction degree of ceria in two-temperature or isothermal thermochemical cycling, namely, can directly affect the cycle efficiency. To obtain a low oxygen partial pressure environment in the reduction step of the thermochemical cycle, a series of attempts have been made, such as vacuum pump pumping or cascade decompression, inert gas sweeping, or various combinations.[244] Researches indicated that vacuum pump scheme requires small energy relative to the energy stored chemically in fuels, but the efficiency of the vacuum pump performance becomes extremely poor when the air pressure is less than 10^{-3} atm.[245] The inert gas sweeping method can reduce the oxygen partial pressure to a very low level, but the energy required for heating the inert gas from ambient temperature to reactor temperature and subsequent separation of the inert gas and oxygen is very large.[19] Reducing energy consumption for low oxygen partial pressure in the reduction step is significant to improve the efficiency of thermochemical cycle, which can be considered as a challenge of thermochemical fuel production and need to be further studied.

Energy loss in the synthesis process of liquid fuels depends on the level of synthesis technologies for different kinds of hydrocarbon fuels. Namely, the syngas-to-liquid fuel conversion is determined by targeted product, catalyst, and syngas composition. By far, liquid fuels synthesis technologies are relatively mature and have been applied in industrial-scale production. In other words, the existing synthesis technologies have rendered the energy loss as low as possible and cost to be acceptable in the market. For example, around 91% of the produced syngas can be converted into liquid fuel containing 16% kerosene and 40% diesel in recent publication.[53] The syngas-to-methanol conversion rate can also reach 90% and efficiency considering equivalent thermal energy penalty can be 75% in reported experimental data.[36] In contrast to energy loss in solar collection unit and liquid fuels synthesis unit, thermal energy loss in thermochemical redox cycle needs to be further studied as only a small fraction of thermal energy is converted into chemical energy in thermochemical cycle process, which seriously limits the solar-to-fuel efficiency in the entire sustainable fuel production chain. Its breakthrough will significantly improve the solar-to-fuel conversion

efficiency. Therefore, reducing thermal energy loss in the thermochemical reactor has become one of the most important pathways to provide competitive advantages and realize industrial production. How to reduce thermal energy loss during two-step thermochemical cycle for syngas production is discussed in the following section.

Heat recovery concepts

Energy distribution discussed in Limiting factors states the research direction for improving solar-to-fuel efficiency, which is to reduce the energy losses that occur in the sustainable fuel production system. The maximum energy loss occurs at thermochemical redox cycle process in the solar receiver-reactor mainly due to the sensible heat rejected during the temperature-swing cycling, which accounts for more than 60% of the absorbed solar energy according to the energy balance analysis. If most of such sensible heat of receiver-reactor can be recovered, the potential solar-to-syngas efficiency will rise above 20%.[18,19,36,246] Therefore, heat recovery technology becomes a powerful driving force pushing solar-driven thermochemical fuel production toward a commercial scale, and the integration design of heat exchanger and solar reactor is next research focus to improve the conversion efficiency from solar to fuel.

The sensible heat caused by temperature-swing cycling required for reduction and oxidation reactions can be classified into two categories: solid phase sensible heat and gas phase sensible heat. The solid phase sensible heat refers to redox material between reduction and oxidation temperatures, and the large temperature difference and specific heat of solid material would generate large energy required to leave the receiver-reactor to drive oxidation reaction associated with syngas production. The gas phase sensible heat includes two parts: one is from the high-temperature O_2 released (usually accompanied by inert gas) at reduction step; and the other is from the syngas generated at oxidation step. What is expected to be done is to recover both solid and gas phase sensible heats by using heat recovery technologies. Heat exchanger technology has been developed for several decades and various heat exchanger designs have been successfully employed in lots of industrial fields. In other words, heat recovery concept is technically feasible and of low risk by referencing existing heat exchanger designs. What we need to do is just try to combine solar reactor technology and heat exchanger technology. The key is to give a reasonable integration scheme taking swing of redox cycle and structure of reactor into account, especially for solid phase sensible heat recovery of redox materials which is extremely difficult to achieve. Currently some heat recovery concept designs have also been proposed and applied in solar-driven thermochemical splitting of H_2O and CO_2 to improve solar conversion efficiency. A partial listing of various heat recovery concept designs integrated with solar thermochemical reactor in the existing literatures are presented in Table 4, and detailed introductions are given in the following section.

Solid phase sensible heat recovery concepts

For solid phase sensible heat recovery concepts, the heat exchange is mainly based on the solid-solid heat transfer which can be subdivided into conduction exchange between particles and radiation exchange between porous medium. Typical particle-based heat recovery concept cases are presented in Refs. [247–249] For instance, Felinks et al.[247] designed a quasi-counter-current heat exchanger integrated with thermochemical reactor in which redox material is made into small spherical particles with a diameter of 0.8mm. The heat transfer medium is made into large spherical shape with a diameter of 4mm to separate from redox particles through a sieve after finishing heat exchange as shown in Figure 21A. To improve the heat recovery rate, the authors proposed multi-stage heat exchanges based on the counter-current principle. The high-temperature redox particles leaving the reduction zone flow downward under gravity and were cooled by heat transfer spheres in each stage via direct contact. A quasi-counter-current heat exchange process was realized when the redox particles and heat transfer spheres pass through all the stages in opposed order as shown in Figure 21B. If six stages were set in the system, an over 70% of heat recovery rate could be obtained. Such design idea is excellent in term of heat recovery rate, but the integration system of reactor and heat exchanger is complex. It is still in the conceptual stage, as well as the experimental system and prototype have not yet been implemented by far. Next study should focus on transferring such idea to practical application.

Falter et al.[248] established a generic double-walled heat exchanger in which reduced and oxidized particles flow in the opposite direction (i.e., counter-flow) and investigated the potential of heat recuperation from sensible heat of solid redox particles. As shown in Figure 22, the particles which are reduced under directly concentrated solar radiation flow downward along the annular inner tube of the heat exchanger while the heat of "hot" reduced particles (1800K) is transferred to the "cold" oxidized particles (1000K) in annular outer tube of the heat exchanger through a separating wall. The reduced particles leaving heat exchanger are inserted into the oxidation chamber in which they are re-oxidized by H_2O or/and CO_2. The oxidized particles are eventually fed into the bottom and moved upward along the outer tube of the heat exchanger. A cycle is completed and the sensible heat of redox particles is recovered.

Brendelberger et al.[249] proposed a quasi-countercurrent heat recovery system which includes an arrangement of flow pattern stages as shown in Figure 23. The redox material and heat transfer medium are made into particles with different sizes, respectively, to be separated conveniently. This system consists of reduction zone, oxidation zone, and two heat exchange zones (cooling zone and heating zone). First, the reduced redox particles enter the cooling zone (left heat exchange zone) after finishing reduction reaction with concentrated solar radiation at reduction zone. Afterward, the reduced redox particles transfer heat to the low temperature heat transfer particles via conduction during direct contact in multi stages. When the temperature of reduced redox particles drops to the oxidation temperature, they are moved into oxidation zone and participate in oxidation reaction accompanied by syngas production. After that, the oxidized redox particles enter heating zone (right heat exchange zone), while the high temperature heat transfer particles are also moved from cooling zone to heating zone. The oxidized redox particles are heated by the high temperature heat transfer particles in the same form as that occurring in cooling zone. When the temperature of redox particles increases to reduction temperature, they return to the reduction zone and participate in reduction

Table 4. Heat recovery concepts for sensible heat of thermochemical reactors

Heat recovery concepts	Designs	Reduction temperature	Oxidation temperature	Oxygen partial pressure in reduction step	Redox material and its shape	Heat transfer medium and its shape	Heat exchange style	Maximum heat exchanger efficiency	Maximum solar-to-syngas efficiency	Reference
Solid phase sensible heat recovery	Moving brick receiver-reactor solid-solid heat exchanger	1800K	1100K	10Pa	Ceria porous brick	/	Radiation	/	~25%	Siegrist et al.[243]
	Quasi-counter-current heat exchanger	1400°C	1000°C	/	Ceria particle	Alumina sphere	Conduction	>70%	/	Felinks et al.[247]
	Counter-flow particle heat exchanger	1800K	1000K	/	Ceria particle	/	Conduction	>80%	/	Falter and Pitz-Paal[248]
	Quasi-countercurrent heat recovery system	1500°C	900°C	100Pa	Ceria particle	Particle	Conduction	~70%	/	Brendelberger et al.[249]
	Counter-flow solid heat exchanger	1800K	1000K	10^{-3}atm	Ceria reticulated porous ceramic brick	/	Radiation	~70%	~12%	Falter and Pitz-Paal[250]
	Heat recovery based on dual heat storage system	1450-1500°C	900-650°C	20-22mbar	Ceria porous eight side brick		Conduction, convection, and radiation	~70%	~2.83%	Lidor et al.[254]
	Counter-flow solid heat exchanger	1800K	1000K	10^{-5}atm	Ceria porous brick	/	Radiation	~80%	/	Falter et al.[258]
	Solid–solid heat exchanger	1773.15K	1073.15K	10^{-3}bar	/	/	/	/	/	Holzemer-Zerhusen et al.[259]
	Reactor train system for heat recovery	1773K	1073K	10Pa	Ceria porous brick	/	Radiation	~80%	~30%	Patankar et al.[251]
	Counter-rotating inert solid heat exchanger	/	/	/	Ceria porous medium	Inert material cylinder solid	Radiation	>50%	/	Lapp et al.[202]
Gas phase sensible heat recovery	Reticulated ceramic foam heat exchanger	1773K	1773K	/	Ceria porous particle	/	Conduction and convection	/	~2.4%	Bala Chandran et al.[257]
Simultaneous solid and gas phase sensible heat recovery	Simultaneous solid and gas phase heat recovery design	1980K	1073K	0.01atm	Ceria	/	Conduction convection and radiation	/	~40.8%	Lapp et al.[19]

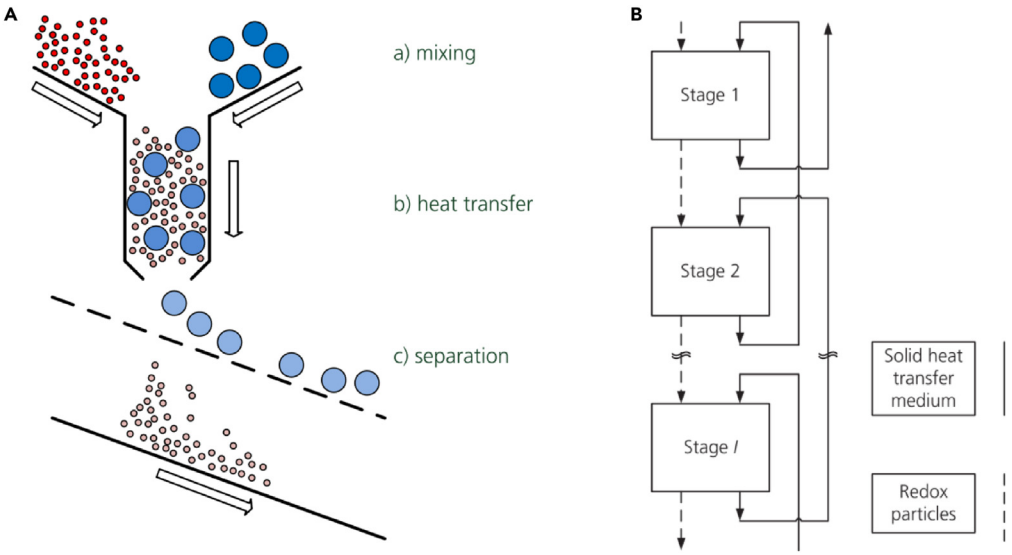

Figure 21. Heat recovery model using a solid heat transfer medium

(A) Heat exchange design.

(B) Multi-stage heat exchange design.

Reproduced with permission.[247] Copyright 2014, Elsevier.

reaction. Meanwhile, the high temperature heat transfer particles become low temperature heat transfer particles after finishing heat exchange and are redelivered into cooling zone. A complete redox cycle associated with heat recovery is therefore achieved, and analysis indicated that heat recovery rate of about 70% can be achieved if assuming six stages in both cooling and heating zones and 10 s in each stage.

Typical medium-based heat recovery concept cases are well discussed in Refs.[250,251] Falter et al.[250] discussed the counter-flow solid heat exchange and internal heat diffusion in a generic solar-thermochemical reactor model they established. Elements of redox material with porous structure were reduced under concentrated solar radiation in the reduction chamber and moved into the oxidation chamber in which they were re-oxidized with H_2O or/and CO_2. Oxidized elements were moved into the reduction chamber again to finish the redox cycle. During the counter-flow moving process through the heat exchanger chambers, heat exchange between reduced elements and oxidized elements is realized by radiation heat transfer as shown in Figure 24. The authors analyzed effects of porosity, residence time, and heat exchanger length on the heat recovery based on heat diffusion calculations. An adequate parameter combinations were suggested to obtain close to 70% of heat exchange efficiency.

Similar with idea of Falter et al.,[250] Patankar et al.[251] proposed their design of heat recovery concept which adopted moving reactors instead of moving redox materials, because the outer reactor temperature can be minimized with good insulation. As shown in Figure 25, a series of identical reactors are arranged in a closed-loop and cycling between the reduction and oxidation zones. The reduction and oxidation zone are located at the left-hand and right-hand sides of the system, respectively. When the reactor finishes reduction step, it will be moved into the heat recovery zone at the top where the reduced reactor with high temperature delivers energy to the oxidized reactor at the bottom by radiation heat transfer. After arriving at the oxidation zone, reduced material in the reactor is oxidized with H_2O or/and CO_2. The oxidized reactor thereafter leaves the oxidation zone and enters into the heat recovery zone at the bottom where it absorbs the energy from the reduced reactor at the top. The oxidized reactor eventually returns to the reduction zone and completes a cycle in which the sensible heat of redox material is recovered. Results showed that a heat recovery effectiveness of 80% can be achieved for a train producing 100kg-H_2/day with a 60 min cycle time.

Diver et al.[178,203,214,252,253] designed a Counter-Rotating-Ring Receiver/Reactor/Recuperator (CR5) prototype which used a stack of counter-rotating rings or disks with fins along the perimeter. As shown in Figure 26, each ring rotates in the opposite direction to its neighbor at a rotational speed on the order of 1 rpm or less. Solar flux penetrates in depth through gap between adjacent reactant fins and drive the splitting of H_2O and CO_2. Solar flux illuminates the fins on the stack of rings on the edge along nominally 1/4 of the perimeter. The moving "volumetric absorber" has the advantage of effectively smoothing non-uniform flux distributions inherent in reflective solar concentrators. On the opposite side of the stack, the oxidation reaction takes place and products fuels. While the remaining half of the stack (two 1/4 sections between) is adiabatic and is utilized for countercurrent recuperation, primarily by thermal radiation. Equal pressures are maintained in the two reactors to minimize flow through the recuperator sections. Such solid-to-solid countercurrent recuperation design can perfectly recover sensible heat of solid redox material, and can be considered as one of the most effective integration schemes.

Lidor et al.[254] proposed a novel high-temperature heat recovery method based on the dual storage system, which can avoid the heat losses incurred by an indirect design. As shown in Figure 27, the cycle in this new system consists of four steps: reduction, heat extraction, oxidation, and heat recuperation. First, the solar reactor is heated by the high flux solar simulator up to the temperature required for reduction

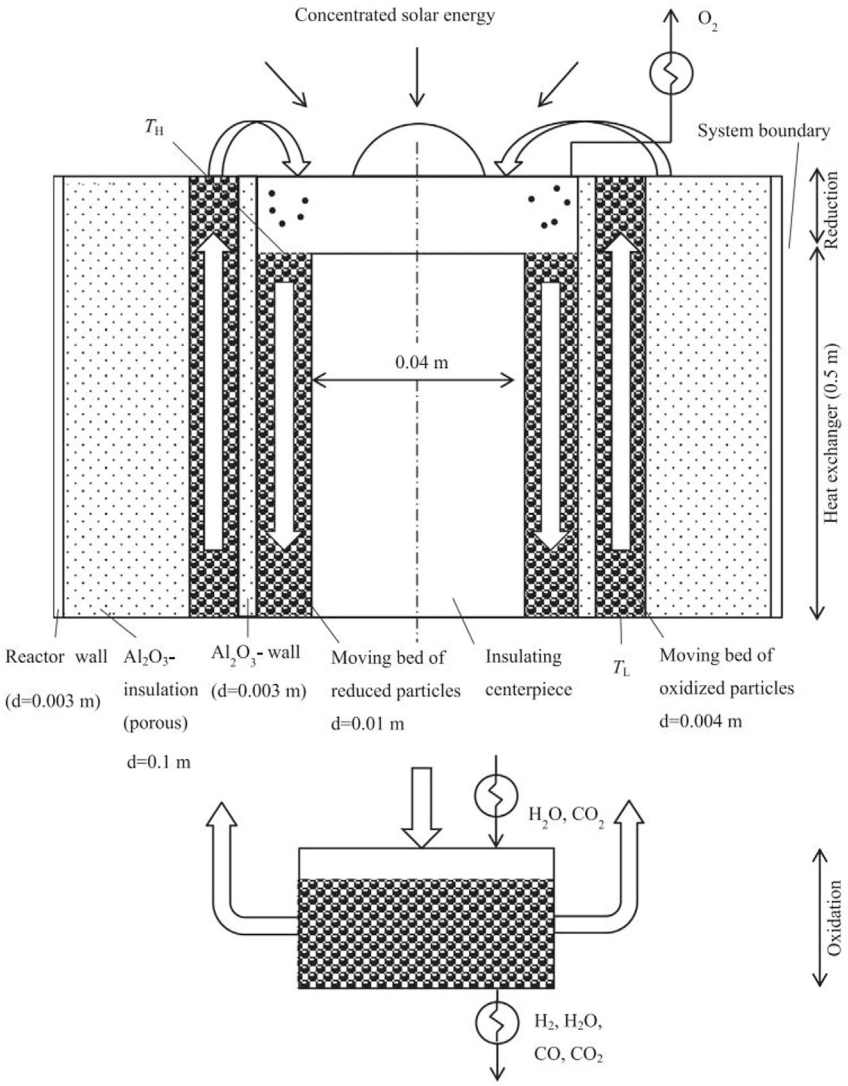

Figure 22. Particle heat exchanger model integrated into thermochemical reactor
Reproduced with permission.[248] Copyright 2018, Elsevier.

reaction which is accompanied with O_2 release. After the reduction reaction, heat transfer fluid (such as N_2) flows through the thermal energy storage unit 2 (TES 2) where it is heated up to oxidation temperature and enters the solar reactor via the main inlet port where it is further heated up to reduction temperature. The high temperature heat transfer fluid then leaves and enters the thermal energy storage unit 1 (TES 1) where it is cooled down to ambient temperature. In this process, the solar reactor is also cooled down to the desired temperature for oxidation. Oxidation reaction eventually occurs at the solar reactor and produces syngas in the presence of H_2O and CO_2, after which the thermal energy stored in the TES 1 is extracted to heat solar reactor by reversing the heat transfer fluid. Such a cycle realizes the sensible heat recovery of redox material, and experimental data showed a heat extraction effectiveness of up to 70% from a 4-kW solar reactor. This is another successful case of heat recovery integrating into reactor except for the CR5 reactor, application of thermal energy storage unit provides a new way to realize heat recovery to improve the solar conversion efficiency in thermochemical fuel production.

Gas phase sensible heat recovery concepts

In contrast to solid phase sensible heat recovery, the importance of gas sensible heat recovery is relatively minimal in terms of improving solar conversion efficiency. This is because the specific heat capacity of gas (oxygen, inert, or syngas) is much less than that of solid redox materials. However, the heat exchange between inlet and outlet gases is beneficial for stable operation of reactor. Moreover, the near isothermal operation scheme was developed by several groups.[55,246,255,256] Such scheme has several advantages: (1) avoiding solid phase sensible heat recovery of redox materials; (2) simplifying solar reactor structure because it eliminates the temperature swing of redox cycle; and (3) being

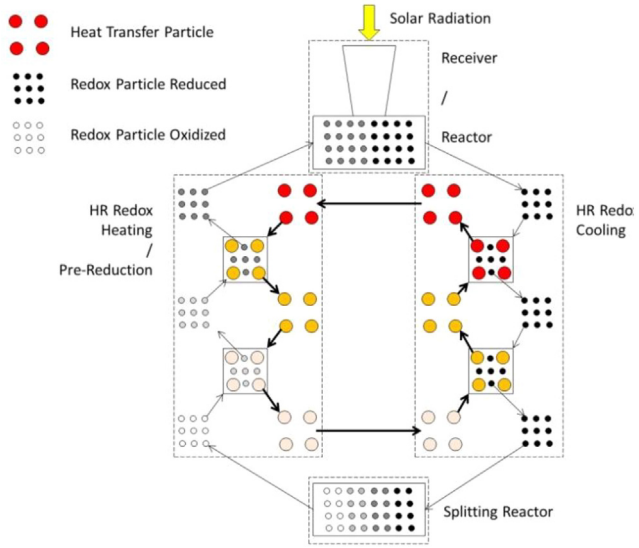

Figure 23. Design of combining thermochemical redox cycle and heat recovery
Reproduced with permission.[249] Copyright 2014, The American Society Mechanical Engineers.

beneficial of devices due to avoiding damage caused by alternating high and low temperature cycling. Meanwhile, the temperature has a significant effect on redox reaction. If the redox temperature is too high, the oxidation kinetics would be decreased, which is not conducive to oxidation step. If the redox temperature is too low, a lower oxygen partial pressure is required to drive reduction reaction, which means a higher energy consumption associated with vacuum pump or inert gas sweep. Except for temperature, redox material is also key factor which is related to operation conditions, for example, isothermal cycling trends to work much better on CO_2 splitting for easily reducible materials than two-temperature thermochemical cycle. At present, the pros and cons of isothermal versus two-temperature thermochemical cycle are under debate. In addition, although the solid phase sensible heat recovery of redox materials can be avoided, the gas phase sensible heat recovery is still unsolved. A large amount of sweep inert gas and oxygen product during reduction step and excessive water vapor or carbon dioxide during oxidation step all carry a large amount of heat away from reactor, which means a heat recovery is still required. It is therefore necessary to study the gas phase sensible heat recovery in the thermochemical redox cycle.

A typical case of gas phase sensible heat recovery was reported by Chandran et al.[257] They designed a counter-flow and tube-in-tube alumina heat exchanger which was integrated with thermochemical reactor based on isothermal operating condition (i.e., reduction temperature is equal to oxidation temperature). The details are shown in Figure 28. There are six reactive elements in the reactor such that each reactive element is made up of concentric and high purity alumina tubes with a closed spherical cap. The annular gap is filled with porous

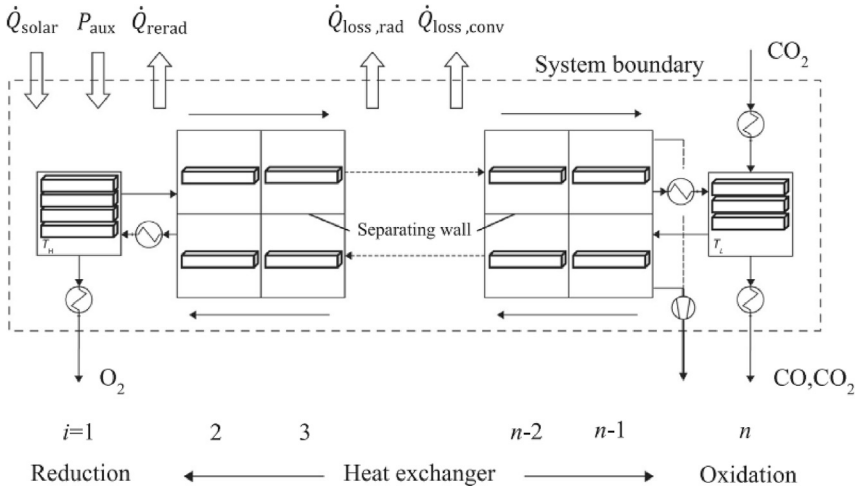

Figure 24. Modular generic rector model including heat exchanger chambers
Reproduced with permission.[250] Copyright 2017, Elsevier.

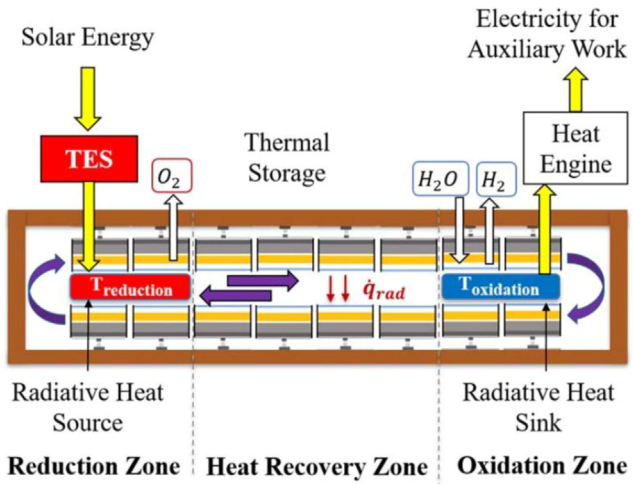

Figure 25. The reactor train system combined with heat recovery
Reproduced with permission.[251] Copyright 2022, The American Society Mechanical Engineers.

cylindrical ceria particles and inert alumina reticulate porous ceramic. In the reactive element, gases with near ambient conditions enter the inner tube of the heat exchanger and then return to the heat exchanger through the annulus after completing redox reaction. Details are as follows: (1) during reduction step, an inert sweep gas with ambient temperature enters the inner tube and is heated by hot gases (mixture of inert gas and released O_2) through outer tube; (2) during oxidation step, CO_2 or/and H_2O steam enter the inner tube and are heated by the syngas (CO or/and H_2) generated from oxidation reaction. In both reduction and oxidation steps, the gas phase sensible heat is recovered from the gases leaving the reactor to preheat the gases entering the reactor. Analysis results predicted that the maximum solar-to-fuel efficiency is about 2.4%.

Simultaneous solid and gas phase sensible heat recovery concepts

Simultaneous solid and gas phase sensible heat recovery concepts are regarded as the most perfect way to increase solar conversion efficiency at the expense of more complex mechanism design. Lapp et al.[19] proposed a simultaneous solid and gas phase heat recovery concept

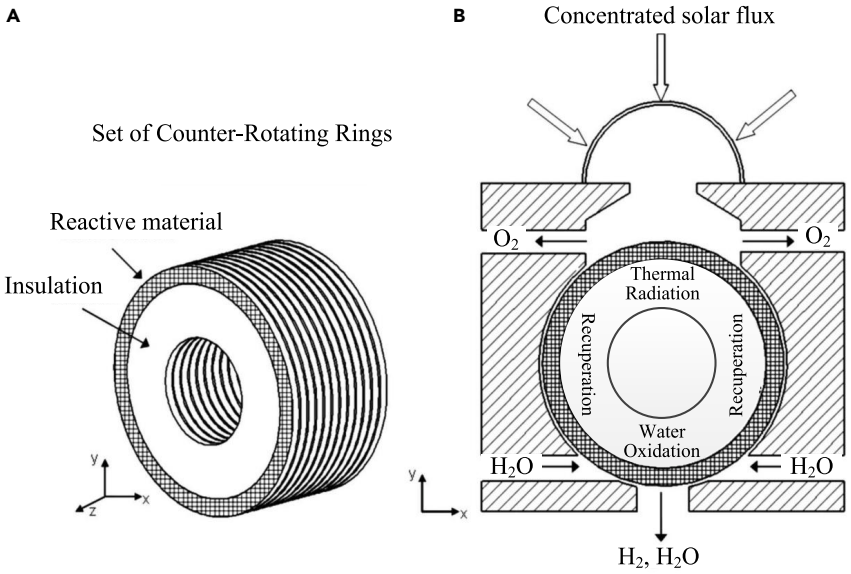

Figure 26. Schematic of counter-rotating-ring receiver/reactor/recuperation
(A) Set of counter-Rotating Rings.
(B) Cross section of reactor.
Reproduced with permission.[203] Copyright 2008, The American Society Mechanical Engineers.

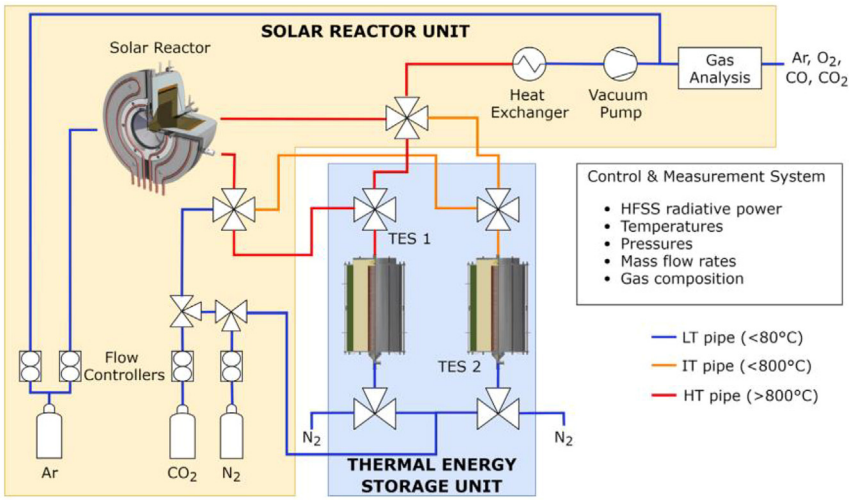

Figure 27. Heat recovery scheme based on dual heat storage system
Reproduced with permission.[254] Copyright 2023, Elsevier.

from redox material and gaseous products. The heat recovery model is shown in Figure 29. In this model, inert gas is preheated from ambient temperature T_0 to the temperature T_1 in heat exchanger 1 in which the mixture of inert gas and O_2 released from the ceria is cooled from reduction temperature T_{red} to temperature T_2. The oxidizing reactants H_2O or/and CO_2 are preheated from ambient temperature T_0 to the temperature T_3 in heat exchanger 2. It is noted that H_2O is liquid at ambient temperature, it is needed to first evaporate, and then the vapor is preheated to T_3. The products H_2 or/and CO are cooled from oxidation temperature T_{ox} to T_4 in heat exchanger 2. Both heat exchange processes complete the heat recovery of gas-phase sensible heat. Solid ceria as non-stoichiometric redox material is designed to continuously cycle between the reduction and oxidation zones, in which ceria undergoes heating from T_{ox} to T_{red} and cooling from T_{red} to T_{ox}. The partial sensible heat of solid ceria is recovered and used in the heating step. The calculation results indicated that a perfect heat recovery enables an order of magnitude increase in cycle efficiency to 40.8%.

At present, a series of heat recovery concepts have been proposed to improve solar-to-syngas efficiency, particularly solid phase sensible heat recovery of redox materials (particles or porous medium) in temperature-swing thermochemical cycles. Theoretical analysis has proven that the heat recovery technology can significantly increase solar conversion efficiency and can be considered to be one of the most potential

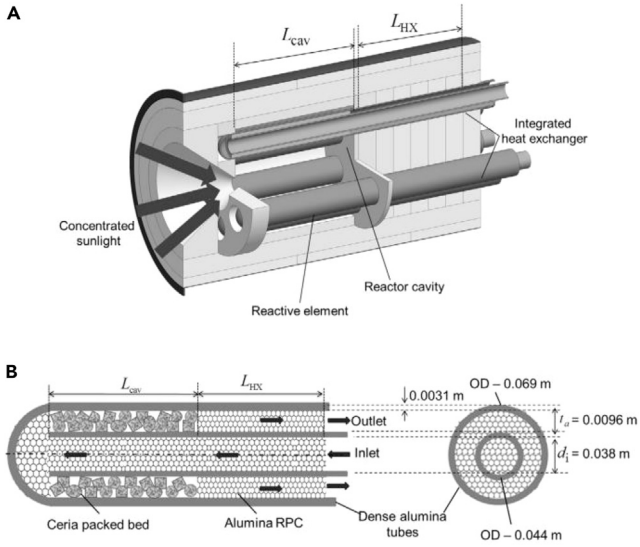

Figure 28. Schematic of integrated solar thermochemical reactor/reticulated ceramic foam heat exchanger
(A) Integrated reactor/heat exchanger prototype.
(B) Expanded cross-sectional views of the reactive element connected to the heat exchanger.
Reproduced with permission.[257] Copyright 2015, Elsevier.

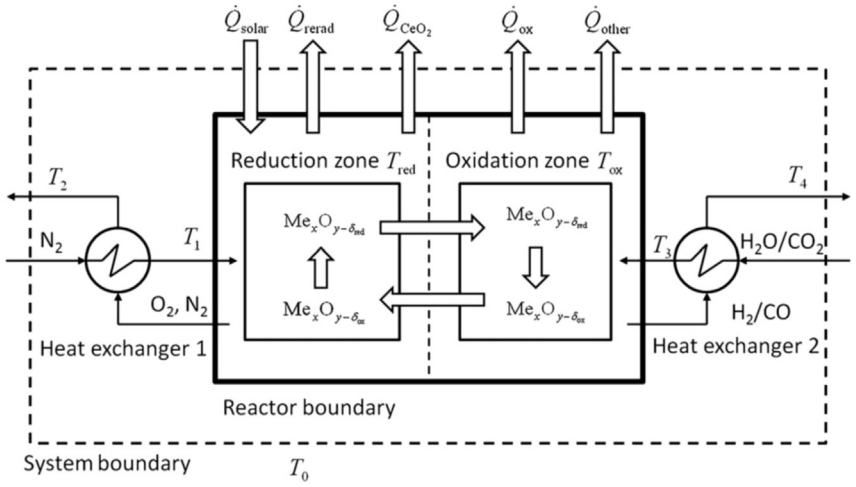

Figure 29. Heat recovery model in thermochemical redox cycle process
Reproduced with permission.[19] Copyright 2012, Elsevier.

pathways to push solar-driven thermochemical fuel production to a commercial scale. However, the idea of heat recovery of reactor is still stuck in the concept and design stage due to a large number of detailed techniques yet to be resolved. Therefore, effective heat exchange designs integrated into the thermochemical reactor is considered as a lingering issue which should be addressed in the future.

CONCLUSIONS

Solar-driven thermochemical conversion of H_2O and CO_2 into sustainable fuels based on redox cycle is considered as one of the most promising pathways for alternative energy. This work describes the complete sustainable fuel production chain including a series of physical and chemical processes which convert solar energy into chemical energy which is stored in sustainable liquid fuels. In the entire production chain, only concentrated solar energy is used as high-temperature heat supply and almost zero cost H_2O and CO_2 are adopted as initial feedstock, which can meet the requirement of human beings for sustainable energy and carbon neutrality. However, such technology is still stuck in theoretical and experimental stages and there is still a long way to realize industrial production. This work therefore reviews the working principle of thermochemical redox cycle with the aid of concentrated solar energy, development of redox materials, and key devices including solar concentrators and solar reactors. Energy losses along the energy flow in the production chain and heat recovery concepts employed to improve solar-to-fuel conversion efficiency are also summarized. Some conclusions from this review are given as follows.

(1) Among the existing three categories of redox materials developed in the past several decades, the non-stoichiometric redox materials can be regarded as the current state-of-the-art redox materials for thermochemical splitting of H_2O or/and CO_2 in terms of operation, efficiency, and stability. Although incomplete reaction content would reduce oxygen released in reduction step and syngas generated in subsequent oxidation step, it can avoid phase transformations which can induce structural disruption, and make redox cycle operate more stably and efficiently. This points out development trends of next generation redox materials which will take both thermochemical kinetics and reaction extent into account. In addition, further reducing the reduction reaction temperature is also a major research focus.

(2) Concentrated solar energy is used as high-temperature heat source for thermochemical redox cycles. At present, only parabolic dish and heliostat field concentrators with 3D point-focus concentration can provide such evaluated temperature for reduction reaction. Compared with parabolic dish concentrator, a tower solar collector with the aid of a controllable heliostat field has been identified as a favorable path for scale-up of thermochemical splitting of H_2O or/and CO_2 based on redox cycle. Thus, combination of solar tower and thermochemical fuels production is a promising technology to realize commercial application. Further work should be focused on solving scientific and technical issues, such as efficiency, cost, intermittent solar energy, weather, optimal design of heliostat and optimal layout of heliostat field, and energy storage design integrated into solar collector.

(3) When solar energy is combined with thermochemical redox, it is reasonable to anticipate that directly irradiated reactors will outperform indirectly irradiated ones due to the relatively high temperatures that will be encountered. However, when combined with an open-loop system, in which a chemical reduction process could reduce the required temperature for the reduction step to levels similar to those indirectly-irradiated and even also thermally heated reactors could become competitive. It is possible to infer that the majority of global research strategies involves reactors with non-moving parts. When catalysts for specific reactions are relatively inexpensive materials like oxides that can be shaped into bulky finished objects (in contrast to cases where functional catalysts are expensive metals), the idea of increasing volumetric product yield of such reactors by manufacturing the bulk of the entire monolithic

body from the active material rather than employing the latter as a mere coating is appealing. As a result, an increased cell density and honeycomb structure made of the redox material will significantly improve syngas yield and reaction rate.

(4) The primary issue hindering commercial application continues to be the low efficiency of reactors. The ceria-foam-based reactor has an average efficiency of 1.73% and a peak efficiency of 3.53% at 1870 K, according to the ETH/PSI team. However, it is widely agreed that the long-term objective is to achieve a practical 20% efficiency of solar-to-syngas energy conversion to ensure commercial viability, environmental performance, and competition with alternative methods of solar-driven thermochemical fuel production. In addition, mechanical vibrations, thermal expansion, thermal shock resistance, inhomogeneous heating of rotating parts, sealing at high temperatures, and some other issues are difficult to resolve and can result in fatalities over time. At the stage of making a scale-up decision at the commercial level, perhaps a compromise between scalability and simplicity of operation is required. Therefore, next generation reactors should be developed toward high efficiency and large scale.

(5) The majority of energy loss in the entire thermochemical fuels production chain from H_2O and CO_2 to sustainable fuels occurs at thermochemical redox cycle process. Sensible heat loss between reduction and oxidation steps accounts for over 60% of solar energy absorbed by thermochemical reactor. Theoretical analysis has proven that if most of such sensible heat of receiver-reactor can be recovered, the potential solar-to-syngas efficiency will rise above 20%. Thus, heat recovery technology is considered as optimal choice to be integrated with the solar reactor to improve solar energy conversion efficiency. However, the idea of heat recovery of reactor is still stuck in the concept and design stage due to a large number of detailed techniques yet to be resolved. Further research works should therefore focus on heat recovery design particularly suitable for thermochemical redox cycle.

ACKNOWLEDGMENTS

The work described in this paper was fully supported by a grant from the National Natural Science Foundation of China (52022003, 52106079) and a grant from the Shenzhen Science and Technology Innovation Commission (JCYJ20190808123011253).

AUTHOR CONTRIBUTIONS

Conceptualization: L.W. and L.A.; Investigation: L.W., Z.P., and X.S.; Writing - Original Draft: L.W., Z.P., X.S., and O.C.E.; Writing - Review and Editing: G.L. and H.Q.; Funding Acquisition: L.W. and L.A.; Project administration: Q.W. and L.A.; Supervision: Q.W. and L.A.

DECLARATION OF INTERESTS

The authors declare no competing interests.

REFERENCES

1. Park, S.W., Lee, J.S., Yang, W.S., Alam, M.T., and Seo, Y.C. (2020). A comparative study of the gasification of solid refuse fuel in downdraft fixed bed and bubbling fluidized bed reactors. Waste Biomass Valori *11*, 2345–2356.
2. Shahabuddin, M., and Bhattacharya, S. (2021). Effect of reactant types (steam, CO_2 and steam + CO_2) on the gasification performance of coal using entrained flow gasifier. Int. J. Energy Res. *45*, 9492–9501.
3. Hosseini, S.E., Abdul Wahid, M., Jamil, M.M., Azli, A.A.M., and Misbah, M.F. (2015). A review on biomass-based hydrogen production for renewable energy supply. Int. J. Energy Res. *39*, 1597–1615.
4. Shahabuddin, M., Alim, M.A., Alam, T., Mofijur, M., Ahmed, S.F., and Perkins, G. (2021). A critical review on the development and challenges of concentrated solar power technologies. Sustain. Energy Techn. *47*, 101434.
5. Eliseev, O.L. (2009). Gas-to-liquid technologies. Russ. J. Gen. Chem. *79*, 2509–2519.
6. Höök, M., and Aleklett, K. (2010). A review on coal-to-liquid fuels and its coal consumption. Int. J. Energy Res. *34*, 848–864.
7. Chueh, W.C., Falter, C., Abbott, M., Scipio, D., Furler, P., Haile, S.M., and Steinfeld, A. (2010). High-flux solar-driven thermochemical dissociation of CO_2 and H_2O using nonstoichiometric ceria. Science *330*, 1797–1801.
8. Cheng, W.H., de la Calle, A., Atwater, H.A., Stechel, E.B., and Xiang, C. (2021). Hydrogen from Sunlight and Water: A Side-by-Side Comparison between Photoelectrochemical and Solar Thermochemical Water-Splitting. ACS Energy Lett. *6*, 3096–3113.
9. Carrillo, R.J., and Scheffe, J.R. (2017). Advances and trends in redox materials for solar thermochemical fuel production. Sol. Energy *156*, 3–20.
10. Abanades, S., Charvin, P., Flamant, G., and Neveu, P. (2006). Screening of water-splitting thermochemical cycles potentially attractive for hydrogen production by concentrated solar energy. Energy *31*, 2805–2822.
11. Schrader, A.J., De Dominicis, G., Schieber, G.L., and Loutzenhiser, P.G. (2017). Solar electricity via an Air Brayton cycle with an integrated two-step thermochemical cycle for heat storage based on Co_3O_4/CoO redox reactions III: Solar thermochemical reactor design and modeling. Sol. Energy *150*, 584–595.
12. Bhosale, R.R., Kumar, A., AlMomani, F., Ghosh, U., and Khraisheh, M. (2017). A comparative thermodynamic analysis of samarium and erbium oxide based solar thermochemical water splitting cycles. Int. J. Hydrogen Energy *42*, 23416–23426.
13. Wheeler, V.M., Bader, R., Kreider, P.B., Hangi, M., Haussener, S., and Lipiński, W. (2017). Modelling of solar thermochemical reaction systems. Sol. Energy *156*, 149–168.
14. Bayon, A., de la Calle, A., Ghose, K.K., Page, A., and McNaughton, R. (2020). Experimental, computational and thermodynamic studies in perovskites metal oxides for thermochemical fuel production: A review. Int. J. Hydrogen Energy *45*, 12653–12679.
15. Bhosale, R.R., and Rashid, S. (2022). Thermodynamic analysis of $Mg_xFe_{3-x}O_4$ redox CO_2 conversion solar thermochemical cycle. Int. J. Energy Res. *46*, 923–936.
16. Li, S., Wheeler, V.M., Kumar, A., Venkataraman, M.B., Muhich, C.L., Hao, Y., and Lipiński, W. (2022). Thermodynamic guiding principles for designing nonstoichiometric redox materials for solar thermochemical fuel production: ceria, perovskites, and beyond. Energy Tech. *10*, 2000925.
17. Wang, B., Li, X., Dai, Y., and Wang, C.H. (2022). Thermodynamic analysis of an epitrochoidal rotary reactor for solar hydrogen production via a water-splitting thermochemical cycle using nonstoichiometric ceria. Energy Convers. Manag. *268*, 115968.
18. Scheffe, J.R., and Steinfeld, A. (2012). Thermodynamic analysis of cerium-based oxides for solar thermochemical fuel production. Energ. Fuel *26*, 1928–1936.
19. Lapp, J., Davidson, J.H., and Lipiński, W. (2012). Efficiency of two-step solar thermochemical non-stoichiometric redox cycles with heat recovery. Energy *37*, 591–600.

20. Abanades, S. (2022). Redox Cycles, Active Materials, and Reactors Applied to Water and Carbon Dioxide Splitting for Solar Thermochemical Fuel Production: A Review. Energies *15*, 7061.
21. Muhich, C.L., Ehrhart, B.D., Al-Shankiti, I., Ward, B.J., Musgrave, C.B., and Weimer, A.W. (2016). A review and perspective of efficient hydrogen generation via solar thermal water splitting. WIRES Energy Environ *5*, 261–287.
22. Gokon, N., Murayama, H., Nagasaki, A., and Kodama, T. (2009). Thermochemical two-step water splitting cycles by monoclinic ZrO_2-supported $NiFe_2O_4$ and Fe_3O_4 powders and ceramic foam devices. Sol. Energy *83*, 527–537.
23. Ramos, A.E., Maiti, D., Daza, Y.A., Kuhn, J.N., and Bhethanabotla, V.R. (2019). Co, Fe, and Mn in La-perovskite oxides for low temperature thermochemical CO_2 conversion. Catal. Today *338*, 52–59.
24. Jiang, Q., Gao, Y., Haribal, V.P., Qi, H., Liu, X., Hong, H., Jin, H., and Li, F. (2020). Mixed conductive composites for 'low-temperature' thermo-chemical CO_2 splitting and syngas generation. J. Mater. Chem. A. *8*, 13173–13182.
25. Le Gal, A., Abanades, S., and Flamant, G. (2011). CO_2 and H_2O splitting for thermochemical production of solar fuels using nonstoichiometric ceria and ceria/zirconia solid solutions. Energy Fuels *25*, 4836–4845.
26. Meng, Q.L., Lee, C.i., Ishihara, T., Kaneko, H., and Tamaura, Y. (2011). Reactivity of CeO_2-based ceramics for solar hydrogen production via a two-step water-splitting cycle with concentrated solar energy. Int. J. Hydrogen Energy *36*, 13435–13441.
27. Singh, P., and Hegde, M.S. (2010). $Ce_{0.67}Cr_{0.33}O_{2.11}$: A new low-temperature O_2 evolution material and H_2 generation catalyst by thermochemical splitting of water. Chem. Mater. *22*, 762–768.
28. Gao, K., Liu, X., Jiang, Z., Zheng, H., Song, C., Wang, X., Tian, C., Dang, C., Sun, N., and Xuan, Y. (2022). Direct solar thermochemical CO_2 splitting based on Ca-and Al-doped $SmMnO_3$ perovskites: Ultrahigh CO yield within small temperature swing. Renew Energ *194*, 482–494.
29. Rao, C.N.R., and Dey, S. (2017). Solar thermochemical splitting of water to generate hydrogen. Proc. Natl. Acad. Sci. *114*, 13385–13393.
30. Agrafiotis, C., Roeb, M., and Sattler, C. (2015). A review on solar thermal syngas production via redox pair-based water/carbon dioxide splitting thermochemical cycles. Renew. Sustain. Energy Rev. *42*, 254–285.
31. Yadav, D., and Banerjee, R. (2016). A review of solar thermochemical processes. Renew. Sustain. Energy Rev. *54*, 497–532.
32. Zsembinszki, G., Solé, A., Barreneche, C., Prieto, C., Fernández, A., and Cabeza, L. (2018). Review of reactors with potential use in thermochemical energy storage in concentrated solar power plants. Energies *11*, 2358.
33. Bhosale, R.R., Takalkar, G., Sutar, P., Kumar, A., AlMomani, F., and Khraisheh, M. (2019). A decade of ceria based solar thermochemical H_2O/CO_2 splitting cycle. Int. J. Hydrogen Energy *44*, 34–60.
34. Pullar, R.C., Novais, R.M., Caetano, A.P.F., Barreiros, M.A., Abanades, S., and Oliveira, F.A.C. (2019). A review of solar thermochemical CO_2 splitting using ceria-based ceramics with designed morphologies and microstructures. Front. Chem. *7*, 601.
35. Warren, K.J., and Weimer, A.W. (2022). Solar thermochemical fuels: Present status and future prospects. Sol. Compass. *1*, 100010.
36. Schäppi, R., Rutz, D., Dähler, F., Muroyama, A., Haueter, P., Lilliestam, J., Patt, A., Furler, P., and Steinfeld, A. (2022). Drop-in fuels from sunlight and air. Nature *601*, 63–68.
37. Romero, M., González-Aguilar, J., Sizmann, A., Batteiger, V., Falter, C., Steinfeld, A., Zoller, S., Brendelberger, S., and Lieftink, D. (2019). Solar-driven thermochemical production of sustainable liquid fuels from H_2O and CO_2 in a heliostat field. Proceedings of the ISES Solar World Congress.
38. Romero, M., and Steinfeld, A. (2012). Concentrating solar thermal power and thermochemical fuels. Energy Environ. Sci. *5*, 9234–9245.
39. Rostrup-Nielsen, J.R. (2002). Syngas in perspective. Catal. Today *71*, 243–247.
40. Rostrup-Nielsen, J.R., Sehested, J., and Nørskov, J.K. (2002). Hydrogen and synthesis gas by steam-and CO_2 reforming. Adv. Catal. *47*, 65–139.
41. Marxer, D., Furler, P., Scheffe, J., Geerlings, H., Falter, C., Batteiger, V., Sizmann, A., and Steinfeld, A. (2015). Demonstration of the entire production chain to renewable kerosene via solar thermochemical splitting of H_2O and CO_2. Energy Fuels *29*, 3241–3250.
42. Herron, J.A., Kim, J., Upadhye, A.A., Huber, G.W., and Maravelias, C.T. (2015). A general framework for the assessment of solar fuel technologies. Energy Environ. Sci. *8*, 126–157.
43. Villafán-Vidales, H., Arancibia-Bulnes, C., Riveros-Rosas, D., Romero-Paredes, H., and Estrada, C. (2017). An overview of the solar thermochemical processes for hydrogen and syngas production: Reactors, and facilities. Renew. Sustain. Energy Rev. *75*, 894–908.
44. Van Der Laan, G.P., and Beenackers, A.A.C.M. (1999). Kinetics and selectivity of the Fischer–Tropsch synthesis: a literature review. Catal. Rev. *41*, 255–318.
45. Furler, P., Marxer, D., Scheffe, J., Reinalda, D., Geerlings, H., Falter, C., Batteiger, V., Sizmann, A., and Steinfeld, A. (2017). Solar kerosene from H2O and CO2. AIP Conference Proceedings, AIP Publishing LLC. 1850, 100006. https://doi.org/10.1063/1.4984463.
46. Ozin, G.A. (2015). Throwing new light on the reduction of CO_2. Adv. Mater. *27*, 1957–1963.
47. Detz, R.J., Reek, J.N.H., and van der Zwaan, B.C.C. (2018). The future of solar fuels: when could they become competitive? Energy Environ. Sci. *11*, 1653–1669.
48. Prats-Salvado, E., Monnerie, N., and Sattler, C. (2021). Synergies between Direct Air Capture Technologies and Solar Thermochemical Cycles in the Production of Methanol. Energies *14*, 4818.
49. Steinfeld, A., and Palumbo, R. (2003). Solar thermochemical process technology. Encyclopedia of Physical Science and Technology (Third Edition) *15*, 237–256.
50. Funk, J.E., and Reinstrom, R.M. (1966). Energy requirements in production of hydrogen from water. Ind. Eng. Chem. Proc. Des. Dev. *5*, 336–342.
51. Vázquez, F.V., Koponen, J., Ruuskanen, V., Bajamundi, C., Kosonen, A., Simell, P., Ahola, J., Frilund, C., Elfving, J., Reinikainen, M., et al. (2018). Power-to-X technology using renewable electricity and carbon dioxide from ambient air: SOLETAIR proof-of-concept and improved process concept. J. CO_2 Util. *28*, 235–246.
52. Schulz, H. (1999). Short history and present trends of Fischer–Tropsch synthesis. Appl. Catal. A-Gen. *186*, 3–12.
53. Zoller, S., Koepf, E., Nizamian, D., Stephan, M., Patané, A., Haueter, P., Romero, M., González-Aguilar, J., Lieftink, D., de Wit, E., et al. (2022). A solar tower fuel plant for the thermochemical production of kerosene from H_2O and CO_2. Joule *6*, 1606–1616.
54. Bulfin, B., Miranda, M., and Steinfeld, A. (2021). Performance indicators for benchmarking solar thermochemical fuel processes and reactors. Front. Energy Res. *9*, 677980.
55. Kong, H., Hao, Y., and Jin, H. (2018). Isothermal versus two-temperature solar thermochemical fuel synthesis: A comparative study. Appl. Energy *228*, 301–308.
56. Hao, Y., Yang, C.K., and Haile, S.M. (2013). High-temperature isothermal chemical cycling for solar-driven fuel production. Phys. Chem. Chem. Phys. *15*, 17084–17092.
57. Muhich, C.L., Evanko, B.W., Weston, K.C., Lichty, P., Liang, X., Martinek, J., Musgrave, C.B., and Weimer, A.W. (2013). Efficient generation of H_2 by splitting water with an isothermal redox cycle. Science *341*, 540–542.
58. Roeb, M., and Sattler, C. (2013). Isothermal water splitting. Science *341*, 470–471.
59. Gálvez, M.E., Loutzenhiser, P.G., Hischier, I., and Steinfeld, A. (2008). CO_2 splitting via two-step solar thermochemical cycles with Zn/ZnO and FeO/Fe_3O_4 redox reactions: thermodynamic analysis. Energy Fuels *22*, 3544–3550.
60. Loutzenhiser, P.G., Gálvez, M.E., Hischier, I., Stamatiou, A., Frei, A., and Steinfeld, A. (2009). CO_2 splitting via two-step solar thermochemical cycles with Zn/ZnO and FeO/Fe_3O_4 redox reactions II: Kinetic analysis. Energy Fuels *23*, 2832–2839.
61. Loutzenhiser, P.G., and Steinfeld, A. (2011). Solar syngas production from CO_2 and H_2O in a two-step thermochemical cycle via Zn/ZnO redox reactions: Thermodynamic cycle analysis. Int. J. Hydrogen Energy *36*, 12141–12147.
62. Steinfeld, A. (2012). Thermochemical production of syngas using concentrated solar energy. Annual Rev. Heat Transfer *15*, 255–275. https://doi.org/10.1615/AnnualRevHeatTransfer.2012004537.
63. Stamatiou, A., Steinfeld, A., and Jovanovic, Z.R. (2013). On the effect of the presence of solid diluents during Zn oxidation by CO_2. Ind. Eng. Chem. Res. *52*, 1859–1869.
64. Ambriz, J., Ducarroir, M., and Sibieude, F. (1982). Preparation of cadmium by thermal dissociation of cadmium oxide using solar energy. Int. J. Hydrogen Energy *7*, 143–153.
65. Bilgen, E., and Bilgen, C. (1982). Solar hydrogen production using two-step thermochemical cycles. Int. J. Hydrogen Energy *7*, 637–644.
66. Sibieude, F., Ducarroir, M., Tofighi, A., and Ambriz, J. (1982). High temperature experiments with a solar furnace: The decomposition of Fe_3O_4, Mn_3O_4. Int. J. Hydrogen Energy *7*, 79–88.

67. Charvin, P., Abanades, S., Lemont, F., and Flamant, G. (2008). Experimental study of SnO_2/SnO/Sn thermochemical systems for solar production of hydrogen. AIChE J. *54*, 2759–2767.
68. Abanades, S., Charvin, P., Lemont, F., and Flamant, G. (2008). Novel two-step SnO_2/SnO water-splitting cycle for solar thermochemical production of hydrogen. Int. J. Hydrogen Energy *33*, 6021–6030.
69. Chambon, M., Abanades, S., and Flamant, G. (2009). Kinetic investigation of hydrogen generation from hydrolysis of SnO and Zn solar nanopowders. Int. J. Hydrogen Energy *34*, 5326–5336.
70. Abanades, S. (2012). CO_2 and H_2O reduction by solar thermochemical looping using SnO_2/SnO redox reactions: Thermogravimetric analysis. Int. J. Hydrogen Energy *37*, 8223–8231.
71. Kang, K.S., Kim, C.H., Cho, W.C., Bae, K.K., Kim, S.H., and Park, C.S. (2009). Novel two-step thermochemical cycle for hydrogen production from water using germanium oxide: KIER 4 thermochemical cycle. Int. J. Hydrogen Energy *34*, 4283–4290.
72. Charvin, P., Abanades, S., Flamant, G., and Lemort, F. (2007). Two-step water splitting thermochemical cycle based on iron oxide redox pair for solar hydrogen production. Energy *32*, 1124–1133.
73. Abanades, S., and Villafan-Vidales, H.I. (2011). CO_2 and H_2O conversion to solar fuels via two-step solar thermochemical looping using iron oxide redox pair. Chem. Eng. J. *175*, 368–375.
74. Abanades, S., and Villafan-Vidales, I. (2013). CO_2 valorisation based on Fe_3O_4/FeO thermochemical redox reactions using concentrated solar energy. Int. J. Energy Res. *37*, 598–608.
75. Abanades, S., and Flamant, G. (2006). Thermochemical hydrogen production from a two-step solar-driven water-splitting cycle based on cerium oxides. Sol. Energy *80*, 1611–1623.
76. Kaneko, H., Yokoyama, T., Fuse, A., Ishihara, H., Hasegawa, N., and Tamaura, Y. (2006). Synthesis of new ferrite, Al–Cu ferrite, and its oxygen deficiency for solar H_2 generation from H_2O. Int. J. Hydrogen Energy *31*, 2256–2265.
77. Scheffe, J.R., Li, J., and Weimer, A.W. (2010). A spinel ferrite/hercynite water-splitting redox cycle. Int. J. Hydrogen Energy *35*, 3333–3340.
78. Arifin, D., Aston, V.J., Liang, X., McDaniel, A.H., and Weimer, A.W. (2012). $CoFe_2O_4$ on a porous Al_2O_3 nanostructure for solar thermochemical CO_2 splitting. Energy Environ. Sci. *5*, 9438–9443.
79. Nakamura, T. (1977). Hydrogen production from water utilizing solar heat at high temperatures. Sol. Energy *19*, 467–475.
80. Tamaura, Y., Ueda, Y., Matsunami, J., Hasegawa, N., Nezuka, M., Sano, T., and Tsuji, M. (1999). Solar hydrogen production by using ferrites. Sol. Energy *65*, 55–57.
81. Lorentzou, S., Dimitrakis, D., Zygogianni, A., Karagiannakis, G., and Konstandopoulos, A. (2017). Thermochemical H_2O and CO_2 splitting redox cycles in a $NiFe_2O_4$ structured redox reactor: Design, development and experiments in a high flux solar simulator. Sol. Energy *155*, 1462–1481.
82. Guene Lougou, B., Geng, B., Jiang, B., Zhang, H., Sun, Q., Shuai, Y., Qu, Z., Zhao, J., and Wang, C.H. (2022). Copper ferrite and cobalt oxide two-layer coated macroporous SiC substrate for efficient CO_2-splitting and thermochemical energy conversion. J. Colloid Interface Sci. *627*, 516–531.
83. Cho, H., Gokon, N., Kodama, T., Kang, Y., and Lee, H. (2015). Improved operation of solar reactor for two-step water-splitting H_2 production by ceria-coated ceramic foam device. Int. J. Hydrogen Energy *40*, 114–124.
84. Lu, Y., Zhu, L., Agrafiotis, C., Vieten, J., Roeb, M., and Sattler, C. (2019). Solar fuels production: two-step thermochemical cycles with cerium-based oxides. Prog. Energ. Combust. *75*, 100785.
85. Rhodes, N.R., Bobek, M.M., Allen, K.M., and Hahn, D.W. (2015). Investigation of long term reactive stability of ceria for use in solar thermochemical cycles. Energy *89*, 924–931.
86. Bulfin, B., Call, F., Lange, M., Lübben, O., Sattler, C., Pitz-Paal, R., and Shvets, I.V. (2015). Thermodynamics of CeO_2 thermochemical fuel production. Energ. Fuel *29*, 1001–1009.
87. Vieten, J., Bulfin, B., Huck, P., Horton, M., Guban, D., Zhu, L., Lu, Y., Persson, K.A., Roeb, M., and Sattler, C. (2019). Materials design of perovskite solid solutions for thermochemical applications. Energy Environ. Sci. *12*, 1369–1384.
88. Liu, X., Wang, T., Gao, K., Meng, X., Xu, Q., Song, C., Zhu, Z., Zheng, H., Hao, Y., and Xuan, Y. (2021). Ca-and Ga-doped $LaMnO_3$ for solar thermochemical CO_2 splitting with high fuel yield and cycle stability. ACS Appl. Energy Mater. *4*, 9000–9012.
89. Naik, J.M., Ritter, C., Bulfin, B., Steinfeld, A., Erni, R., and Patzke, G.R. (2021). Reversible Phase Transformations in Novel Ce-Substituted Perovskite Oxide Composites for Solar Thermochemical Redox Splitting of CO_2. Adv. Energy Mater. *11*, 2003532.
90. Haeussler, A., Julbe, A., and Abanades, S. (2022). Investigation of reactive perovskite materials for solar fuel production via two-step redox cycles: thermochemical activity, thermodynamic properties and reduction kinetics. Mater. Chem. Phys. *276*, 125358.
91. Boretti, A. (2021). Perspectives of Perovskites for Solar Thermochemical Splitting of CO_2 or H_2O Molecules. Adv. Energy and Sustain. Res. *2*, 2100067.
92. Roeb, M., Säck, J.P., Rietbrock, P., Prahl, C., Schreiber, H., Neises, M., de Oliveira, L., Graf, D., Ebert, M., Reinalter, W., et al. (2011). Test operation of a 100 kW pilot plant for solar hydrogen production from water on a solar tower. Sol. Energy *85*, 634–644.
93. Aoki, H., Kaneko, H., Hasegawa, N., Ishihara, H., Suzuki, A., and Tamaura, Y. (2004). The $ZnFe_2O_4$/(ZnO+Fe_3O_4) system for H_2 production using concentrated solar energy. Solid State Ionics *172*, 113–116.
94. Agrafiotis, C., Zygogianni, A., Pagkoura, C., Kostoglou, M., and Konstandopoulos, A.G. (2013). Hydrogen production via solar-aided water splitting thermochemical cycles with nickel ferrite: experiments and modeling. AIChE J. *59*, 1213–1225.
95. Miller, J.E., Allendorf, M.D., Diver, R.B., Evans, L.R., Siegel, N.P., and Stuecker, J.N. (2008). Metal oxide composites and structures for ultra-high temperature solar thermochemical cycles. J. Mater. Sci. *43*, 4714–4728.
96. Tamaura, Y., Kojima, M., Sano, T., Ueda, Y., Hasegawa, N., and Tsuji, M. (1998). Thermodynamic evaluation of water splitting by a cation-excessive (Ni, Mn) ferrite. Int. J. Hydrogen Energy *23*, 1185–1191.
97. Inoue, M., Hasegawa, N., Uehara, R., Gokon, N., Kaneko, H., and Tamaura, Y. (2004). Solar hydrogen generation with H_2O/ZnO/$MnFe_2O_4$ system. Sol. Energy *76*, 309–315.
98. Fresno, F., Fernández-Saavedra, R., Belén Gómez-Mancebo, M., Vidal, A., Sánchez, M., Isabel Rucandio, M., Quejido, A.J., and Romero, M. (2009). Solar hydrogen production by two-step thermochemical cycles: Evaluation of the activity of commercial ferrites. Int. J. Hydrogen Energy *34*, 2918–2924.
99. Kostoglou, M., Lorentzou, S., and Konstandopoulos, A.G. (2014). Improved kinetic model for water splitting thermochemical cycles using Nickel Ferrite. Int. J. Hydrogen Energy *39*, 6317–6327.
100. Gokon, N., Hasegawa, T., Takahashi, S., and Kodama, T. (2008). Thermochemical two-step water-splitting for hydrogen production using Fe-YSZ particles and a ceramic foam device. Energy *33*, 1407–1416.
101. Coker, E.N., Ambrosini, A., Rodriguez, M.A., and Miller, J.E. (2011). Ferrite-YSZ composites for solar thermochemical production of synthetic fuels: in operando characterization of CO_2 reduction. J. Mater. Chem. *21*, 10767–10776.
102. Coker, E.N., Ohlhausen, J.A., Ambrosini, A., and Miller, J.E. (2012). Oxygen transport and isotopic exchange in iron oxide/YSZ thermochemically-active materials via splitting of $C(^{18}O)_2$ at high temperature studied by thermogravimetric analysis and secondary ion mass spectrometry. J. Mater. Chem. *22*, 6726–6732.
103. Go, K., Son, S., and Kim, S. (2008). Reaction kinetics of reduction and oxidation of metal oxides for hydrogen production. Int. J. Hydrogen Energy *33*, 5986–5995.
104. Neises, M., Roeb, M., Schmücker, M., Sattler, C., and Pitz-Paal, R. (2010). Kinetic investigations of the hydrogen production step of a thermochemical cycle using mixed iron oxides coated on ceramic substrates. Int. J. Energ. Res. *34*, 651–661.
105. Scheffe, J.R., Jacot, R., Patzke, G.R., and Steinfeld, A. (2013). Synthesis, characterization, and thermochemical redox performance of Hf^{4+}, Zr^{4+}, and Sc^{3+} doped ceria for splitting CO_2. J. Phys. Chem. C *117*, 24104–24114.
106. Takacs, M., Scheffe, J.R., and Steinfeld, A. (2015). Oxygen nonstoichiometry and thermodynamic characterization of Zr doped ceria in the 1573–1773 K temperature range. Phys. Chem. Chem. Phys. *17*, 7813–7822.
107. Le Gal, A., and Abanades, S. (2012). Dopant incorporation in ceria for enhanced water-splitting activity during solar thermochemical hydrogen generation. J. Phys. Chem. C *116*, 13516–13523.
108. Meng, Q.L., Lee, C.i., Kaneko, H., and Tamaura, Y. (2012). Solar thermochemical process for hydrogen production via two-step water splitting cycle based on $Ce_{1-x}Pr_xO_{2-\delta}$ redox reaction. Thermochim. Acta *532*, 134–138.
109. Bhosale, R., and Takalkar, G. (2018). Nanostructured co-precipitated $Ce_{0.9}Ln_{0.1}O_2$ (Ln= La, Pr, Sm, Nd, Gd, Tb, Dy, or Er) for thermochemical conversion of CO_2. Ceram. Int. *44*, 16688–16697.
110. Zhu, L., and Lu, Y. (2018). Reactivity and efficiency of ceria-based oxides for solar

CO_2 splitting via isothermal and near-isothermal cycles. Energ. Fuel *32*, 736–746.
111. Zhu, L., Lu, Y., and Li, F. (2018). Reactivity of Ni, Cr and Zr doped ceria in CO_2 splitting for CO production via two-step thermochemical cycle. Int. J. Hydrogen Energy *43*, 13754–13763.
112. Takalkar, G.D., Bhosale, R.R., Kumar, A., AlMomani, F., Khraisheh, M., Shakoor, R.A., and Gupta, R.B. (2018). Transition metal doped ceria for solar thermochemical fuel production. Sol. Energy *172*, 204–211.
113. Takalkar, G., Bhosale, R.R., Rashid, S., AlMomani, F., Shakoor, R.A., and Al Ashraf, A. (2020). Application of Li-Mg-Ba-Sr-Ca- and Sn-doped ceria for solar-driven thermochemical conversion of carbon dioxide. J. Mater. Sci. *55*, 11797–11807.
114. Arifin, D., Ambrosini, A., Wilson, S.A., Mandal, B., Muhich, C.L., and Weimer, A.W. (2020). Investigation of Zr, Gd/Zr, and Pr/Zr–doped ceria for the redox splitting of water. Int. J. Hydrogen Energy *45*, 160–174.
115. Portarapillo, M., Russo, D., Landi, G., Luciani, G., and Di Benedetto, A. (2021). K-doped CeO_2–ZrO_2 for CO_2 thermochemical catalytic splitting. RSC Adv. *11*, 39420–39427.
116. Portarapillo, M., Landi, G., Luciani, G., Imparato, C., Vitiello, G., Deorsola, F.A., Aronne, A., and Di Benedetto, A. (2022). Redox behavior of potassium doped and transition metal co-doped $Ce_{0.75}Zr_{0.25}O_2$ for thermochemical H_2O/CO_2 splitting. RSC Adv. *12*, 14645–14654.
117. Chueh, W.C., and Haile, S.M. (2010). A thermochemical study of ceria: exploiting an old material for new modes of energy conversion and CO_2 mitigation. Philos. T. R. Soc A. *368*, 3269–3294.
118. Orfila, M., Sanz, D., Linares, M., Molina, R., Sanz, R., Marugán, J., and Botas, J.Á. (2021). H_2 production by thermochemical water splitting with reticulated porous structures of ceria-based mixed oxide materials. Int. J. Hydrogen Energy *46*, 17458–17471.
119. Lorentzou, S., Pagkoura, C., Zygogianni, A., Karagiannakis, G., and Konstandopoulos, A. (2017). Thermochemical cycles over redox structured reactors. Int. J. Hydrogen Energy *42*, 19664–19682.
120. Furler, P., Scheffe, J., Gorbar, M., Moes, L., Vogt, U., and Steinfeld, A. (2012). Solar thermochemical CO_2 splitting utilizing a reticulated porous ceria redox system. Energy Fuels *26*, 7051–7059.
121. Furler, P., Scheffe, J., Marxer, D., Gorbar, M., Bonk, A., Vogt, U., and Steinfeld, A. (2014). Thermochemical CO_2 splitting via redox cycling of ceria reticulated foam structures with dual-scale porosities. Phys. Chem. Chem. Phys. *16*, 10503–10511.
122. Haeussler, A., Abanades, S., Julbe, A., Jouannaux, J., Drobek, M., Ayral, A., and Cartoixa, B. (2020). Remarkable performance of microstructured ceria foams for thermochemical splitting of H_2O and CO_2 in a novel high–temperature solar reactor. Chem. Eng. Res. Des. *156*, 311–323.
123. Haeussler, A., Abanades, S., Julbe, A., Jouannaux, J., and Cartoixa, B. (2020). Solar thermochemical fuel production from H_2O and CO_2 splitting via two-step redox cycling of reticulated porous ceria structures integrated in a monolithic cavity-type reactor. Energy *201*, 117649.
124. Marxer, D., Furler, P., Takacs, M., and Steinfeld, A. (2017). Solar thermochemical splitting of CO_2 into separate streams of CO and O_2 with high selectivity, stability, conversion, and efficiency. Energy Environ. Sci. *10*, 1142–1149.
125. Costa Oliveira, F.A., Barreiros, M.A., Abanades, S., Caetano, A.P., Novais, R.M., and Pullar, R.C. (2018). Solar thermochemical CO_2 splitting using cork-templated ceria ecoceramics. J. CO_2 Util. *26*, 552–563.
126. Costa Oliveira, F.A., Barreiros, M.A., Haeussler, A., Caetano, A.P.F., Mouquinho, A.I., Oliveira e Silva, P.M., Novais, R.M., Pullar, R.C., and Abanades, S. (2020). High performance cork-templated ceria for solar thermochemical hydrogen production via two-step water-splitting cycles. Sustain. Energy Fuels *4*, 3077–3089.
127. Haeussler, A., Abanades, S., Costa Oliveira, F.A., Barreiros, M.A., Caetano, A.P.F., Novais, R.M., and Pullar, R.C. (2020). Solar redox cycling of ceria structures based on fiber boards, foams, and biomimetic cork-derived ecoceramics for two-step thermochemical H_2O and CO_2 splitting. Energy Fuels *34*, 9037–9049.
128. Abanades, S., Haeussler, A., and Julbe, A. (2021). Synthesis and thermochemical redox cycling of porous ceria microspheres for renewable fuels production from solar-aided water-splitting and CO_2 utilization. Appl. Phys. Lett. *119*, 023902.
129. Abanades, S., Haeussler, A., and Julbe, A. (2021). Thermochemical solar-driven reduction of CO_2 into separate streams of CO and O_2 via an isothermal oxygen-conducting ceria membranec reactor. Chem. Eng. J. *422*, 130026.
130. Haeussler, A., and Abanades, S. (2021). Additive manufacturing and two-step redox cycling of ordered porous ceria structures for solar-driven thermochemical fuel production. Chem. Eng. Sci. *246*, 116999.
131. Abanades, S., and Haeussler, A. (2021). Two-step thermochemical cycles using fibrous ceria pellets for H_2 production and CO_2 reduction in packed-bed solar reactors. Sustain. Mater. Techno. *29*, e00328.
132. Hoes, M., Ackermann, S., Theiler, D., Furler, P., and Steinfeld, A. (2019). Additive-manufactured ordered porous structures made of ceria for concentrating solar applications. Energy Tech. *7*, 1900484.
133. Haile, S.M. (2003). Fuel cell materials and components. Acta Mater. *51*, 5981–6000.
134. Scheffe, J.R., Weibel, D., and Steinfeld, A. (2013). Lanthanum–strontium–manganese perovskites as redox materials for solar thermochemical splitting of H_2O and CO_2. Energy Fuels *27*, 4250–4257.
135. Ezbiri, M., Takacs, M., Stolz, B., Lungthok, J., Steinfeld, A., and Michalsky, R. (2017). Design principles of perovskites for solar-driven thermochemical splitting of CO_2. J. Mater. Chem. A. *5*, 15105–15115.
136. Emery, A.A., Saal, J.E., Kirklin, S., Hegde, V.I., and Wolverton, C. (2016). High-throughput computational screening of perovskites for thermochemical water splitting applications. Chem. Mater. *28*, 5621–5634.
137. Fedunik-Hofman, L., Bayon, A., and Donne, S.W. (2019). Kinetics of solid-gas reactions and their application to carbonate looping systems. Energies *12*, 2981.
138. Bulfin, B., Lange, M., de Oliveira, L., Roeb, M., and Sattler, C. (2016). Solar thermochemical hydrogen production using ceria zirconia solid solutions: efficiency analysis. Int. J. Hydrogen Energy *41*, 19320–19328.
139. Bulfin, B., Hoffmann, L., de Oliveira, L., Knoblauch, N., Call, F., Roeb, M., Sattler, C., and Schmücker, M. (2016). Statistical thermodynamics of non-stoichiometric ceria and ceria zirconia solid solutions. Phys. Chem. Chem. Phys. *18*, 23147–23154.
140. de la Calle, A., and Bayon, A. (2019). Annual performance of a thermochemical solar syngas production plant based on non-stoichiometric CeO_2. Int. J. Hydrogen Energy *44*, 1409–1424.
141. Bayon, A., and Calle, A.d.l. (2018). Dynamic modelling of a continuous hydrogen production plant based on a CeO2 thermochemical cycle. AIP Conference Proceedings, AIP Publishing LLC. 130002. https://doi.org/10.1063/1.5067136.
142. Muhich, C.L., Blaser, S., Hoes, M.C., and Steinfeld, A. (2018). Comparing the solar-to-fuel energy conversion efficiency of ceria and perovskite based thermochemical redox cycles for splitting H_2O and CO_2. Int. J. Hydrogen Energy *43*, 18814–18831.
143. Gao, K., Liu, X., Wang, T., Zhu, Z., Li, P., Zheng, H., Song, C., Xuan, Y., Li, Y., and Ding, Y. (2021). Sr-doped $SmMnO_3$ perovskites for high-performance near-isothermal solar thermochemical CO_2-to-fuel conversion. Sustain. Energy Fuels *5*, 4295–4310.
144. Barcellos, D.R., Coury, F.G., Emery, A., Sanders, M., Tong, J., McDaniel, A., Wolverton, C., Kaufman, M., and O'Hayre, R. (2019). Phase Identification of the Layered Perovskite $Ce_xSr_{2-x}MnO_4$ and Application for Solar Thermochemical Water Splitting. Inorg. Chem. *58*, 7705–7714.
145. Sai Gautam, G., Stechel, E.B., and Carter, E.A. (2020). Exploring Ca–Ce–M–O (M= 3d Transition Metal) Oxide Perovskites for Solar Thermochemical Applications. Chem. Mater. *32*, 9964–9982.
146. Qian, X., He, J., Mastronardo, E., Baldassarri, B., Wolverton, C., and Haile, S.M. (2020). Favorable redox thermodynamics of $SrTi_{0.5}Mn_{0.5}O_{3-\delta}$ in solar thermochemical water splitting. Chem. Mater. *32*, 9335–9346.
147. Qian, X., He, J., Mastronardo, E., Baldassarri, B., Yuan, W., Wolverton, C., and Haile, S.M. (2021). Outstanding properties and performance of $CaTi_{0.5}Mn_{0.5}O_{3-\delta}$ for solar-driven thermochemical hydrogen production. Matter *4*, 688–708.
148. Carrillo, A.J., Kim, K.J., Hood, Z.D., Bork, A.H., and Rupp, J.L.M. (2020). $La_{0.6}Sr_{0.4}Cr_{0.8}Co_{0.2}O_3$ perovskite decorated with exsolved Co nanoparticles for stable CO_2 splitting and syngas production. ACS Appl. Energy Mater. *3*, 4569–4579.
149. Heo, S.J., Sanders, M., O'Hayre, R., and Zakutayev, A. (2021). Double-site substitution of Ce into (Ba, Sr) MnO_3 perovskites for solar thermochemical hydrogen production. ACS Energy Lett. *6*, 3037–3043.
150. Carrillo, A.J., Bork, A.H., Moser, T., Sediva, E., Hood, Z.D., and Rupp, J.L.M. (2019). Modifying $La_{0.6}Sr_{0.4}MnO_3$ perovskites with Cr incorporation for fast isothermal CO_2-splitting kinetics in solar-driven thermochemical cycles. Adv. Energy Mater. *9*, 1803886.
151. Şanlı, S.B., and Pişkin, B. (2022). Effect of B-site Al substitution on hydrogen production of $La_{0.4}Sr_{0.6}Mn_{1-x}Al_x$ (x = 0.4, 0.5

and 0.6) perovskite oxides. Int. J. Hydrogen Energy *47*, 19411–19421.
152. Demont, A., Abanades, S., and Beche, E. (2014). Investigation of perovskite structures as oxygen-exchange redox materials for hydrogen production from thermochemical two-step water-splitting cycles. J. Phys. Chem. C *118*, 12682–12692.
153. Gálvez, M.E., Jacot, R., Scheffe, J., Cooper, T., Patzke, G., and Steinfeld, A. (2015). Physico-chemical changes in Ca, Sr and Al-doped La–Mn–O perovskites upon thermochemical splitting of CO_2 via redox cycling. Phys. Chem. Chem. Phys. *17*, 6629–6634.
154. Yang, C.K., Yamazaki, Y., Aydin, A., and Haile, S.M. (2014). Thermodynamic and kinetic assessments of strontium-doped lanthanum manganite perovskites for two-step thermochemical water splitting. J. Mater. Chem. A *2*, 13612–13623.
155. Wang, L., Al-Mamun, M., Liu, P., Wang, Y., Yang, H.G., and Zhao, H. (2018). Notable hydrogen production on $La_xCa_{1-x}CoO_3$ perovskites via two-step thermochemical water splitting. J. Mater. Sci. *53*, 6796–6806.
156. Wang, L., Al-Mamun, M., Zhong, Y.L., Liu, P., Wang, Y., Yang, H.G., and Zhao, H. (2018). Enhanced thermochemical water splitting through formation of oxygen vacancy in $La_{0.6}Sr_{0.4}BO_{3-\delta}$ (B = Cr, Mn, Fe, Co, and Ni) Perovskites. ChemPlusChem *83*, 924–928.
157. Orfila, M., Linares, M., Molina, R., Botas, J.Á., Sanz, R., and Marugán, J. (2016). Perovskite materials for hydrogen production by thermochemical water splitting. Int. J. Hydrogen Energy *41*, 19329–19338.
158. Nair, M., and Abanades, S. (2018). Experimental screening of perovskite oxides as efficient redox materials for solar thermochemical CO_2 conversion. Sustain. Energy Fuels *2*, 843–854.
159. Nair, M.M., and Abanades, S. (2016). Insights into the redox performance of non–stoichiometric lanthanum manganite perovskites for solar thermochemical CO_2 splitting. ChemistrySelect *1*, 4449–4457.
160. Rodenbough, P.P., and Chan, S.W. (2018). Thermal oxygen exchange cycles in mixed manganese perovskites. Ceram. Int. *44*, 1343–1347.
161. Dey, S., Naidu, B.S., and Rao, C.N.R. (2015). $Ln_{0.5}A_{0.5}MnO_3$ (Ln = Lanthanide, A = Ca, Sr) perovskites exhibiting remarkable performance in the thermochemical generation of CO and H_2 from CO_2 and H_2O. Chemistry *21*, 7077–7081.
162. R Barcellos, D., Sanders, M.D., Tong, J., McDaniel, A.H., and O'Hayre, R.P. (2018). $BaCe_{0.25}Mn_{0.75}O_{3-\delta}$—A promising perovskite-type oxide for solar thermochemical hydrogen production. Energy Environ. Sci. *11*, 3256–3265.
163. Kabir, E., Kumar, P., Kumar, S., Adelodun, A.A., and Kim, K.H. (2018). Solar energy: Potential and future prospects. Renew. Sustain. Energy Rev. *82*, 894–900.
164. Boretti, A., Nayfeh, J., and Al-Maaitah, A. (2021). Hydrogen production by solar thermochemical water-splitting cycle via a beam down concentrator. Front. Energy Res. *9*, 116.
165. Islam, M.T., Huda, N., Abdullah, A., and Saidur, R. (2018). A comprehensive review of state-of-the-art concentrating solar power (CSP) technologies: Current status and research trends. Renew. Sustain. Energy Rev. *91*, 987–1018.
166. Yaqi, L., Yaling, H., and Weiwei, W. (2011). Optimization of solar-powered Stirling heat engine with finite-time thermodynamics. Renew. Energy *36*, 421–427.
167. He, Y.L., Wang, K., Qiu, Y., Du, B.C., Liang, Q., and Du, S. (2019). Review of the solar flux distribution in concentrated solar power: non-uniform features, challenges, and solutions. Appl. Therm. Eng. *149*, 448–474.
168. López, O., Baños, A., and Arenas, A. (2020). On the thermal performance of flat and cavity receivers for a parabolic dish concentrator and low/medium temperatures. Sol. Energy *199*, 911–923.
169. Dähler, F., Wild, M., Schäppi, R., Haueter, P., Cooper, T., Good, P., Larrea, C., Schmitz, M., Furler, P., and Steinfeld, A. (2018). Optical design and experimental characterization of a solar concentrating dish system for fuel production via thermochemical redox cycles. Sol. Energy *170*, 568–575.
170. Kim, K., Siegel, N., Kolb, G., Rangaswamy, V., and Moujaes, S.F. (2009). A study of solid particle flow characterization in solar particle receiver. Sol. Energy *83*, 1784–1793.
171. Z'Graggen, A., and Steinfeld, A. (2008). A two-phase reactor model for the steam-gasification of carbonaceous materials under concentrated thermal radiation. Chem. Eng. Process *47*, 655–662.
172. Zhang, H., and Smith, J.D. (2019). Investigating influences of geometric factors on a solar thermochemical reactor for two-step carbon dioxide splitting via CFD models. Sol. Energy *188*, 935–950.
173. Binotti, M., Marcoberardino, G.D., Biassoni, M., Manzolini, G. (2017). Solar hydrogen production with cerium oxides thermochemical cycle. AIP Conference Proceedings, AIP Publishing LLC. 100002. https://doi.org/10.1063/1.4984459.
174. Mehrpooya, M., Tabatabaei, S.H., Pourfayaz, F., and Ghorbani, B. (2021). High-temperature hydrogen production by solar thermochemical reactors, metal interfaces, and nanofluid cooling. J. Therm. Anal. Calorim. *145*, 2547–2569.
175. Hoes, M., Muhich, C.L., Jacot, R., Patzke, G.R., and Steinfeld, A. (2017). Thermodynamics of paired charge-compensating doped ceria with superior redox performance for solar thermochemical splitting of H_2O and CO_2. J. Mater. Chem. A. *5*, 19476–19484.
176. Rytter, E., Soušková, K., Lundgren, M.K., Ge, W., Nannestad, Å.D., Venvik, H.J., and Hillestad, M. (2016). Process concepts to produce syngas for Fischer–Tropsch fuels by solar thermochemical splitting of water and/or CO_2. Fuel Process. Technol. *145*, 1–8.
177. Kong, H., Kong, X., Wang, H., and Wang, J. (2019). A strategy for optimizing efficiencies of solar thermochemical fuel production based on nonstoichiometric oxides. Int. J. Hydrogen Energy *44*, 19585–19594.
178. Diver, R.B., Miller, J.E., Siegel, N.P., and Moss, T.A. (2010). Testing of a CR5 solar thermochemical heat engine prototype. ASME 2010 4th International Conference on Energy Sustainability *2*, 97–104.
179. Schäppi, R., Rutz, D., Basler, P., Muroyama, A., Haueter, P., Furler, P., and Steinfeld, A. (2019). Solar thermochemical splitting of CO2 in a modular solar dish-reactor system. Proc. ISES-SWC2019 Solar World Congress. 4-7. https://doi.org/10.18086/swc.2019.24.08.
180. Alexopoulos, S., and Hoffschmidt, B. (2017). Advances in solar tower technology. WIRES Energy Environ *6*, e217.
181. Segal, A., and Epstein, M. (2001). The optics of the solar tower reflector. Sol. Energy *69*, 229–241.
182. Milidonis, K., Blanco, M.J., Grigoriev, V., Panagiotou, C.F., Bonanos, A.M., Constantinou, M., Pye, J., and Asselineau, C.A. (2021). Review of application of AI techniques to Solar Tower Systems. Sol. Energy *224*, 500–515.
183. Srilakshmi, G., Venkatesh, V., Thirumalai, N., and Suresh, N. (2015). Challenges and opportunities for Solar Tower technology in India. Renew. Sustain. Energy Rev. *45*, 698–709.
184. Wei, X., Lu, Z., Wang, Z., Yu, W., Zhang, H., and Yao, Z. (2010). A new method for the design of the heliostat field layout for solar tower power plant. Renew. Energy *35*, 1970–1975.
185. Schlaich, J., Bergermann, R., Schiel, W., and Weinrebe, G. (2005). Design of commercial solar updraft tower systems-utilization of solar induced convective flows for power generation. J. Sol. Energy Eng. *127*, 117–124.
186. Lilliestam, J., Labordena, M., Patt, A., and Pfenninger, S. (2017). Empirically observed learning rates for concentrating solar power and their responses to regime change. Nat. Energy *2*, 17094.
187. Behar, O., Khellaf, A., and Mohammedi, K. (2013). A review of studies on central receiver solar thermal power plants. Renew. Sustain. Energy Rev. *23*, 12–39.
188. Wei, X., Lu, Z., Lin, Z., Zhang, H., and Ni, Z. (2007). Optimization procedure for design of heliostat field layout of a 1MWe solar tower thermal power plant. Solid State Lighting and Solar Energy Technologies, SPIE *6841*, 236–245.
189. Wei, X., Herbst, A., Ma, D., Aiken, J., and Li, L. (2011). Tracking and ray tracing equations for the target-aligned heliostat for solar tower power plants. Renew. Energ. *10*, 2687–2702.
190. Wei, X., Lu, Z., Yu, W., and Wang, Z. (2010). A new code for the design and analysis of the heliostat field layout for power tower system. Sol. Energy *84*, 685–690.
191. Wei, X., Lu, Z., Yu, W., and Xu, W. (2013). Ray tracing and simulation for the beam-down solar concentrator. Renew. Energy *50*, 161–167.
192. Kolb, G.J., Diver, R.B., and Siegel, N. (2007). Central-station solar hydrogen power plant. J. Sol. Energy Eng. *129*, 179–183.
193. Martinek, J., Channel, M., Lewandowski, A., and Weimer, A.W. (2010). Considerations for the design of solar-thermal chemical processes. J. Sol. Energy Eng. *132*, 031013.
194. Roca, L., de la Calle, A., and Yebra, L.J. (2013). Heliostat-field gain-scheduling control applied to a two-step solar hydrogen production plant. Appl. Energy *103*, 298–305.
195. Agrafiotis, C., von Storch, H., Roeb, M., and Sattler, C. (2014). Solar thermal reforming of methane feedstocks for hydrogen and syngas production—A review. Renew. Sustain. Energy Rev. *29*, 656–682.
196. Kodama, T., Bellan, S., Gokon, N., and Cho, H.S. (2017). Particle reactors for solar thermochemical processes. Sol. Energy *156*, 113–132.
197. Ávila-Marín, A.L. (2011). Volumetric receivers in Solar Thermal Power Plants with Central

Receiver System technology: A review. Sol. Energy *85*, 891–910.
198. Bailera, M., Lisbona, P., Romeo, L.M., and Espatolero, S. (2017). Power to Gas projects review: Lab, pilot and demo plants for storing renewable energy and CO_2. Renew. Sustain. Energy Rev. *69*, 292–312.
199. Schunk, L., Lipiński, W., and Steinfeld, A. (2009). Heat transfer model of a solar receiver-reactor for the thermal dissociation of ZnO—Experimental validation at 10 kW and scale-up to 1 MW. Chem. Eng. J. *150*, 502–508.
200. Koepf, E., Advani, S.G., Steinfeld, A., and Prasad, A.K. (2012). A novel beam-down, gravity-fed, solar thermochemical receiver/reactor for direct solid particle decomposition: Design, modeling, and experimentation. Int. J. Hydrogen Energy *37*, 16871–16887.
201. Ermanoski, I., Siegel, N.P., and Stechel, E.B. (2013). A new reactor concept for efficient solar-thermochemical fuel production. J. Sol. Energy Eng. *135*, 031002.
202. Lapp, J., Davidson, J.H., and Lipiński, W. (2013). Heat transfer analysis of a solid-solid heat recuperation system for solar-driven nonstoichiometric redox cycles. J. Sol. Energ-T. ASME. *135*, 031004.
203. Diver, R.B., Miller, J.E., Allendorf, M.D., Siegel, N.P., and Hogan, R.E. (2008). Solar thermochemical water-splitting ferrite-cycle heat engines. J. Sol. Energy Eng. *130*, 041001.
204. Haueter, P., Moeller, S., Palumbo, R., and Steinfeld, A. (1999). The production of zinc by thermal dissociation of zinc oxide—solar chemical reactor design. Sol. Energy *67*, 161–167.
205. Villasmil, W., Brkic, M., Wuillemin, D., Meier, A., and Steinfeld, A. (2013). Pilot Scale Demonstration of a 100-kWth Solar Thermochemical Plant for the Thermal Dissociation of ZnO. J. Sol. Energy Eng. *136*, 011016.
206. Chambon, M., Abanades, S., and Flamant, G. (2010). Design of a Lab-Scale Rotary Cavity-Type Solar Reactor for Continuous Thermal Dissociation of Volatile Oxides Under Reduced Pressure. J. Sol. Energy Eng. *132*, 021006.
207. Chambon, M., Abanades, S., and Flamant, G. (2011). Thermal dissociation of compressed ZnO and SnO_2 powders in a moving-front solar thermochemical reactor. AIChE J. *57*, 2264–2273.
208. Perkins, C., Lichty, P.R., and Weimer, A.W. (2008). Thermal ZnO dissociation in a rapid aerosol reactor as part of a solar hydrogen production cycle. Int. J. Hydrogen Energy *33*, 499–510.
209. Gokon, N., Mataga, T., Kondo, N., and Kodama, T. (2011). Thermochemical two-step water splitting by internally circulating fluidized bed of $NiFe_2O_4$ particles: Successive reaction of thermal-reduction and water-decomposition steps. Int. J. Hydrogen Energy *36*, 4757–4767.
210. Kaneko, H., Miura, T., Fuse, A., Ishihara, H., Taku, S., Fukuzumi, H., Naganuma, Y., and Tamaura, Y. (2007). Rotary-Type Solar Reactor for Solar Hydrogen Production with Two-step Water Splitting Process. Energ. Fuel *21*, 2287–2293.
211. Ermanoski, I., Siegel, N.P., and Stechel, E.B. (2013). A New Reactor Concept for Efficient Solar-Thermochemical Fuel Production. J. Sol. Energy Eng. *135*, 031002.
212. Kaneko, H., Fuse, A., Miura, T., Ishihara, H., and Tamara, Y. (2006). Two-Step Water Splitting with Concentrated Solar Heat Using Rotary-Type Solar Furnace. 13th International Symposium on Concentrated Solar Power and Chemical Energy Technologies, Seville (Spain). https://www.osti.gov/etdeweb/biblio/20811738.
213. Diver, R.B., Miller, J.E., Allendorf, M.D., Siegel, N.P., and Hogan, R.E. (2008). Solar Thermochemical Water-Splitting Ferrite-Cycle Heat Engines. J. Sol. Energy Eng. *130*, 041001.
214. Miller, J.E., Evans, L.R., Stuecker, J.N., Allendorf, M.D., Siegel, N.P., and Diver, R.B. (2006). Materials Development for the CR5 Solar Thermochemical Heat Engine. Sol. Energy, 311–320.
215. Johnson, T.A., Hogan, J.R.E., McDaniel, A.H., Siegel, N.P., Dedrick, D.E., Stechel, E.B., Diver, J.R.B., Miller, J.E., Allendorf, M.D., Ambrosini, A., Coker, E.N., Staiger, C.L., Chen, K.S., Ermanoski, I., and Kellog, G.L. (2012). Reimagining liquid transportation fuels: sunshine to petrol. Sandia National Laboratories (SNL), Albuquerque, NM, and Livermore, CA (United States). https://doi.org/10.2172/1035344.
216. Miller, J. E., Allendorf, M.A., Ambrosini, A., Coker, E.N., Diver, R.B., Ermanoski, I., Evans, L.R., Hogan, R.E., McDaniel, A.H. (2012). Development and assessment of solar-thermal-activated fuel production. Phase 1, summary. Sandia National Laboratories (SNL), Albuquerque, NM, and Livermore, CA (United States). https://www.osti.gov/servlets/purl/1055617.
217. Kim, J., Miller, J.E., Maravelias, C.T., and Stechel, E.B. (2013). Comparative analysis of environmental impact of S2P (Sunshine to Petrol) system for transportation fuel production. Appl. Energy *111*, 1089–1098.
218. Tamaura, Y., Steinfeld, A., Kuhn, P., and Ehrensberger, K. (1995). Production of solar hydrogen by a novel, 2-step, water-splitting thermochemical cycle. Energy *20*, 325–330.
219. Gokon, N., Takahashi, S., Yamamoto, H., and Kodama, T. (2008). Thermochemical two-step water-splitting reactor with internally circulating fluidized bed for thermal reduction of ferrite particles. Int. J. Hydrogen Energy *33*, 2189–2199.
220. Gokon, N., Takahashi, S., Yamamoto, H., and Kodama, T. (2009). New solar water-splitting reactor with ferrite particles in an internally circulating fluidized bed. J. Sol. Energy Eng. *131*, 011007.
221. Kodama, T., Enomoto, S.i., Hatamachi, T., and Gokon, N. (2008). Application of an internally circulating fluidized bed for windowed solar chemical reactor with direct irradiation of reacting particles. J. Sol. Energy Eng. *130*, 014504.
222. Roeb, M., Neises, M., Säck, J.P., Rietbrock, P., Monnerie, N., Dersch, J., Schmitz, M., and Sattler, C. (2009). Operational strategy of a two-step thermochemical process for solar hydrogen production. Int. J. Hydrogen Energy *34*, 4537–4545.
223. Neises, M., Goehring, F., Roeb, M., Sattler, C., and Pitz-Paal, R. (2009). Simulation of a solar receiver-reactor for hydrogen production. Proceedings of the ASME 2009 3th International Conference Energy Sustainability, 295–304.
224. Agrafiotis, C., Roeb, M., Konstandopoulos, A.G., Nalbandian, L., Zaspalis, V., Sattler, C., Stobbe, P., and Steele, A. (2005). Solar water splitting for hydrogen production with monolithic reactors. Sol. Energy *79*, 409–421.
225. Roeb, M., Monnerie, N., Schmitz, M., Sattler, C., Konstandopoulos, A., Agrafiotis, C., Zaspalis, V., Nalbandian, L., Steele, A., and Stobbe, P. (2006). Thermo-chemical production of hydrogen from water by metal oxides fixed on ceramic substrates. Proceedings of the 16th World Hydrogen Energy Conference, Lyon, France *13*, 16–27. https://www.researchgate.net/publication/224985351.
226. Walker, L.S., Miller, J.E., Hilmas, G.E., Evans, L.R., and Corral, E.L. (2012). Coextrusion of zirconia–iron oxide honeycomb substrates for solar-based thermochemical generation of carbon monoxide for renewable fuels. Energy Fuels *26*, 712–721.
227. Houaijia, A., Sattler, C., Roeb, M., Lange, M., Breuer, S., and Säck, J.P. (2013). Analysis and improvement of a high-efficiency solar cavity reactor design for a two-step thermochemical cycle for solar hydrogen production from water. Sol. Energy *97*, 26–38.
228. Gokon, N., Kodama, T., Imaizumi, N., Umeda, J., and Seo, T. (2011). Ferrite/zirconia-coated foam device prepared by spin coating for solar demonstration of thermochemical water-splitting. Int. J. Hydrogen Energy *36*, 2014–2028.
229. Gokon, N., Mizuno, T., Takahashi, S., and Kodama, T. (2006). A two-step water splitting with ferrite particles and its new reactor concept using an internally circulating fludized-bed. Sol. Energy, 205–214.
230. Ávila-Marín, A.L. (2011). Volumetric receivers in solar thermal power plants with central receiver system technology: a review. Sol. Energy *85*, 891–910.
231. Agrafiotis, C., Mavroidis, I., Konstandopoulos, A., Hoffschmidt, B., Stobbe, P., Romero, M., and Fernandez-Quero, V. (2007). Evaluation of porous silicon carbide monolithic honeycombs as volumetric receivers/collectors of concentrated solar radiation. Sol. Energ. Mat. Sol. C. *91*, 474–488.
232. Roeb, M., Sattler, C., Klüser, R., Monnerie, N., de Oliveira, L., Konstandopoulos, A.G., Agrafiotis, C., Zaspalis, V.T., Nalbandian, L., Steele, A., and Stobbe, P. (2006). Solar Hydrogen Production by a Two-step Cycle Based on Mixed Iron Oxides. J. Sol. Energy Eng. *128*, 125–133.
233. Hoffschmidt, B., Te'llez, F.M., Valverde, A., Ferna'ndez, J., and Ferna'ndez, V. (2003). Performance evaluation of the 200-kW th HiTRec-II open volumetric air receiver. J. Sol. Energy Eng. *125*, 87–94.
234. Heck, R.M., Gulati, S., and Farrauto, R.J. (2001). The application of monoliths for gas phase catalytic reactions. Chem. Eng. J. *82*, 149–156.
235. Levy, M., Rubin, R., Rosin, H., and Levitan, R. (1992). Methane reforming by direct solar irradiation of the catalyst. Energy *17*, 749–756.
236. Furler, P., Scheffe, J.R., and Steinfeld, A. (2012). Syngas production by simultaneous splitting of H_2O and CO_2 via ceria redox reactions in a high-temperature solar reactor. Energy Environ. Sci. *5*, 6098–6103.
237. Brendelberger, S., Vieten, J., Vidyasagar, M.J., Roeb, M., and Sattler, C. (2018). Demonstration of thermochemical oxygen pumping for atmosphere control in

reduction reactions. Sol. Energy *170*, 273–279.

238. Bai, W., Huang, H., Suter, C., Haussener, S., and Lin, M. (2022). Enhanced Solar-to-Fuel Efficiency of Ceria-Based Thermochemical Cycles via Integrated Electrochemical Oxygen Pumping. ACS Energy Lett. *7*, 2711–2716.
239. Haeussler, A., Abanades, S., Jouannaux, J., and Julbe, A. (2021). Demonstration of a ceria membrane solar reactor promoted by dual perovskite coatings for continuous and isothermal redox splitting of CO_2 and H_2O. J. Memb. Sci. *634*, 119387.
240. Tou, M., Michalsky, R., and Steinfeld, A. (2017). Solar-driven thermochemical splitting of CO_2 and in situ separation of CO and O_2 across a ceria redox membrane reactor. Joule *1*, 146–154.
241. Tou, M., Jin, J., Hao, Y., Steinfeld, A., and Michalsky, R. (2019). Solar-driven co-thermolysis of CO_2 and H_2O promoted by in situ oxygen removal across a non-stoichiometric ceria membrane. React. Chem. Eng. *4*, 1431–1438.
242. Siegel, N.P., Miller, J.E., Ermanoski, I., Diver, R.B., and Stechel, E.B. (2013). Factors affecting the efficiency of solar driven metal oxide thermochemical cycles. Ind. Eng. Chem. Res. *52*, 3276–3286.
243. Siegrist, S., Storch, H.v., Roeb, M., and Sattler, C. (2019). Moving brick receiver–reactor: a solar thermochemical reactor and process design with a solid–solid heat exchanger and on-demand production of hydrogen and/or carbon monoxide. J. Sol. Energ-T. ASME. *141*, 021009.
244. Chen, J., Kong, H., and Wang, H. (2023). A novel high-efficiency solar thermochemical cycle for fuel production based on chemical-looping cycle oxygen removal. Appl. Energy *343*, 121161.
245. Jarrett, C., Chueh, W., Yuan, C., Kawajiri, Y., Sandhage, K.H., and Henry, A. (2016). Critical limitations on the efficiency of two-step thermochemical cycles. Sol. Energy *123*, 57–73.
246. Ermanoski, I., Miller, J.E., and Allendorf, M.D. (2014). Efficiency maximization in solar-thermochemical fuel production: challenging the concept of isothermal water splitting. Phys. Chem. Chem. Phys. *16*, 8418–8427.
247. Felinks, J., Brendelberger, S., Roeb, M., Sattler, C., and Pitz-Paal, R. (2014). Heat recovery concept for thermochemical processes using a solid heat transfer medium. Appl. Therm. Eng. *73*, 1006–1013.
248. Falter, C.P., and Pitz-Paal, R. (2018). Modeling counter-flow particle heat exchangers for two-step solar thermochemical syngas production. Appl. Therm. Eng. *132*, 613–623.
249. Brendelberger, S., Felinks, J., Roeb, M., and Sattler, C. (2014). Solid phase heat recovery and multi chamber reduction for redox cycles. Proceedings of the ASME 2014 8th International Conference on Energy Sustainability. V001T002A016, 1-9. https://doi.org/10.1115/ES2014-6421.
250. Falter, C.P., and Pitz-Paal, R. (2017). A generic solar-thermochemical reactor model with internal heat diffusion for counter-flow solid heat exchange. Sol. Energy *144*, 569–579.
251. Patankar, A.S., Wu, X.Y., Choi, W., Tuller, H.L., and Ghoniem, A.F. (2022). A Reactor Train System for Efficient Solar Thermochemical Fuel Production. J. Sol. Energy Eng. *144*, 061014.
252. Hogan, R.E., Miller, J.E., James, D.L., Chen, K.S., and Diver, R.B. (2012). Modeling Chemical and Thermal States of Reactive Metal Oxides in a CR5 Solar Thermochemical Heat Engine. ASME 2012 6th International Conference on Energy Sustainability. ES2012-91490, 1137-1144. https://doi.org/10.1115/ES2012-91490.
253. James, D.L., Siegel, N.P., Diver, R.B., Boughton, B.D., and Hogan, R.E. (2008). Numerical Modeling of Solar Thermo-Chemical Water-Splitting Reactor. Sol. Energy *ISEC2006–99141*, 221–227.
254. Lidor, A., Aschwanden, Y., Häseli, J., Reckinger, P., Haueter, P., and Steinfeld, A. (2023). High-temperature heat recovery from a solar reactor for the thermochemical redox splitting of H_2O and CO_2. Appl. Energy *329*, 120211.
255. Carrillo, R.J., and Scheffe, J.R. (2019). Beyond ceria: theoretical investigation of isothermal and near-isothermal redox cycling of perovskites for solar thermochemical fuel production. Energ Fuel *33*, 12871–12884.
256. Warren, K.J., Tran, J.T., and Weimer, A.W. (2022). A thermochemical study of iron aluminate-based materials: A preferred class for isothermal water splitting. Energy Environ. Sci. *15*, 806–821.
257. Bala Chandran, R., De Smith, R.M., and Davidson, J.H. (2015). Model of an integrated solar thermochemical reactor/reticulated ceramic foam heat exchanger for gas-phase heat recovery. Int. J. Heat Mass Transf. *81*, 404–414.
258. Falter, C.P., Sizmann, A., and Pitz-Paal, R. (2015). Modular reactor model for the solar thermochemical production of syngas incorporating counter-flow solid heat exchange. Sol. Energy *122*, 1296–1308.
259. Holzemer-Zerhusen, P., Brendelberger, S., Roeb, M., and Sattler, C. (2021). Oxygen Crossover in Solid–Solid Heat Exchangers for Solar Water and Carbon Dioxide Splitting: A Thermodynamic Analysis. J. Energ. Resour-ASME. *143*, 071301.